

DEVELOPMENT OF A CONTROL STRATEGY FOR ROAD VEHICLES
WITH SEMI-ACTIVE SUSPENSIONS USING A FULL VEHICLE RIDE
MODEL

A THESIS SUBMITTED TO
THE GRADUATE SCHOOL OF NATURAL AND APPLIED SCIENCES
OF
MIDDLE EAST TECHNICAL UNIVERSITY

BY

ZEYNEP ERDOĞAN

IN PARTIAL FULFILLMENT OF THE REQUIREMENTS
FOR
THE DEGREE OF MASTER OF SCIENCE
IN
MECHANICAL ENGINEERING

FEBRUARY 2009

Approval of the thesis:

**DEVELOPMENT OF A CONTROL STRATEGY FOR ROAD
VEHICLES WITH SEMI-ACTIVE SUSPENSIONS USING A FULL
VEHICLE RIDE MODEL**

submitted by **ZEYNEP ERDOĞAN** in partial fulfilment of the requirements for the degree of **Master of Science in Mechanical Engineering Department, Middle East Technical University** by,

Prof.Dr.Canan Özgen _____
Dean, Graduate School of **Natural Applied Sciences**

Prof.Dr.Süha Oral _____
Head of Department, **Mechanical Engineering**

Prof.Dr.Y.Samim Ünlüsoy _____
Supervisor, **Mechanical Engineering Dept., METU**

Examining Committee Members:

Prof. Dr. Mehmet Çalışkan _____
Mechanical Engineering Dept., METU

Prof. Dr. Y. Samim Ünlüsoy _____
Mechanical Engineering Dept., METU

Asst. Prof. Dr. Yiğit Yazıcıoğlu _____
Mechanical Engineering Dept., METU

Dr. Gökhan Özgen _____
Mechanical Engineering Dept., METU

Asst. Prof. Dr. Kutluk Bilge Arıkan _____
Mechatronics Engineering Dept., Atılım University

Date: 12.02.2009

I hereby declare that all information in this document has been obtained and presented in accordance with academic rules and ethical conduct. I also declare that, as required by these rules and conduct, I have fully cited and referenced all material and results that are not original to this work.

Name, Last name: Zeynep, Erdoğan

Signature:

ABSTRACT

DEVELOPMENT OF A CONTROL STRATEGY FOR ROAD VEHICLES WITH SEMI-ACTIVE SUSPENSIONS USING A FULL RIDE VEHICLE MODEL

Erdoğan, Zeynep

M.S., Department of Mechanical Engineering

Supervisor: Prof. Dr. Y. Samim Ünlüsoy

February 2009, 112 pages

The main motivation of this study is the design of a control strategy for semi-active vehicle suspension systems to improve ride comfort for road vehicles. In order to achieve this objective, firstly the damping characteristics of Magnetorheological dampers will be reviewed. Then an appropriate semi-active control strategy manipulating the inputs of the dampers to create suitable damping forces will be designed. Linear Quadratic Regulator (LQR) control strategy is the primary focus area on semi-active control throughout this study. Further, skyhook controllers are examined and compared with optimal LQR controllers. The semi-active controller is tuned using a linearized full (4 wheel) vehicle ride model with seven degrees of freedom. Some selected simulations are carried out by using a nonlinear model to tune LQR controller in an effort to optimize bounce, pitch, and roll motion of the vehicle. Time domain simulations and frequency response analysis are used to justify the effectiveness of the proposed LQR control strategy.

Keywords: Semi-active Suspensions, Magnetorheological Damper, Linear Quadratic Regulator, Optimal Control, Optimization, Skyhook, Full Vehicle Ride Model

ÖZ

YARI AKTİF SÜSPANSİYONLAR İÇİN TAM ARAÇ MODELİ KULLANILAN KONTROL STRATEJİLERİNİN GELİŞTİRİLMESİ

Erdoğan, Zeynep

Yüksek Lisans, Makine Mühendisliği Bölümü

Tez Yöneticisi: Prof. Dr. Y. Samim Ünlüsoy

Şubat 2009, 112 sayfa

Bu tez çalışmasının amacı, yarı-aktif süspansiyon sistemleri için kullanılan kontrol stratejilerinin yol araçlarının sürüş konforunu geliştirmek için tasarlanmasıdır. Bu çalışmada öncelikle manyetoreolojik sönümleyiciler araştırılmış, daha sonra araç modelinde süspansiyonların uygulaması gereken sönümleme kuvvetlerinin belirlenebilmesi için yarı-aktif kontrol stratejisi geliştirilmiştir. Lineer Karesel Durum Regülatörü (LKR) bu çalışmada öncelikle kullanılan yarı-aktif kontrol stratejisidir. Buna ek olarak “Skyhook” kontrolcüsü incelenmiş ve LKR kontrolcüsüyle performans açısından karşılaştırılmıştır. Yarı-aktif kontrol stratejisi doğrusal yedi serbestlik dereceli (4 tekerlekli) araç modeli kullanılarak ayarlanmış; seçilen bazı simülasyonlarla, doğrusal olmayan modelde sistemin zıplama, başvurma ve yalpalama davranışları eniyelenmiştir. Zamana bağlı simülasyonlarla ve frekans cevabı analizleriyle LKR denetleyicisinin yeterliliği gösterilmiştir.

Anahtar Kelimeler: Yarı aktif Süspansiyon, Manyetoreolojik Sönümleyici, Lineer Karesel durum Regülatörü, Eniyi Denetim, Eniyileme, “Skyhook”, Tam Araç Sürüş Konforu Modeli

ACKNOWLEDGEMENTS

First, I would like to express my special thanks to my supervisor Prof. Dr. Y. Samim Ünlüsoy, who has guided me to this topic with his experience, endlessly supported and encouraged me. Additionally I want to thank Prof. Dr. Bülent Platin for opening his doors when I needed help. I would also like to state my gratitude to my colleague Kemal Çalışkan for his assistance in developing user interfaces in Matlab. Also, financial support of TÜBİTAK is also gratefully acknowledged.

It would not be easy for me to write my master degree thesis without the help and support of my friends Tuğçe Yüksel, Ali Murat Kayıran, Zekai Murat Kılıç and Bekir Bediz.

I would like to express my special thanks to Gökhan Tekin who has supported and cheered me up in all my hard times and gave me the strength to carry on.

Finally I would also like to thank my precious parents Şükran and Esat Erdoğan for their unconditional continuous support throughout my life. The last but not the least, I would like to thank my sister Bilge Erdoğan for making me feel she is always standing by my side despite the long distances between us.

TABLE OF CONTENTS

ABSTRACT	iv
ÖZ	v
ACKNOWLEDGEMENTS	vi
TABLE OF CONTENTS	vii
LIST OF FIGURES	x
LIST OF TABLES	xiv
LIST OF SYMBOLS	xv
LIST OF ABBREVIATIONS	xvii
1 INTRODUCTION	1
1.1 RESEARCH OBJECTIVES.....	1
1.2 APPROACH.....	2
1.3 BACKGROUND	2
1.3.1 MAGNETORHEOLOGICAL FLUID TECHNOLOGY	3
1.4 LITERATURE SURVEY.....	8
1.5 OUTLINE.....	13
2 FULL-CAR VEHICLE RIDE MODEL	15
2.1 INTRODUCTION.....	15
2.2 EQUATIONS OF MOTION OF THE FULL-CAR RIDE MODEL	16
2.2.1 NONLINEAR EQUATIONS WITH PASSIVE SUSPENSIONS	16
2.2.2 STATE SPACE REPRESENTATION OF THE LINEAR PASSIVE SYSTEM....	18
2.2.3 EQUATIONS OF MOTION IN STATE SPACE FORM	20
2.2.4 STATE SPACE REPRESENTATION OF THE LINEAR SEMI-ACTIVE SYSTEM	24
3 SEMI-ACTIVE CONTROL STRATEGY	29

3.1	INTRODUCTION	29
3.2	SENSOR REQUIREMENTS	30
3.3	MR MODELLING	31
3.4	OPTIMAL CONTROL/ LINEAR QUADRATIC REGULATOR CONTROL STRATEGY	31
3.4.1	A THEORETICAL LOOK INTO LINEAR QUADRATIC REGULATOR CONTROL STRATEGY.....	32
3.4.2	THE LIMITATIONS OF TIME-INVARIANT LINEAR QUADRATIC REGULATOR.....	33
3.4.3	FEASIBILITY OF LQR CONTROL INPUTS FOR SEMI-ACTIVE DAMPERS.....	34
3.5	SKYHOOK, GROUNDHOOK CONTROL STRATEGY	39
4	SIMULATION MODEL.....	41
4.1	SIMULINK MODEL	41
4.2	OPTIMAL CONTROLLER BLOCKS	41
4.3	SKYHOOK CONTROLLER BLOCKS	44
5	OPTIMIZATION PROCESS.....	45
5.1	THEORETICAL BACKGROUND	45
5.1.1	TRANSMISSIBILITY ANALYSIS OF QUARTER CAR MODEL.....	45
5.1.2	VIBRATION ANALYSIS OF FULL CAR RIDE MODEL.....	51
5.2	OPTIMIZATION FOR OPTIMAL CONTROL USING BUMP INPUT	52
5.2.1	STAGE 1: OPTIMIZATION WITH RESPECT TO ONLY BOUNCE WEIGHTING FACTOR.....	53
5.2.2	STAGE 2: OPTIMIZATION WITH RESPECT TO ONLY PITCH WEIGHTING FACTOR	55
5.2.3	STAGE 3: OPTIMIZATION WITH RESPECT TO BOUNCE ACCELERATION FACTOR AND PITCH WEIGHTING FACTOR.....	58
5.2.4	STAGE 4: OPTIMIZATION WITH RESPECT TO BOUNCE ACCELERATION, PITCH AND ROLL WEIGHTING FACTOR	64
5.3	3D BUMP OPTIMIZATION FOR SKYHOOK CONTROL STRATEGIES	68
5.4	3D CHIRP INPUT ANALYSIS	69
6	SIMULATION TESTS	75
6.1	SINUOSIDAL INPUT TEST.....	75
6.2	BUMP&HUMP TEST.....	78
6.2.1	HALF SINUSOIDAL BUMP TEST SIMULATION 1	78

6.2.2	HALF SINUSOIDAL BUMP TEST SIMULATION 2	82
6.2.3	HALF SINUSOIDAL HUMP TEST	85
6.3	STEP INPUT TEST	87
6.4	RANDOM ROAD INPUT TEST	90
7	CONCLUSION	95
	REFERENCES	97
APPENDICES		
	APPENDIX A	101
A.1	GENERAL VIEW OF THE SIMULATION MODEL SIMULATION MODEL	101
A.2	ROLL AND PITCH MOTION OF THE VEHICLE.....	102
A.3	COMPABILITY EQUATIONS BETWEEN CENTRE OF MASS AND CORNERS OF THE VEHICLE.....	103
A.4	UNSPRUNG MASS MOTION.....	104
A.5	BOUNCE MOTION OF THE VEHICLE.....	105
	APPENDIX B	106
	APPENDIX C	107
	APPENDIX D	110
	APPENDIX E	112

LIST OF FIGURES

FIGURES

Figure 1.1 Illustrative Sketch	5
Figure 1.2 The Characteristics of CARRERA™ MagneShock™ Damper	6
Figure 1.3 MR Damper Characteristics of MR CDC damper of Daewoo Precision Industries, Ltd., Korea.....	7
Figure 1.4 MR Damper selection Guide	8
Figure 2.1 Full Car Ride Model	16
Figure 3.1 Semi-Active Damper Control Concept.....	30
Figure 3.2 Admissible Damping Region of a Typical Semi-Active Damper	34
Figure 3.3 Process of Clipping Optimal Forces to Admissible Damping Region	36
Figure 3.4 Quarter Car Model.....	40
Figure 4.1 Full State Feedback Optimal Control Simulink Model.....	42
Figure 4.2 MR Modelling And Force Clipping Simulink Model	43
Figure 4.3 Skyhook Controller Simulink Model.....	44
Figure 5.1 Quarter Car Model.....	45
Figure 5.2 Transmissibility of Sprung Mass Acceleration with Respect to Road Input	46
Figure 5.3 Transmissibility of Sprung Mass Displacement with Respect to Road Input	46
Figure 5.4 Transmissibility of Rattle Space with respect to Road Input	47
Figure 5.5 Transmissibility of Unsprung Mass Acceleration with respect to Road Input	48
Figure 5.6 Transmissibility of Tire Deflection with respect to Road Input.....	48

Figure 5.7 Weighting Constants for Sinusoidal Bump Body Bounce Acceleration Optimization.....	54
Figure 5.8 Bump Simulation Results (RMS Body Bounce Acceleration).....	54
Figure 5.9 Sinusoidal Bump Simulation Results (Peak To Peak Body Bounce Acceleration).....	55
Figure 5.10 Weighting Constants for Sinusoidal Bump Pitch Angle Optimization ..	56
Figure 5.11 Sinusoidal Bump Simulation Results (RMS of Pitch Angle).....	57
Figure 5.12 Sinusoidal Bump Simulation Results (Peak To Peak Pitch Angle).....	57
Figure 5.13 Sinusoidal Bump Simulation Results (RMS of Bounce Acceleration) ..	60
Figure 5.14 Sinusoidal Bump Simulation Results (RMS of Pitch Angle).....	60
Figure 5.15 Sinusoidal Bump Simulation Results (RMS of Bounce Acceleration) ..	63
Figure 5.16 Sinusoidal Bump Simulation Results (RMS of Pitch Angle).....	63
Figure 5.17 Sinusoidal Bump 3D Simulation Results (RMS of Bounce Acceleration)	67
Figure 5.18 Sinusoidal Bump 3D Simulation Results (RMS of Pitch Angle).....	67
Figure 5.19 Sinusoidal Bump 3D Simulation Results (RMS of Roll Angle)	68
Figure 5.20 Power Spectral Density of Bounce Displacement and Acceleration - Chirp Input from 4 Wheels	71
Figure 5.21 Power Spectral Density of Bounce Acceleration - Chirp Input from one Wheel	71
Figure 5.22 Power Spectral Density of Pitch Motion - Chirp Input from one Wheel	72
Figure 5.23 Power Spectral Density Of Roll Motion - Chirp Input From One Wheel	73
Figure 5.24 Power Spectral Density of Rattle Space Motion - Chirp Input from One Wheel	74
Figure 6.1 Bounce Displacement and Acceleration versus Time – Sinusoidal Input	76
Figure 6.2 Pitch Angle versus Time - Sinusoidal Input.....	76
Figure 6.3 Roll Angle versus Time - Sinusoidal Input	77
Figure 6.4 Rattle Space versus Time - Sinusoidal Input.....	77

Figure 6.5 Road Input versus Time - Half Sinusoidal Bump Input Case 1	79
Figure 6.6 Bounce Displacement and Bounce Acceleration versus Time - Half Sinusoidal Bump Case 1	80
Figure 6.7 Pitch Angle versus Time - Half Sinusoidal Bump Case 1	80
Figure 6.8 Roll Angle versus Time - Half Sinusoidal Bump Input Case 1	81
Figure 6.9 Rattle Space Motion of Front Left Suspension and Rear Right Suspension versus Time - Half Sinusoidal Bump Input Case 1	81
Figure 6.10 Road Input versus Time - Half Sinusoidal Bump Input Case 2	82
Figure 6.11 Bounce Motion And Bounce Acceleration versus - Half Sinusoidal Bump Input Case 2	83
Figure 6.12 Pitch Motion versus Time - Half Sinusoidal Bump Input Case 2	83
Figure 6.13 Roll Motion versus Time - Half Sinusoidal Bump Input Case 2	84
Figure 6.14 Rattle Space Motion of Front Left Suspension and Rear Right Suspension versus Time - Half Sinusoidal Bump Input Case 2	84
Figure 6.15 Road Input versus Time - Half Sinusoidal Hump Input	85
Figure 6.16 Bounce Motion And Bounce Acceleration versus - Half Sinusoidal Hump Input	86
Figure 6.17 Pitch Motion versus Time - Half Sinusoidal Hump Input	86
Figure 6.18 Rattle Space Motion of Front Left Suspension and Rear Right Suspension versus Time - Half Sinusoidal Hump Input	87
Figure 6.19 Step Road Input versus Time	88
Figure 6.20 Bounce Motion versus Time Step Input	88
Figure 6.21 Pitch Motion versus Time Step Input	89
Figure 6.22 Rattle Space Motion of Front Left Suspension and Rear Right Suspension versus Time - Step Input	89
Figure 6.23 Random Road Input versus Time	90
Figure 6.24 MR and Passive Damper Characteristics	92
Figure 6.25 Power Spectral Density of Bounce Displacement and Bounce Acceleration of the existing MR damper	92

Figure 6.26 Power Spectral Density of Bounce Displacement and Bounce Acceleration of the fictitious MR damper	93
Figure A.1 General view of the Simulink Model.....	101
Figure A.2 Simulink Model for Roll and Pitch Motion.....	102
Figure A.3 Simulink Model for Compatibility Equations	103
Figure A.4 Simulink Model of Unsprung Mass Motion.....	104
Figure A.5 Simulink Model for Bounce Motion.....	105
Figure E.1 MR Data used in Simulations	112

LIST OF TABLES

TABLES

Table 1 Natural Frequencies of Full Car Ride Model.....	51
Table 2 Weighting Constants for 2D Optimization	59
Table 3 Weighting Constants for 3D Bump Optimization.....	65
Table 4 Performance Results for the MR Damper under Random Road Input	94
Table 5 Performance Results for the Fictitious MR Damper under Random Road Input	94
Table 6 Vehicle Data Used in Vehicle Simulations.....	106

LIST OF SYMBOLS

φ = pitch angle
 ρ =road roughness parameter
 ρ_n =weighting factor
 σ^2 = covariance
 θ = roll angle
 a = longitudinal distance from sprung mass center to front suspension
 A = state matrix of the vehicle in state space representation
 b = longitudinal distance from sprung mass center to rear suspension
 B = disturbance matrix in state space representation
 c = lateral distance from sprung mass center to right suspension
 C =input matrix in state space representation/damping matrix
 c_{bl1} = damping constant of rear left tyre
 c_{bl2} = rear left MR damping constant between sprung and unsprung masses
 c_{br1} = damping constant of rear right tyre
 c_{br2} = rear right MR damping constant between sprung and unsprung masses
 c_{fl1} = damping constant of front left tyre
 c_{fl2} = front left MR damping constant between sprung and unsprung masses
 c_{fr1} = damping constant of front right tyre
 c_{fr2} = front right MR damping constant between sprung and unsprung masses
 d = lateral distance from sprung mass center to right suspension
 G_g =groundhook constant
 G_s =skyhook constant
 K =closed loop gain matrix/stiffness matrix
 m_{bl} = rear left unsprung mass
 m_{br} = rear right unsprung mass
 m_{fl} = front left unsprung mass
 m_{fr} = front right unsprung mass
 M = sprung mass of the car
 P_1, P_2, P_3 =performance indices
 Q, R, N =design matrices for quadratic cost functions
 S =solution of algebraic riccati equation

u =input

v =velocity

w =disturbance

W =white noise

x =states in the state space representation of the vehicle model

z_{bl0} = road input to rear left tyre

z_{bl1} = position of rear left unsprung mass

z_{bl2} = position of rear left sprung mass

z_{br0} = road input to rear right tyre

z_{br1} = position of rear right unsprung mass

z_{br2} = position of rear right sprung mass

z_{cg} = position of sprung mass

z_{fl0} = road input to front left tyre

z_{fl1} = position of front left unsprung mass

z_{fl2} = position of front left sprung mass

z_{fr0} =road input to front right tyre

z_{fr1} = position of front right unsprung mass

z_{fr2} = position of front right sprung mass

z_1 = position of unsprung mass in a quarter car model

z_2 = position of sprung mass in a quarter car model

all first derivatives will have upscript " ' " and second derivatives will have "'' "

LIST OF ABBREVIATIONS

ER	Electrorheological
FAMOS	Frequency Adaptive Multi-objective
H_2	H_2 control
H_∞	H infinity control
HILS	Hardware-in-the-Loop Simulations
IMU	Inertial Measurement Unit
LDT	Linear Displacement Transducer
LQG	Linear Quadratic Gaussian
LQR	Linear Quadratic Regulator
MIMO	Multi Input Multi Output System
MR	Magnetorheological
OGS	Optimal Gain Switching Target
PID	Proportional Integral Derivative
PSD	Power Spectral Density
RMS	Root Mean Square
SID	Simplified Inverse Dynamics
SISO	Single Input Single Output System

CHAPTER 1

INTRODUCTION

1.1 RESEARCH OBJECTIVES

In classical vehicle dynamics, there exists three main subjects of interest: vehicle handling, ride comfort, and performance. The first subject is mainly concerned on stability and controllability of the vehicle by the driver during cornering manoeuvres. The second subject refers to the quality of the isolation of vehicle passengers from outer disturbances such as road bumps and roughness, external inputs, etc. Without any doubt, the design of appropriate suspension systems is the most crucial part for obtaining ride comfort objectives which will inevitably affect vehicle handling.

There are three types of suspension systems namely passive, semi-active, and active suspension systems. The latter suspension systems are developed to improve conventional passive suspension characteristics. Semi-active and active dampers can adjust their forces according to road conditions. Active suspension systems are superior in improving handling and ride characteristics of a vehicle whereas passive dampers have the advantage of the simplicity and low cost. A semi-active suspension system using magnetorheological (MR) dampers is a compromise between active and passive suspension systems. They have lower cost than active suspension systems and while they are superior in improving ride comfort and road holding to passive suspensions. More general information on suspension system types can be found in section 2.1.

The main objective of this study is to build a design methodology for constructing a controller system for the semi active vehicle suspension systems to improve ride

comfort. The methodology targets basic ride comfort through controlling the vehicle suspension system. The suspension system is to be designed to obtain a compromise between different ride comfort objectives such as sprung mass acceleration roll and pitch motions of the vehicle. The designed controller system will be tested in order to verify its performance.

1.2 APPROACH

The study on semi-active suspensions is carried with Magnetorheological(MR) dampers which are discussed in detail in section 2.2. Clipped Linear Quadratic Regulator (LQR) optimal control strategy is chosen as the main control strategy to minimize bounce acceleration, and roll and pitch motions of the vehicle by modifying the damper characteristics. The full ride model (seven degree of freedom) with the proposed controller is tested for several road inputs and the controller is tuned based on the simulation tests that will be discussed in chapter 4.

1.3 BACKGROUND

In conventional vehicles, the suspension system between sprung and unsprung masses is usually composed of a spring and a conventional damper in parallel. The parameters of the spring and damper are set to make a compromise between ride comfort and handling. To get better handling and ride comfort characteristics simultaneously, the use of active and semi-active suspension systems has become a recent focus area in automotive industry.

Active systems can supply and dissipate energy to/from a system. There is a force actuator that can provide necessary force to the system. The response of the system can be adjusted according to road inputs. The main disadvantage is the high power demand from the vehicle power sources.

Semi-active damper systems can provide the variation of damping coefficient of the damper. They, however, can only dissipate energy from the system. Power requirement of these systems is usually lower than active suspensions. Although active suspensions has superiority in performance, semi-active suspensions are more feasible for implementation in vehicles because of their cost advantage, low power requirement and simplicity.

Some varieties of semi-active devices are controllable friction devices, variable orifice dampers, electrorheological (ER) fluid dampers, and magnetorheological (MR) fluid dampers. The friction coefficient can be regulated in controllable friction dampers, more information on controllable friction devices can be taken from (Guglielmino, 2008). The orifice openings consequently are regulated in variable orifice dampers such that necessary damping forces are generated (Rajamani, 2006). MR and ER semi-active dampers are fluid dampers which change their viscosity according to the current supplied to the system.

MR dampers have become the search focus for semi-active dampers, since their available damping range and the response time are almost as good as active dampers in spite of the lower power requirement. The next section provides more detailed information on MR fluids and MR dampers.

1.3.1 MAGNETORHEOLOGICAL FLUID TECHNOLOGY

In the 1940's, MR fluid technology and its possible application areas have become known in the scientific areas. However the availability of MR fluids was greatly enhanced later on by the development of electronic technology such as controllers, microprocessors and sensors. After 1980, MR fluids have started to be used in many application areas (Grad, 2006). The application areas of the MR technology are quite wide. These applications can be seen from (Klingenberg, 2001). MR technology can be used in prosthetic knees, in civil engineering to reduce earthquake effects in structures, polishing industry, gun recoil mechanisms, and washing machines. One of

the main application areas is in the automotive industry. Besides its obvious use in shock absorbers; it can also be used in clutches, passenger seat suspensions, and brakes. The paper by Klingenberg also addresses the possible challenges in MR technology like decreasing cost, overcoming sedimentation, and oxidation of iron particles.

MR dampers were used as primary suspensions on models of Acura MDX, Audi TT, Audi R8, Buick Lucerne, Cadillac DTS, Cadillac SLR, Cadillac SRX, Cadillac STS, Chevrolet Corvette, Ferrari 599GTB and Holden HSV Commodore (Primary Suspension, 2008).

1.3.1.1 Magnetorheological Fluid Characteristics

Magnetorheological (MR) fluids are kind of a fluid with magnetic particles that change rheological characteristics in response to application of a magnetic field. Magnetic particles align and develop yield strength in the presence of a magnetic field. The yield strength of the fluid can be modified by changing the magnetic field strength. Usually the yield stress increases by the magnetic field applied. In the work of Klingenberg (Klingenberg, 2001), it is stated that the flow behaviour of MR fluids is typically like a Bingham fluid which does not flow unless the stress exerted is above the yield strength of the fluid. In the absence of a magnetic field, the fluid behaviour is like Newtonian fluids. It is also claimed that the MR fluids are not sensitive to contaminants and unaffected by temperature and the changes in rheological behaviour of the fluid take less than 10 milliseconds (Technology Compared, n.d.).

1.3.1.2 MR Damper Characteristics

MR dampers have received attention in engineering environments because they offer variable damping characteristics. They are mainly used as semi active automotive suspension systems. Thus, semi active devices are expected to offer effective performance over a variety of amplitude and frequency ranges. Although the active

dampers are superior in order to reach that goal, they have higher power requirements than semi active dampers and they cost. Considering the performances of suppressing vibration of the sprung and unsprung masses, they achieve significant performance achievement when compared to conventional passive suspensions.

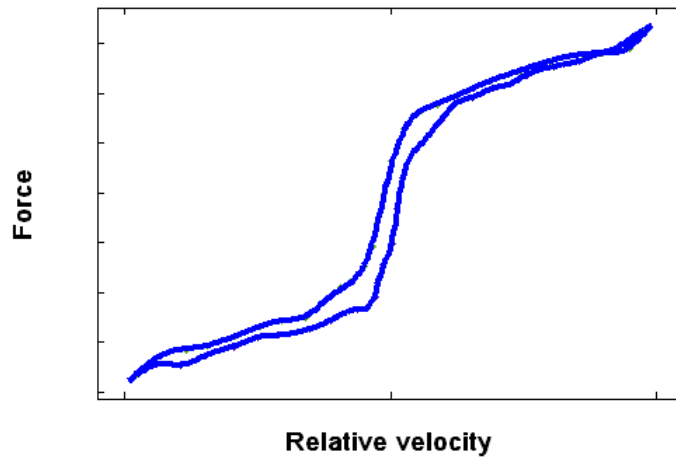


Figure 1.1 Illustrative Sketch

MR dampers have nonlinear damping characteristics with hysteresis. MR damper characteristics depend on both input current and the relative velocity across suspension ends. The hysteresis can be seen from the illustrative Figure 1.1 which is inspired from the article of Butz et. al. (Butz, 2002). Figure 1.1 shows the damping force changes due to relative velocity at a specified constant current value. In low relative velocity region across the suspension, the damping behaviour is quite unpredictable, however in high relative velocity regions; the damping characteristic is quite linear. The models used in simulations generally do not include hysteresis in order to simplify and linearize the system.

Generally as the input current becomes higher, the damping force available at a particular relative velocity becomes higher. From Figure 1.2 which shows the

characteristics of CARRERA™ MagneShock™ damper (Giua A. M., 2004) and from Figure 1.3 which shows the characteristics MR CDC damper of Daewoo Precision Industries, Ltd., Korea (Hong, Kim, & Kim, 2007)., the increase in damping force with increased input currents can be clearly seen. In simulations the hysteresis is generally not included. Nonlinear variations are linearized and the hysteresis dominance in small relative velocity regions is neglected by setting the damping force to zero force at zero relative velocity.

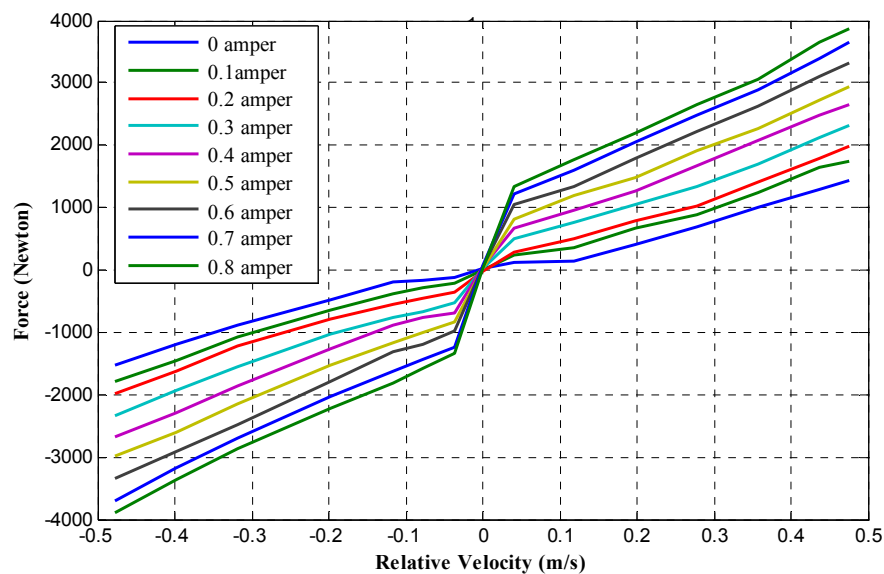


Figure 1.2 The Characteristics of CARRERA™ MagneShock™ Damper

Comparison between Figure 1.2 and Figure 1.3 implies that the damping forces of the Daewoo damper at zero current level and maximum current level is lower. Although the softer zero current level damping characteristics are favourable, the larger damping forces at maximum current levels are also favourable. How to choose a suitable damper will be discussed in the following paragraphs.

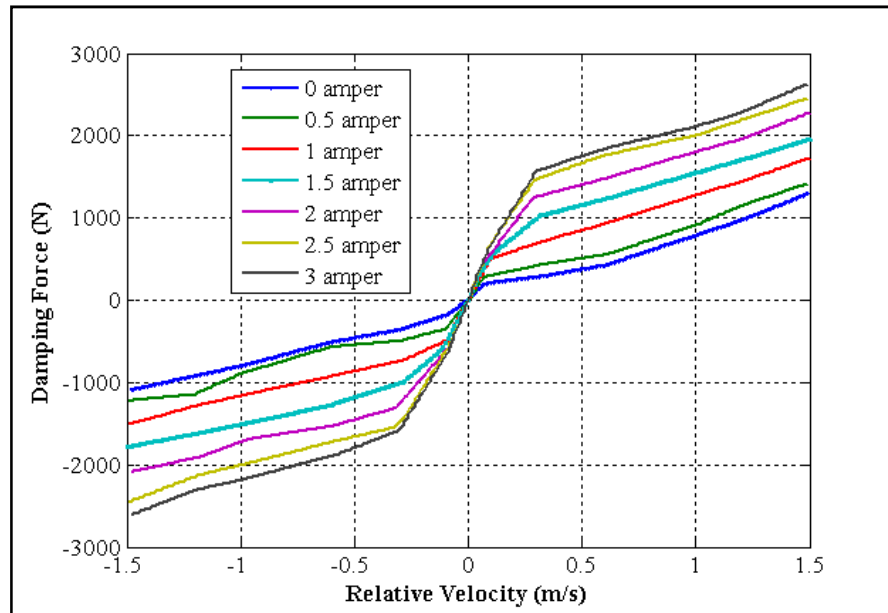


Figure 1.3 MR Damper Characteristics of MR CDC damper of Daewoo Precision Industries, Ltd., Korea

The selection of a specific MR damper is mainly based on the vehicle type and vehicle size. The easiest way to select suitable MR dampers is to obtain the characteristic of a classical damper used in the same class of the vehicle and then to find a MR damper whose damping range contains the classical damper characteristics. The MR damper should have softer characteristics when no input current supplied and harder characteristics when a nonzero current level is maintained.

In an ideal MR damper, in case of no current the damping forces at any relative velocity across the damper should be as low as possible. Figure 3 shows the range of an appropriate MR damper and the characteristic for an ideal classical damper. In reality the characteristic of a classical damper is not a straight line, is not symmetric about origin, and does not pass through the zero force-zero velocity point.

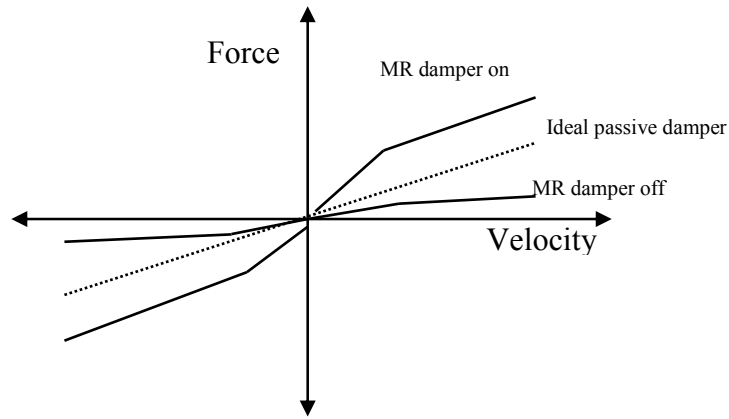


Figure 1.4 MR Damper selection Guide

The published works on parametric and nonparametric MR damper modelling that may include hysteresis are given in section 1.4. In the method of inverse modelling, the necessary input current to generate desired damping force should be found by inverse modelling methods.

1.4 LITERATURE SURVEY

MR dampers have decreased reaction times of vibration control systems to millisecond scales and their power requirement is much lower than active dampers which can be stated as generally no more than 50 Watts. In addition, space requirement of MR dampers is less compared with other active and semi active suspension systems. The yield properties and technical properties are given in detail by Butz et al. Since in the design of MR damper there exists less moving parts, they provide long-term endurance. Besides for the case of MR devices, the interface mechanical and electronic units is fast which makes the control of these devices easier (Butz, 2002).

The chemical structure of MR damper fluids and the additives which prevent settling of iron particles, inhibit wear lubrication, etc. can be studied in detail on the website of LORD Corporation. (LORD Corporation – Adhesives, Coatings, Vibration, Shock

& Motion Control., n.d.). LORD Corporation is one of the leading companies in MR technology in corporation with Delphi's MagneRide™ shock absorbers, and Carrera's MagneShock™ automotive racing shocks absorbers. MR technology has been adapted to Cadillac Seville STS and Chevrolet Corvette. Today the MagneRide system is in production on the Cadillac SRX, SLR, and DTS and the new Buick Lucerne. From the website of LORD Corporation (Primary Suspension, 2008), introductory technical papers about the rheological, magnetic, and material properties of various commercial MR fluids can be found. Also possible application areas can be found in the article by Jolly et al.(Mark R. Jolly, 1999).

Modelling MR damper characteristics and behaviour estimation is generally done by constructing look-up tables or estimated behaviour curves. Sung et al. (Sung K. C., 2005) studied three modes of operation of MR dampers; namely flow (valve), shear mode, and squeeze mode. The flow mode is more related to the thesis subject since this mode is suitable for shock absorbers and dampers. The paper also discusses other application areas of MR fluids and the problems encountered in application of MR fluids.

To control MR dampers in real life including hysteresis, the modelling of hysteresis phenomena by parametric and nonparametric models is studied by Butz et al (Butz, 2002). The parametric models include Bingham model, Bouc Wen hysteresis model, and modified Bouc Wen model. Non-parametric models are based on a specific fluid device. In the study reported by Dominguez et al, the Bouc–Wen model which is extensively used to simulate the hysteresis behaviour of MR dampers is studied to eliminate the differences between simulation and experimental results (Dominguez, 2004). In this work, the proposed methodology takes into consideration of the effect of each term in the Bouc–Wen model over the hysteretic loop to tune this model.

To use the characteristics from the MR dampers properly, the inputs to the dampers should be determined. This process is more applicable in inverse dynamic models. However, since the MR damper models are highly nonlinear, Tsang et al. (Tsang, 2006) suggested simplification in the models. Simplified inverse dynamics (SID)

models were built for Bingham plasticity model and the Bouc–Wen hysteresis model. In SID models the fluid yield stress or input current are computed to generate the desirable damping forces demanded by various control strategies. Two algorithms named “Piston Velocity Feedback (PVF)” and “Damper Force Feedback (DFF)” were formulated. Numerical simulations are claimed to show the effectiveness of the simulations.

Song et al. (Song, 2005) claim that efficiency of the models in computation time can be enhanced by nonparametric models. It is stated that nonparametric models can be solved with bigger integration step sizes than parametric models which enable real time model based control algorithms. The study claims that the proposed nonparametric models are able to accurately predict the damper force characteristics, damper bilinear behaviour, hysteresis, and electromagnetic saturation.

The adaptation of the MR dampers to automotive suspensions will be studied in the following. The semi-active suspensions will be tested for handling and ride comfort criteria. The number of criteria that can be observed is based on the complexity of the vehicle models. Full car models are the more complex models compared with quarter and half car models.

Different control strategies exist for controlling the response of MR dampers. Skyhook-groundhook, H_2 / H_∞ , sliding mode, LQR/LQG, on-off, fuzzy, and PID control strategies are commonly adapted to semi-active suspension systems involving MR dampers. In the following paragraphs the literature survey on control strategies will be given.

The first and commonly encountered type of control strategies is of skyhook control type. Ahmadian et al. (Ahmadian M. P., 2000) have studied skyhook, groundhook, and hybrid (a combination of skyhook and ground hook control strategies) control experimentally on a quarter car model. According to the simulation results, the hybrid control seems to have a compromise between skyhook and groundhook control policy for vehicle handling and comfort. To get further details of skyhook

policy two publications are useful. Ahmadian et al. (Ahmadian M. S., 2004) proposed two different formulations of skyhook policy to eliminate the sudden rise in the damping force when the relative velocity across the suspension is zero. By eliminating the rise, the increase of the sprung mass acceleration is prevented in heavy truck suspension applications. Also in another paper by Ahmadian et al. (Ahmadian M., 2004), skyhook control policy was used to minimize lateral and pitch accelerations of the vehicle during maneuvers. Kim (Kim, 2007) is one of the contributors to apply skyhook control strategy using a full car ride model on semi-active suspension with MR dampers using four relative displacement sensors. Estimation of absolute velocity of the sprung mass is also studied in this paper. A field test study on skyhook controllers is done by Choi et al. This paper (Choi, Han, & Sung, 2008) presents full vehicle tests with sky-hook controllers for bump and random road inputs. In the bump test results, a reduction in vertical acceleration, pitch angle, and suspension travel was claimed to be observed.

Optimal control strategies are widely used for MR dampers. H_∞ and H_2 control are among most known types of optimal control strategies. These control strategies enable robustness, which makes the system more stable. Du et al. (Du, 2005) has given a H_∞ example in a quarter car model. H_∞ controller was designed using the measurable suspension deflection and sprung mass velocity signals. Simulation results under random excitation were claimed to indicate improvements comparable to active suspensions. (Choi S. L., 2002) has also extended H_∞ control of MR dampers to full car ride model. This paper explains the design and manufacturing of a MR damper based on Bingham model and H_∞ controller was formulated with robustness to the sprung mass uncertainties. This was accomplished by adopting the loop shaping design procedure.

Another widely known optimal control strategy is LQR/LQG control strategy. If the damper is ideal such that the damping forces can be generated without any constraints, this control strategy would work without any need of modifications because of the physical constraints in semi-active dampers that will be covered in section 3.4.3. So modifications to LQR/LQG techniques should be developed. Zhang

et al. (Zhang, 2006) implemented Hrovat control algorithm which is a combination of LQR and clipped optimal control laws implemented in a two degree of freedom tracklayer suspension system. In the simulations carried, the improvement in reducing vertical and rocking acceleration is claimed to be more than 30%. A similar study on a two degree of vibration model was carried by Martynowicz et al.(Martynowicz, 2007). In this study, the skyhook and LQ control algorithms were compared. LQ control algorithm was found superior. Again, in a half car model which involves passenger dynamics two MR dampers are adapted to a vehicle suspension by Karkoub et al.(Karkoub, 2006). All the papers show that LQR approach to MR dampers is a feasible idea.

While using LQR technique, there are some methods developed to constrain the force generated by MR dampers. One of them is the two-phase design technique by Giua et .al.(Giua, Seatzu, & Usai, 1999). The method used in the first phase is called Optimal Gain Switching method which gives a bounded target control force by switching different feedback gains. This method also calculates the region of state space in which the control forces are bounded. In the second phase, the target control force is approximated by controlling the damper coefficient. The article claims that the use of a semi-active suspension leads to minimal loss with respect to optimal performance of an active suspension. This work was carried on a quarter car model. Same work was carried on a four degree of freedom model by Giua et al. (Giua A. S., 2000). The same methodology was applied to a mixed suspension system for the axletree of a road vehicle based on a linear model.

In another paper by Seatzu et al. (Giua A. M., 2004). LQR methodology was adapted to two kinds of semi-active dampers named MR and solenoid valve damper in a quarter car model. The updating frequency of the damping coefficient was taken into consideration, and the expected value of damper coefficient was predicted. “An asymptotic state observer was designed by minimizing the H_2 norm of the transfer function matrix among the error state estimate and the external disturbance”. Then, the control law was formulated as an LQR problem.

Fuzzy control strategy is generally used as a combination of other control methods. Wang et al. (Wang, 2005) made a study on optimal fuzzy control of a semi-active suspension of a full vehicle model. Yu et al. (Yu, 2006) studied a combination of fuzzy and groundhook control strategy on a quarter car model. Another fuzzy application with a sliding mode controller is given by Zheng et al.(Zheng, 2007). In this paper chattering of the sliding mode controller is claimed to be reduced considerably and the controller is claimed to have good robustness. Li et al. (Li, 2004) has made a study on hybrid control with fuzzy control. The hybrid control strategy changes the ratio of the groundhook and skyhook forces according to fuzzy intelligent controller. The coordination controller is designed to coordinate the four independent semi-active fuzzy logic controllers by adjusting their output parameters according to the system feedback.

There are a number of other control strategies. To name some papers, one may mention Liu et al.(Liu, 2004) has studied the variable control theory on car body vibrations. Lu (Lu, 2004) has studied FAMOS (A frequency adaptive multi objective suspension control strategy) which adjusts the control strategy for a given frequency excitation on a quarter car model. In the paper by Choi et al. (Choi Y. P., 2000) sliding mode controller was adapted to full car model with four independent Electrorheological dampers. A sliding mode controller was formulated by treating the sprung mass as uncertain parameter.

1.5 OUTLINE

The thesis work starts with a background of the state of the art of basic elements used in the semi-active suspensions. Firstly suspension system types, MR technology and MR damper properties are discussed in chapter 1. Literature survey on the control of the MR dampers are given at the end of the chapter.

In chapter 2, the seven degree of freedom ride model is presented and the equations of motions are derived with Newtonian approach. The state space representation is also derived at the end of the chapter.

In chapter 3, the possible control strategies for semi-active dampers are studied and the theoretical background of the control strategies is given, whereas in chapter 4, the Matlab/Simulink model for seven degree ride model is studied. In chapter 5, the chosen control strategy is examined considering its optimization phases.

In chapter 6, the inputs to the vehicle model is discussed and the results of simulations of the controllers are presented accordingly. Finally chapter 0 serves as the conclusive chapter of all former chapters and consists of conclusions reached on this particular thesis subject.

CHAPTER 2

FULL-CAR VEHICLE RIDE MODEL

2.1 INTRODUCTION

Simulation of control strategies of semi-active suspensions needs a vehicle model to be analyzed for various road inputs. In this study a two axle simulation model involving seven degrees of freedom will be used for all simulations. This model is adequate for small and mid-sized cars to determine bounce, pitch, and roll responses of the vehicle. A moving coordinate system xyz is fixed at the center of gravity of the car. The degrees of freedom are positions of unsprung masses, position of the vehicle center of gravity in z direction, pitch motion and roll motion at the center of gravity. Elimination of the yaw motion simplifies the equation by reducing equation couplings. There are four independent inputs from the road surface at the contact patches of the tires.

As seen from Figure 2.1, the model has four suspension systems connected to car body which is represented in the model with a rigid body frame. The tires are represented with unsprung mass, stiffness, and damper. The dampers between sprung mass and unsprung masses are MR dampers whose damping constants are adjusted by a suitable control strategy. The nomenclature used in the model can be found in the List of Symbols. The nonlinear equations of motion will be derived by using Newtonian approach in section 2.2. After obtaining the nonlinear equations of motion in section 2.2.1, they are linearized by using small angle assumption in section 2.2.2, and finally state space representation is developed in section 2.2.3 by using fourteen state variables which consist of seven degrees of freedom and their derivatives.

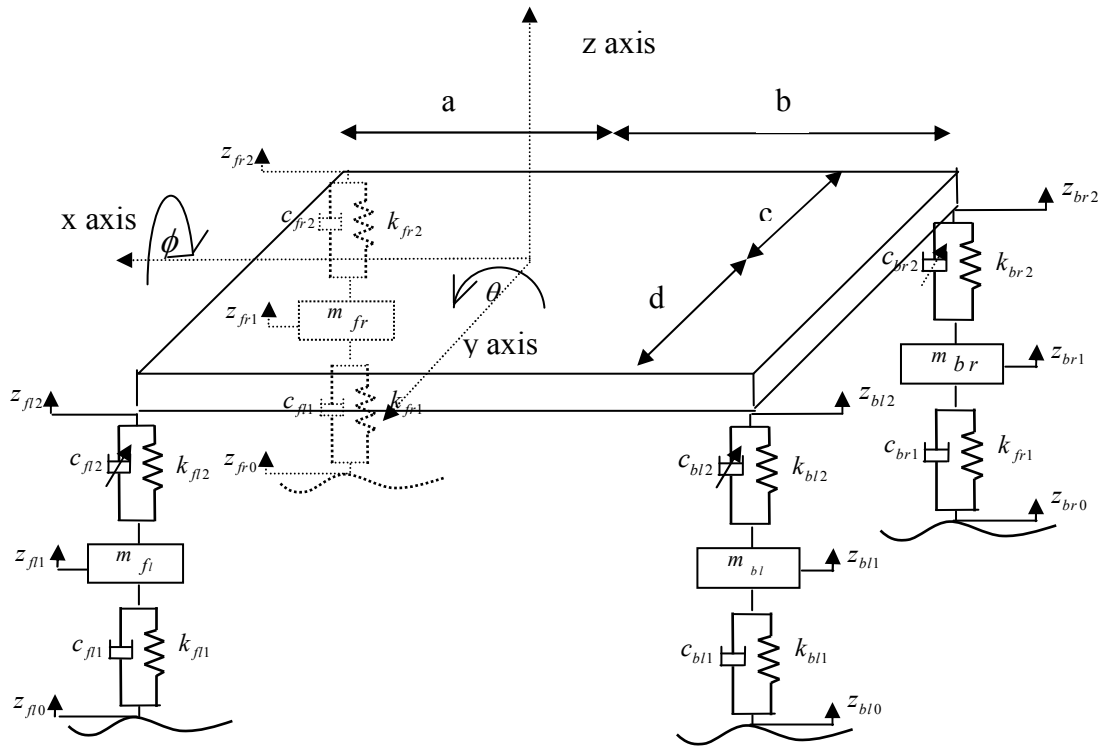


Figure 2.1 Full Car Ride Model

2.2 EQUATIONS OF MOTION OF THE FULL-CAR RIDE MODEL

2.2.1 NONLINEAR EQUATIONS WITH PASSIVE SUSPENSIONS

In passive suspensions, damping coefficients are assumed to be constant.

The equations of motions are derived using small angle assumption. Force balances along the z-direction for each of the unsprung masses:

$$m_{fi} \ddot{z}_{fi1} = k_{fi1} z_{fi0} + c_{fi1} \dot{z}_{fi0} - (k_{fi1} + k_{fi2}) z_{fi1} - (c_{fi1} + c_{fi2}) \dot{z}_{fi1} + k_{fi2} z_{fi2} + c_{fi2} \dot{z}_{fi2} \quad (2.1)$$

$$m_{fr} \ddot{z}_{fr1} = k_{fr1} z_{fr0} + c_{fr1} \dot{z}_{fr0} - (k_{fr1} + k_{fr2}) z_{fr1} - (c_{fr1} + c_{fr2}) \dot{z}_{fr1} + k_{fr2} z_{fr2} + c_{fr2} \dot{z}_{fr2} \quad (2.2)$$

$$m_{bl} \ddot{z}_{bl1} = k_{bl1} z_{bl0} + c_{bl1} \dot{z}_{bl0} - (k_{bl1} + k_{bl2}) z_{bl1} - (c_{bl1} + c_{bl2}) \dot{z}_{bl1} + k_{bl2} z_{bl2} + c_{bl2} \dot{z}_{bl2} \quad (2.3)$$

$$m_{br} \ddot{z}_{br1} = k_{br1} z_{br0} + c_{br1} \dot{z}_{br0} - (k_{br1} + k_{br2}) z_{fr1} - (c_{br1} + c_{br2}) \dot{z}_{br1} + k_{br2} z_{br2} + c_{br2} \dot{z}_{br2} \quad (2.4)$$

Force balance along the z-direction for the sprung mass:

$$\begin{aligned} M \ddot{z}_{cg} = & k_{fl2} z_{fl1} + c_{fl2} \dot{z}_{fl1} - k_{fl2} z_{fl2} - c_{fl2} \dot{z}_{fl2} + k_{bl2} z_{bl1} + c_{bl2} \dot{z}_{bl1} - k_{bl2} z_{bl2} - c_{bl2} \dot{z}_{bl2} \\ & + k_{fr2} z_{fr1} + c_{fr2} \dot{z}_{fr1} - k_{fr2} z_{fr2} - c_{fr2} \dot{z}_{fr2} + k_{br2} z_{br1} + c_{br2} \dot{z}_{br1} - k_{br2} z_{br2} - c_{br2} \dot{z}_{br2} \end{aligned} \quad (2.5)$$

Torque balance around the x-axis of the vehicle:

$$\begin{aligned} I_{xx} \ddot{\phi} = & k_{fl2} z_{fl1} d \cos(\phi) + c_{fl2} \dot{z}_{fl1} d \cos(\phi) - k_{fl2} z_{fl2} d \cos(\phi) - c_{fl2} \dot{z}_{fl2} d \cos(\phi) \\ & + k_{bl2} z_{bl1} d \cos(\phi) + c_{bl2} \dot{z}_{bl1} d \cos(\phi) - k_{bl2} z_{bl2} d \cos(\phi) - c_{bl2} \dot{z}_{bl2} d \cos(\phi) \\ & - k_{fr2} z_{fr1} c \cos(\phi) - c_{fr2} \dot{z}_{fr1} c \cos(\phi) + k_{fr2} z_{fr2} c \cos(\phi) + c_{fr2} \dot{z}_{fr2} c \cos(\phi) \\ & - k_{br2} z_{br1} c \cos(\phi) - c_{br2} \dot{z}_{br1} c \cos(\phi) + k_{br2} z_{br2} c \cos(\phi) + c_{br2} \dot{z}_{br2} c \cos(\phi) \end{aligned} \quad (2.6)$$

Torque balance around the y-axis of the sprung mass:

$$\begin{aligned} I_{yy} \ddot{\theta} = & -k_{fl2} z_{fl1} a \cos(\theta) - c_{fl2} \dot{z}_{fl1} a \cos(\theta) + k_{fl2} z_{fl2} a \cos(\theta) + c_{fl2} \dot{z}_{fl2} a \cos(\theta) \\ & + k_{bl2} z_{bl1} b \cos(\theta) + c_{bl2} \dot{z}_{bl1} b \cos(\theta) - k_{bl2} z_{bl2} b \cos(\theta) - c_{bl2} \dot{z}_{bl2} b \cos(\theta) \\ & - k_{fr2} z_{fr1} a \cos(\theta) - c_{fr2} \dot{z}_{fr1} a \cos(\theta) + k_{fr2} z_{fr2} a \cos(\theta) + c_{fr2} \dot{z}_{fr2} a \cos(\theta) \\ & + k_{br2} z_{br1} b \cos(\theta) + c_{br2} \dot{z}_{br1} b \cos(\theta) - k_{br2} z_{br2} b \cos(\theta) - c_{br2} \dot{z}_{br2} b \cos(\theta) \end{aligned} \quad (2.7)$$

The geometrical relations for suspension connection points to the sprung mass:

$$z_{fl2} = z_{cg} + d \sin(\phi) - a \sin(\theta) \quad (2.8)$$

$$z_{fr2} = z_{cg} - c \sin(\phi) - a \sin(\theta) \quad (2.9)$$

$$z_{bl2} = z_{cg} + d \sin(\phi) + b \sin(\theta) \quad (2.10)$$

$$z_{br2} = z_{cg} - c \sin(\phi) + b \sin(\theta) \quad (2.11)$$

$$\dot{z}_{fl2} = \dot{z}_{cg} + d \cos(\phi) \dot{\phi} - a \cos(\theta) \dot{\theta} \quad (2.12)$$

$$\dot{z}_{fr2} = \dot{z}_{cg} - c \cos(\phi) \dot{\phi} - a \cos(\theta) \dot{\theta} \quad (2.13)$$

$$\dot{z}_{bl2} = \dot{z}_{cg} + d \dot{\phi} \cos(\phi) + b \dot{\theta} \cos(\theta) \quad (2.14)$$

$$\dot{z}_{br2} = \dot{z}_{cg} - c \cos(\phi) \dot{\phi} + b \cos(\theta) \dot{\theta} \quad (2.15)$$

To obtain the linear equations for a passive suspension:

$$\cos(\theta) = 1; \cos(\phi) = 1; \sin(\theta) = \theta; \sin(\phi) = \phi \quad (2.16)$$

The geometrical relations become:

$$z_{fr2} = z_{cg} - c\phi - a\theta \quad (2.17)$$

$$z_{bl2} = z_{cg} + d\phi + b\theta \quad (2.18)$$

$$z_{br2} = z_{cg} - c\phi + b\theta \quad (2.19)$$

$$\dot{z}_{fl2} = \dot{z}_{cg} + d\dot{\phi}\dot{\phi} - a\dot{\theta}\dot{\theta} \quad (2.20)$$

$$\dot{z}_{fr2} = \dot{z}_{cg} - c\dot{\phi}\dot{\phi} - a\dot{\theta}\dot{\theta} \quad (2.21)$$

$$\dot{z}_{bl2} = \dot{z}_{cg} + d\dot{\phi}\dot{\phi} + b\dot{\theta}\dot{\theta} \quad (2.22)$$

$$\dot{z}_{br2} = \dot{z}_{cg} - c\dot{\phi}\dot{\phi} + b\dot{\theta}\dot{\theta} \quad (2.23)$$

2.2.2 STATE SPACE REPRESENTATION OF THE LINEAR PASSIVE SYSTEM

In the state space representation of the vehicle model with passive suspensions, all equations of motion should be put in the form,

$$\dot{x} = Ax + Cw \quad (2.24)$$

where w represents the road disturbances:

$$w^T = [w_1 \quad w_2 \quad w_3 \quad w_4 \quad w_5 \quad w_6 \quad w_7 \quad w_8]$$

$$w_1 = z_{fl0}; w_2 = z_{bl0}; w_3 = z_{fr0}; w_4 = z_{br0}; w_5 = \dot{z}_{bl0}; w_6 = \dot{z}_{bl0}; w_7 = \dot{z}_{bl0}; w_8 = \dot{z}_{bl0}$$

And x represents the state variables:

$$x^T = [x_1 \quad x_2 \quad x_3 \quad x_4 \quad x_5 \quad x_6 \quad x_7 \quad x_8 \quad x_9 \quad x_{10} \quad x_{11} \quad x_{12} \quad x_{13} \quad x_{14}]$$

$$x_1 = z_{fl1}; x_2 = z_{bl1}; x_3 = z_{fr1}; x_4 = z_{br1}; x_5 = z_{cg}; x_6 = \phi; x_7 = \theta$$

$$x_8 = \dot{z}_{fl1}; x_9 = \dot{z}_{bl1}; x_{10} = \dot{z}_{fr1}; x_{11} = \dot{z}_{br1}; x_{12} = \dot{z}_{cg}; x_{13} = \dot{\phi}; x_{14} = \dot{\theta}$$

Derivatives will have " " and second derivatives will have " " .

$$\begin{aligned} \dot{x}_8 &= 1/m_n k_{fl1} \cdot u_1 + 1/m_n c_{fl1} \cdot u_2 - 1/m_n (k_{fl1} + k_{fl2}) \cdot x_1 + 1/m_n k_{fl2} \cdot x_5 \\ &+ 1/m_n k_{fl2} \cdot d \cdot x_6 - 1/m_n k_{fl2} \cdot a \cdot x_7 - 1/m_n (c_{fl1} + c_{fl2}) \cdot x_8 \\ &+ 1/m_n c_{fl2} \cdot x_{12} + 1/m_n c_{fl2} \cdot d \cdot x_{13} - 1/m_n c_{fl2} \cdot a \cdot x_{14} \end{aligned} \quad (2.25)$$

$$\begin{aligned}
\dot{x}_9 = & 1/m_{bl}k_{bl1} \cdot u_3 + 1/m_{bl}c_{bl1} \cdot u_4 - 1/m_{bl}(k_{bl1} + k_{bl2}) \cdot x_2 + 1/m_{bl}k_{bl2} \cdot x_5 \\
& + 1/m_{bl}k_{bl2}d \cdot x_6 + 1/m_{bl}k_{bl2}b \cdot x_7 - 1/m_{bl}(c_{bl1} + c_{bl2}) \cdot x_9 + 1/m_{bl}c_{blr2} \cdot x_{12} \\
& + 1/m_{bl}c_{blr2}d \cdot x_{13} + 1/m_{bl}c_{blr2}b \cdot x_{14}
\end{aligned} \tag{2.26}$$

$$\begin{aligned}
\dot{x}_{10} = & 1/m_{fr}k_{fr1} \cdot u_5 + 1/m_{fr}c_{fr1} \cdot u_6 - 1/m_{fr}(k_{fr1} + k_{fr2}) \cdot x_3 + 1/m_{fr}k_{fr2} \cdot x_5 \\
& - 1/m_{fr}k_{fr2}c \cdot x_6 - 1/m_{fr}k_{fr2}a \cdot x_7 - 1/m_{fr}(c_{fr1} + c_{fr2}) \cdot x_{10} + 1/m_{fr}c_{fr2} \cdot x_{12} \\
& - 1/m_{fr}c_{fr2}c \cdot x_{13} - 1/m_{fr}c_{fr2}a \cdot x_{14}
\end{aligned} \tag{2.27}$$

$$\begin{aligned}
\dot{x}_{11} = & 1/m_{br}k_{br1} \cdot u_7 + 1/m_{br}c_{br1} \cdot u_8 - 1/m_{br}(k_{br1} + k_{br2}) \cdot x_4 + 1/m_{br}k_{br2} \cdot x_5 \\
& - 1/m_{br}k_{br2}c \cdot x_6 + 1/m_{br}k_{br2}b \cdot x_7 - 1/m_{br}(c_{br1} + c_{br2}) \cdot x_{11} + 1/m_{br}c_{br2} \cdot x_{12} \\
& - 1/m_{br}c_{br2}c \cdot x_{13} + 1/m_{br}c_{br2}b \cdot x_{14}
\end{aligned} \tag{2.28}$$

$$\begin{aligned}
\dot{x}_{12} = & +1/Mk_{fl2} \cdot x_1 + 1/Mk_{bl2} \cdot x_2 + 1/Mk_{fr2} \cdot x_3 + 1/Mk_{br2} \cdot x_4 \\
& + 1/M(-k_{fl2} - k_{bl2} - k_{fr2} - k_{br2}) \cdot x_5 \\
& + 1/M(-k_{fl2}d - k_{bl2}d + k_{fr2}c + k_{br2}c) \cdot x_6 \\
& + 1/M(+k_{fl2}a - k_{bl2}b + k_{fr2}a - k_{br2}b) \cdot x_7 + 1/M \cdot c_{fl2} \cdot x_8 + 1/M \cdot c_{bl2} \cdot x_9 \\
& + 1/Mc_{fr2} \cdot x_{10} + 1/Mc_{br2} \cdot x_{11} + 1/M(-c_{fl2} - c_{bl2} - c_{br2} - c_{br2}) \cdot x_{12} \\
& + 1/M(-c_{fl2}d - c_{bl2}d + c_{fr2}c + c_{br2}c) \cdot x_{13} \\
& + 1/M(c_{fl2}a - c_{bl2}b + c_{fr2}a - c_{br2}b) \cdot x_{14}
\end{aligned} \tag{2.29}$$

$$\begin{aligned}
\dot{x}_{13} = & -1/I_{yy}k_{fl2}a \cdot x_1 + 1/I_{yy}k_{bl2}b \cdot x_2 - 1/I_{yy}k_{fr2}a \cdot x_3 + 1/I_{yy}k_{br2}b \cdot x_4 \\
& + 1/I_{yy}(k_{fl2}a - k_{bl2}b + k_{fr2}a - k_{br2}b) \cdot x_5 \\
& + 1/I_{yy} \cdot (k_{fl2}ad - k_{bl2}bd - k_{fr2}ac + k_{br2}bc) \cdot x_6 \\
& + 1/I_{yy}(-k_{fl2}a^2 - k_{bl2}b^2 - k_{fr2}a^2 - k_{br2}b^2) \cdot x_7 - 1/I_{yy}c_{fl2}a \cdot x_8 \\
& + 1/I_{yy}c_{bl2}b \cdot x_9 - 1/I_{yy}c_{fr2}a \cdot x_{10} + 1/I_{yy}c_{br2}b \cdot x_{11} \\
& + 1/I_{yy}(c_{fl2}a - c_{bl2}b + c_{fr2}a - c_{br2}b) \cdot x_{12} \\
& + 1/I_{yy}(c_{fl2}ad - c_{bl2}bd - c_{fr2}ac + c_{br2}bc) \cdot x_{13} \\
& + 1/I_{yy}(-c_{fl2}a^2 - c_{bl2}b^2 - c_{fr2}a^2 - c_{br2}b^2) \cdot x_{14}
\end{aligned} \tag{2.30}$$

$$\begin{aligned}
\dot{x}_{14} = & +1/I_{xx}k_{fl2}d \cdot x_1 + 1/I_{xx}k_{bl2}d \cdot x_2 - 1/I_{xx}k_{fr2}c \cdot x_3 - 1/I_{xx}k_{br2}c \cdot x_4 \\
& + 1/I_{xx}(-k_{fl2}d - k_{bl2}d + k_{fr2}c + k_{br2}c) \cdot x_5 \\
& + 1/I_{xx}(-k_{fl2}d^2 - k_{bl2}d^2 - k_{fr2}c^2 - k_{br2}c^2) \cdot x_6 \\
& + 1/I_{xx}(+k_{fl2}da - k_{bl2}db - k_{fr2}ca + k_{br2}cb) \cdot x_7 \\
& + 1/I_{xx}c_{fl2}d \cdot x_8 + 1/I_{xx}c_{bl2}d \cdot x_9 - 1/I_{xx}c_{fr2}c \cdot x_{10} \\
& - 1/I_{xx}c_{br2}c \cdot x_{11} + 1/I_{xx}(-c_{fl2}d - c_{bl2}d + c_{fr2}c + c_{br2}c) \cdot x_{12} \\
& + 1/I_{xx}(-c_{fl2}d^2 - c_{bl2}d^2 - c_{fr2}c^2 - c_{br2}c^2) \cdot x_{13} \\
& + 1/I_{xx}(+c_{fl2}da - c_{bl2}db - c_{fr2}ca + c_{br2}cb) \cdot x_{14}
\end{aligned} \tag{2.31}$$

2.2.3 EQUATIONS OF MOTION IN STATE SPACE FORM

$$A = [A_{11} \quad A_{12} \quad A_{13} \quad A_{14} \quad A_{15}]$$

$$A_{11} = \begin{bmatrix} 0 & 0 & 0 & 0 \\ 0 & 0 & 0 & 0 \\ 0 & 0 & 0 & 0 \\ 0 & 0 & 0 & 0 \\ 0 & 0 & 0 & 0 \\ 0 & 0 & 0 & 0 \\ 0 & 0 & 0 & 0 \\ -(k_{f11} + k_{f12}) / m_f & 0 & 0 & 0 \\ 0 & -(k_{b11} + k_{b12}) / m_{bl} & 0 & 0 \\ 0 & 0 & -(k_{f11} + k_{f12}) / m_{fr} & 0 \\ 0 & 0 & 0 & -\frac{(k_{br1} + k_{br2})}{m_{br}} \\ k_{f12} / M & k_{b12} / M & k_{f12} / M & k_{br2} / M \\ -k_{f12}a / I_{yy} & k_{b12}b / I_{yy} & -k_{f12}a / I_{yy} & k_{br2}b / I_{yy} \\ k_{f12}d / I_{xx} & k_{b12}d / I_{xx} & -k_{f12}c / I_{xx} & -k_{br2}c / I_{xx} \end{bmatrix} \quad (2.32)$$

$$A_{12} = \begin{bmatrix} 0 & 0 \\ 0 & 0 \\ 0 & 0 \\ 0 & 0 \\ 0 & 0 \\ 0 & 0 \\ 0 & 0 \\ 1 / m_f k_{f12} & 1 / m_f k_{f12} d \\ 1 / m_{bl} k_{b12} & 1 / m_{bl} k_{b12} d \\ 1 / m_{fr} k_{f12} & -1 / m_{fr} k_{f12} c \\ +1 / m_{br} k_{br2} & -1 / m_{br} k_{br2} c \\ -(k_{f12} + k_{b12} + k_{f12} + k_{br2}) / M & (-k_{f12}d - k_{b12}d + k_{f12}c + k_{br2}c) / M \\ (k_{f12}a - k_{b12}b + k_{f12}a - k_{br2}b) / I_{yy} & (k_{f12}ad - k_{b12}bd - k_{f12}ac + k_{br2}bc) / I_{yy} \\ (-k_{f12}d - k_{b12}d + k_{f12}c + k_{br2}c) / I_{xx} & (-k_{f12}d^2 - k_{b12}d^2 - k_{f12}c^2 - k_{br2}c^2) / I_{xx} \end{bmatrix} \quad (2.33)$$

$$A_{13} = \begin{bmatrix}
0 & 0 & 1 & 0 \\
0 & 0 & 0 & 1 \\
0 & 0 & 0 & 0 \\
0 & 0 & 0 & 0 \\
0 & 0 & 0 & 0 \\
0 & 0 & 0 & 0 \\
0 & 0 & 0 & 0 \\
-1/m_{fl}k_{fl2}a & -\frac{(c_{fl1} + c_{fl2})}{m_{fl}} & 0 \\
1/m_{bl}k_{bl2}b & 0 & -\frac{(c_{bl1} + c_{bl2})}{m_{bl}} \\
-1/m_{fr}k_{fr2}a & 0 & 0 \\
+1/m_{br}k_{br2}b & 0 & 0 \\
1/M \cdot (+k_{fl2}a - k_{bl2}b + k_{fr2}a - k_{br2}b) & c_{fl2}/M & c_{bl2}/M \\
(-k_{fl2}a^2 - k_{bl2}b^2 - k_{fr2}a^2 - k_{br2}b^2)/I_{yy} & -c_{fl2}a/I_{yy} & bc_{bl2}/I_{yy} \\
(+k_{fl2}da - k_{bl2}db - k_{fr2}ca + k_{br2}cb)/I_{xx} & c_{fl2}d/I_{xx} & c_{bl2}d/I_{xx}
\end{bmatrix} \quad (2.34)$$

$$A_{14} = \begin{bmatrix}
0 & 0 & 0 \\
0 & 0 & 0 \\
1 & 0 & 0 \\
0 & 1 & 0 \\
0 & 0 & 1 \\
0 & 0 & 0 \\
0 & 0 & 0 \\
0 & 0 & 0 \\
0 & 0 & c_{fl2}/m_{fl} \\
0 & 0 & c_{bl2}/m_{fl} \\
-(c_{bl1} + c_{bl2})/m_{bl} & 0 & c_{fr2}/m_{fl} \\
0 & -(c_{br1} + c_{br2})/m_{br} & c_{br2}/m_{fl} \\
c_{fl2}/M & c_{br2}/M & -(c_{fl2} + c_{bl2} + c_{bl2} + c_{br2})/M \\
-ac_{fr2}/I_{yy} & bc_{br2}/I_{yy} & (-bc_{br2} + ac_{fr2} - bc_{bl2} + ac_{fl2})/I_{yy} \\
-c_{fr2}c/I_{xx} & -c_{br2}c/I_{xx} & (-c_{bl2}d - c_{fl2}d + c_{br2}c + c_{fr2}c)/I_{xx}
\end{bmatrix} \quad (2.35)$$

$$A_{15} = \begin{bmatrix} 0 & 0 \\ 0 & 0 \\ 0 & 0 \\ 0 & 0 \\ 0 & 0 \\ 1 & 0 \\ 0 & 1 \\ \frac{c_{fl2}d}{m_{fl}} & -\frac{c_{fl2}a}{m_{fl}} \\ \frac{c_{bl2}d}{m_{fl}} & \frac{c_{bl2}b}{m_{fl}} \\ -\frac{c_{fr2}c}{m_{fl}} & -\frac{c_{fr2}a}{m_{fl}} \\ -\frac{c_{br2}c}{m_{fl}} & \frac{c_{br2}b}{m_{fl}} \\ \frac{(-c_{bl2}d - c_{fl2}d + c_{br2}c + c_{fr2}c)}{M} & \frac{(-bc_{br2} + ac_{fr2} - bc_{bl2} + ac_{fl2})}{M} \\ \frac{(-ac_{fl2}d + ac_{fr2}c - bc_{br2}c + bc_{bl2}d)}{I_{yy}} & \frac{-(a^2c_{fr2} + a^2c_{fl2} + b^2c_{br2} + b^2c_{bl2})}{I_{yy}} \\ \frac{-(c_{fr2}c^2 + c_{br2}c^2 + c_{fl2}d^2 + c_{bl2}d^2)}{I_{xx}} & \frac{-(-ac_{fl2}d + ac_{fr2}c - bc_{br2}c + bc_{bl2}d)}{I_{xx}} \end{bmatrix} \quad (2.36)$$

$$C = [C_{11} \quad C_{12}]$$

$$C_{11} = \begin{bmatrix} 0 & 0 & 0 & 0 \\ 0 & 0 & 0 & 0 \\ 0 & 0 & 0 & 0 \\ 0 & 0 & 0 & 0 \\ 0 & 0 & 0 & 0 \\ 0 & 0 & 0 & 0 \\ 1/m_{fl}k_{fl} & 0 & 0 & 0 \\ 0 & 1/m_{bl}k_{bl} & 0 & 0 \\ 0 & 0 & 1/m_{fr}k_{fr} & 0 \\ 0 & 0 & 0 & 1/m_{br}k_{br} \\ 0 & 0 & 0 & 0 \\ 0 & 0 & 0 & 0 \\ 0 & 0 & 0 & 0 \\ 0 & 0 & 0 & 0 \end{bmatrix} \quad (2.37)$$

$$C_{12} = \begin{bmatrix} 0 & 0 & 0 & 0 \\ 0 & 0 & 0 & 0 \\ 0 & 0 & 0 & 0 \\ 0 & 0 & 0 & 0 \\ 0 & 0 & 0 & 0 \\ 0 & 0 & 0 & 0 \\ 0 & 0 & 0 & 0 \\ 1/m_{fl}c_{fl} & 0 & 0 & 0 \\ 0 & 1/m_{bl}c_{bl} & 0 & 0 \\ 0 & 0 & 1/m_{fr}c_{fr} & 0 \\ 0 & 0 & 0 & 1/m_{br}c_{br} \\ 0 & 0 & 0 & 0 \\ 0 & 0 & 0 & 0 \\ 0 & 0 & 0 & 0 \\ 0 & 0 & 0 & 0 \end{bmatrix} \quad (2.38)$$

2.2.4 STATE SPACE REPRESENTATION OF THE LINEAR SEMI-ACTIVE SYSTEM

The state space representation of a semi-active suspension is different than passive suspension since the damping coefficients are variable. To overcome this difficulty a state space representation of the form described below will be used.

$$\dot{x} = Ax + Bw + Cu \quad (2.39)$$

The state variables and the disturbances are defined in the same manner like in section 2.2.3 where u represents the semi-active damping forces in the system:

$$u^T = \left[F_{\text{damperfl}} \quad F_{\text{damperbl}} \quad F_{\text{damperfr}} \quad F_{\text{damperbr}} \right] \text{ (See list of symbols)}$$

The equations become:

$$\begin{aligned} \dot{x}_8 = & 1/m_{\text{fl}}k_{\text{fl}0} \cdot u_1 + 1/m_{\text{fl}}c_{\text{fl}1} \cdot u_5 - 1/m_{\text{fl}}(k_{\text{fl}1} + k_{\text{fl}2}) \cdot x_1 + 1/m_{\text{fl}}k_{\text{fl}2} \cdot x_5 \\ & + 1/m_{\text{fl}}k_{\text{fl}2}d \cdot x_6 - 1/m_{\text{fl}}k_{\text{fl}2}a \cdot x_7 - 1/m_{\text{fl}}c_{\text{fl}1} \cdot x_8 + 1/m_{\text{fl}} \cdot F_{\text{damperfl}} \end{aligned} \quad (2.40)$$

$$\begin{aligned} \dot{x}_9 = & 1/m_{\text{bl}}k_{\text{bl}1} \cdot u_2 + 1/m_{\text{bl}}c_{\text{bl}1} \cdot u_6 - 1/m_{\text{bl}}(k_{\text{bl}1} + k_{\text{bl}2}) \cdot x_2 + 1/m_{\text{bl}}k_{\text{bl}2} \cdot x_5 \\ & + 1/m_{\text{bl}}k_{\text{bl}2}d \cdot x_6 + 1/m_{\text{bl}}k_{\text{bl}2}b \cdot x_7 - 1/m_{\text{bl}}c_{\text{bl}1} \cdot x_9 + 1/m_{\text{bl}} \cdot F_{\text{damperbl}} \end{aligned} \quad (2.41)$$

$$\begin{aligned} \dot{x}_{10} = & 1/m_{\text{fr}}k_{\text{fr}1} \cdot u_3 + 1/m_{\text{fr}}c_{\text{fr}1} \cdot u_7 - 1/m_{\text{fr}}(k_{\text{fr}1} + k_{\text{fr}2}) \cdot x_3 + 1/m_{\text{fr}}k_{\text{fr}2} \cdot x_5 \\ & - 1/m_{\text{fr}}k_{\text{fr}2}c \cdot x_6 - 1/m_{\text{fr}}k_{\text{fr}2}a \cdot x_7 - 1/m_{\text{fr}}c_{\text{fr}1} \cdot x_{10} + 1/m_{\text{fr}} \cdot F_{\text{damperfr}} \end{aligned} \quad (2.42)$$

$$\begin{aligned} \dot{x}_{10} = & 1/m_{\text{fr}}k_{\text{fr}1} \cdot u_3 + 1/m_{\text{fr}}c_{\text{fr}1} \cdot u_7 - 1/m_{\text{fr}}(k_{\text{fr}1} + k_{\text{fr}2}) \cdot x_3 + 1/m_{\text{fr}}k_{\text{fr}2} \cdot x_5 \\ & - 1/m_{\text{fr}}k_{\text{fr}2}c \cdot x_6 - 1/m_{\text{fr}}k_{\text{fr}2}a \cdot x_7 - 1/m_{\text{fr}}c_{\text{fr}1} \cdot x_{10} + 1/m_{\text{fr}} \cdot F_{\text{damperfr}} \end{aligned} \quad (2.43)$$

$$\begin{aligned} \dot{x}_{11} = & 1/m_{\text{br}}k_{\text{br}1} \cdot u_4 + 1/m_{\text{br}}c_{\text{br}1} \cdot u_8 - 1/m_{\text{br}}(k_{\text{br}1} + k_{\text{br}2}) \cdot x_4 + 1/m_{\text{br}}k_{\text{br}2} \cdot x_5 \\ & - 1/m_{\text{br}}k_{\text{br}2}c \cdot x_6 + 1/m_{\text{br}}k_{\text{br}2}b \cdot x_7 - 1/m_{\text{br}}c_{\text{br}1} \cdot x_{11} + 1/m_{\text{br}} \cdot F_{\text{damperbr}} \end{aligned} \quad (2.44)$$

$$\begin{aligned} \dot{x}_{12} = & +1/Mk_{\text{fl}2} \cdot x_1 + 1/Mk_{\text{bl}2} \cdot x_2 + 1/Mk_{\text{fr}2} \cdot x_3 + 1/Mk_{\text{br}2} \cdot x_4 \\ & + 1/M(-k_{\text{fl}2} - k_{\text{bl}2} - k_{\text{fr}2} - k_{\text{br}2}) \cdot x_5 \\ & + 1/M(-k_{\text{fl}2}d - k_{\text{bl}2}d + k_{\text{fr}2}c + k_{\text{br}2}c) \cdot x_6 \\ & + 1/M(+k_{\text{fl}2}a - k_{\text{bl}2}b + k_{\text{fr}2}a - k_{\text{br}2}b) \cdot x_7 - 1/M \cdot F_{\text{damperfl}} \\ & - 1/M \cdot F_{\text{damperbl}} - 1/M \cdot F_{\text{damperfr}} - 1/M \cdot F_{\text{damperbr}} \end{aligned} \quad (2.45)$$

$$\begin{aligned}
\dot{x}_{13} = & -1/I_{yy}k_{fl2}a \cdot x_1 + 1/I_{yy}k_{bl2}b \cdot x_2 - 1/I_{yy}k_{fr2}a \cdot x_3 \\
& + 1/I_{yy}k_{br2}b \cdot x_4 + 1/I_{yy}(k_{fl2}a - k_{bl2}b + k_{fr2}a - k_{br2}b) \cdot x_5 \\
& + 1/I_{yy}(k_{fl2}ad - k_{bl2}bd - k_{fr2}ac + k_{br2}bc) \cdot x_6 \\
& + 1/I_{yy}(-k_{fl2}a^2 - k_{bl2}b^2 - k_{fr2}a^2 - k_{br2}b^2) \cdot x_7 \\
& - 1/I_{yy}a \cdot F_{damperfl} - 1/I_{yy}a \cdot F_{damperfr} + 1/I_{yy}b \cdot F_{damperbl} + 1/I_{yy}b \cdot F_{damperbr}
\end{aligned} \tag{2.46}$$

$$\begin{aligned}
\dot{x}_{14} = & +1/I_{xx}k_{fl2}d \cdot x_1 + 1/I_{xx}k_{bl2}d \cdot x_2 - 1/I_{xx}k_{fr2}c \cdot x_3 - 1/I_{xx}k_{br2}c \cdot x_4 \\
& + 1/I_{xx}(-k_{fl2}d - k_{bl2}d + k_{fr2}c + k_{br2}c) \cdot x_5 \\
& + 1/I_{xx}(-k_{fl2}d^2 - k_{bl2}d^2 - k_{fr2}c^2 - k_{br2}c^2) \cdot x_6 \\
& + 1/I_{xx}(+k_{fl2}da - k_{bl2}db - k_{fr2}ca + k_{br2}cb) \cdot x_7 \\
& + 1/I_{xx}c_{fl2}d \cdot x_8 + 1/I_{xx}d \cdot F_{damperfl} - 1/I_{xx}c \cdot F_{damperfr} + 1/I_{xx}d \cdot F_{damperbl} \\
& - 1/I_{xx}c \cdot F_{damperbr}
\end{aligned} \tag{2.47}$$

where

$F_{damperfl}$ =semi-active damping force from front left damper

$F_{damperfr}$ =semi-active damping force from front right damper

$F_{damperbl}$ =semi-active damping force from back left damper

$F_{damperbr}$ =semi-active damping force from back right damper

$$A = [A_{11} \quad A_{12} \quad A_{13}]$$

$$\mathbf{A}_{11} = \begin{bmatrix}
0 & 0 & 0 & 0 \\
0 & 0 & 0 & 0 \\
0 & 0 & 0 & 0 \\
0 & 0 & 0 & 0 \\
0 & 0 & 0 & 0 \\
0 & 0 & 0 & 0 \\
0 & 0 & 0 & 0 \\
-(k_{f11} + k_{f12}) / m_f & 0 & 0 & 0 \\
0 & -(k_{b11} + k_{b12}) / m_{bl} & 0 & 0 \\
0 & 0 & -\frac{(k_{fr1} + k_{fr2})}{m_{fr}} & 0 \\
0 & 0 & 0 & -\frac{(k_{br1} + k_{br2})}{m_{br}} \\
1/M \cdot k_{f12} & k_{b12}/M & k_{fr2}/M & k_{br2}/M \\
-k_{f12}a/I_{yy} & k_{b12}b/I_{yy} & -k_{fr2}a/I_{yy} & k_{br2}b/I_{yy} \\
k_{f12}d/I_{xx} & k_{b12}d/I_{xx} & -k_{fr2}c/I_{xx} & -k_{br2}c/I_{xx}
\end{bmatrix} \quad (2.48)$$

$$\mathbf{A}_{12} = \begin{bmatrix}
0 & 0 \\
0 & 0 \\
0 & 0 \\
0 & 0 \\
0 & 0 \\
0 & 0 \\
0 & 0 \\
1/m_f k_{f12} & 1/m_f k_{f12}d \\
1/m_{bl} k_{b12} & 1/m_{bl} k_{b12}d \\
1/m_{fr} k_{fr2} & -1/m_{fr} k_{fr2}c \\
+1/m_{br} k_{br2} & -1/m_{br} k_{br2}c \\
\frac{-k_{f12} - k_{b12} - k_{fr2} - k_{br2}}{M} & \frac{-k_{f12}d - k_{b12}d + k_{fr2}c + k_{br2}c}{M} \\
\frac{(k_{f12}a - k_{b12}b + k_{fr2}a - k_{br2}b)}{I_{yy}} & \frac{(k_{f12}ad - k_{b12}bd - k_{fr2}ac + k_{br2}bc)}{I_{yy}} \\
\frac{(-k_{f12}d - k_{b12}d + k_{fr2}c + k_{br2}c)}{I_{xx}} & \frac{(-k_{f12}d^2 - k_{b12}d^2 - k_{fr2}c^2 - k_{br2}c^2)}{I_{xx}}
\end{bmatrix} \quad (2.49)$$

$$A_{13} = \begin{bmatrix} 0 & 1 & 0 & 0 & 0 & 0 & 0 & 0 \\ 0 & 0 & 1 & 0 & 0 & 0 & 0 & 0 \\ 0 & 0 & 0 & 1 & 0 & 0 & 0 & 0 \\ 0 & 0 & 0 & 0 & 1 & 0 & 0 & 0 \\ 0 & 0 & 0 & 0 & 0 & 1 & 0 & 0 \\ 0 & 0 & 0 & 0 & 0 & 0 & 1 & 0 \\ 0 & 0 & 0 & 0 & 0 & 0 & 0 & 1 \\ -1/m_f k_{f2} a & 0 & 0 & 0 & 0 & 0 & 0 & 0 \\ 1/m_{bl} k_{bl2} b & 0 & 0 & 0 & 0 & 0 & 0 & 0 \\ -1/m_{fr} k_{fr2} a & 0 & 0 & 0 & 0 & 0 & 0 & 0 \\ +1/m_{br} k_{br2} b & 0 & 0 & 0 & 0 & 0 & 0 & 0 \\ 1/M(k_{f2} a - k_{bl2} b + k_{fr2} a - k_{br2} b) & 0 & 0 & 0 & 0 & 0 & 0 & 0 \\ \frac{(-k_{f2} a^2 - k_{bl2} b^2 - k_{fr2} a^2 - k_{br2} b^2)}{I_{yy}} & 0 & 0 & 0 & 0 & 0 & 0 & 0 \\ \frac{(k_{f2} da - k_{bl2} db - k_{fr2} ca + k_{br2} cb)}{I_{xx}} & 0 & 0 & 0 & 0 & 0 & 0 & 0 \end{bmatrix} \quad (2.50)$$

B matrix

$$B = \begin{bmatrix} 0 & 0 & 0 & 0 & 0 & 0 & 0 & 0 \\ 0 & 0 & 0 & 0 & 0 & 0 & 0 & 0 \\ 0 & 0 & 0 & 0 & 0 & 0 & 0 & 0 \\ 0 & 0 & 0 & 0 & 0 & 0 & 0 & 0 \\ 0 & 0 & 0 & 0 & 0 & 0 & 0 & 0 \\ 0 & 0 & 0 & 0 & 0 & 0 & 0 & 0 \\ 0 & 0 & 0 & 0 & 0 & 0 & 0 & 0 \\ 1/m_f k_{f1} & 0 & 0 & 0 & 0 & 0 & 0 & 0 \\ 0 & 1/m_{bl} k_{bl1} & 0 & 0 & 0 & 0 & 0 & 0 \\ 0 & 0 & 1/m_{fr} k_{fr1} & 0 & 0 & 0 & 0 & 0 \\ 0 & 0 & 0 & 1/m_{br} k_{br1} & 0 & 0 & 0 & 0 \\ 0 & 0 & 0 & 0 & 0 & 0 & 0 & 0 \\ 0 & 0 & 0 & 0 & 0 & 0 & 0 & 0 \\ 0 & 0 & 0 & 0 & 0 & 0 & 0 & 0 \end{bmatrix} \quad (2.51)$$

C Matrix

$$C = \begin{bmatrix} 0 & 0 & 0 & 0 \\ 0 & 0 & 0 & 0 \\ 0 & 0 & 0 & 0 \\ 0 & 0 & 0 & 0 \\ 0 & 0 & 0 & 0 \\ 0 & 0 & 0 & 0 \\ 0 & 0 & 0 & 0 \\ 1/m_{fl} & 0 & 0 & 0 \\ 0 & 1/m_{bl} & 0 & 0 \\ 0 & 0 & 1/m_{fr} & 0 \\ 0 & 0 & 0 & 1/m_{br} \\ -1/M & -1/M & -1/M & -1/M \\ -a/I_{yy} & b/I_{yy} & -a/I_{yy} & b/I_{yy} \\ d/I_{xx} & d/I_{xx} & -c/I_{xx} & -c/I_{xx} \end{bmatrix} \quad (2.52)$$

CHAPTER 3

SEMI-ACTIVE CONTROL STRATEGY

3.1 INTRODUCTION

The semi-active damping control concept is illustrated in Figure 3.1. The 7-dof vehicle model has four force inputs from MR dampers and four disturbance inputs from the road surface profile. The states of the seven degree of freedom model are assumed to be measured or estimated and then fed back to the controller. The controller determines required damper forces needed for a chosen control strategy. The MR dampers should then be actuated by proper currents that will generate the MR damping force inputs determined by the controller. After required currents are calculated, MR dampers are actuated by these. In this work, the currents to provide the desired damping forces are assumed to be correctly determined as long as the forces are in the feasible damping range.

The control strategy is chosen as Linear Quadratic Regulator (LQR) and it will be discussed in the next pages.

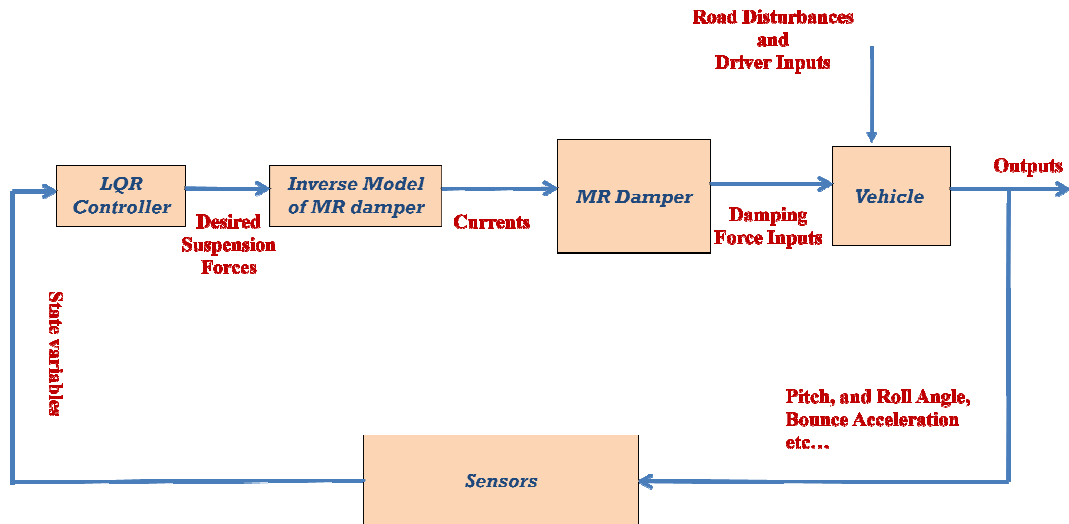


Figure 3.1 Semi-Active Damper Control Concept

3.2 SENSOR REQUIREMENTS

The selected LQR control strategy controls bounce, pitch and roll motions of the seven degrees of freedom vehicle model. Fourteen states, which are degrees of freedoms and related inputs (such bounce rate and bounce, roll rate and roll angle etc.) are needed to be fed back to the controller in order to determine the necessary damper input currents. Thus, four accelerometers for tires and an IMU (Inertial measuring unit) with one accelerometer and a three-axes gyroscope are needed. The four accelerometers should be mounted on wheel hubs to measure unsprung mass accelerations. The IMU and the accelerometer can be placed at the center of gravity of the vehicle to determine roll, and pitch rates (yaw axis is neglected) for easy computation. It can also be placed at other locations of the vehicle. For skyhook control, wire type linear displacement transducers (LDT) are also used to determine rattle space displacement changes (Choi, Han, Song, & Choi, 2007). The rattle space displacements can also be derived from the unsprung mass accelerometers, but for greater accuracy, LDTs are utilized. Following the measurement of these degrees of freedoms, necessary calculations such as integration are performed to obtain fourteen states which will be fed back.

3.3 MR MODELLING

In the simulations to be carried, Matlab/Simulink will be used so that the empirically obtained characteristics of MR dampers are simulated via lookup-tables which do not rely on parametric or nonparametric models. Since the interpolation will be carried between adjacent characteristics points, the characteristics are sampled as data points from the experimental plots of characteristics curves by the help of a data digitalization program. The sampling rate of the data points should be fine enough in order to provide good accuracy and enable feasible computational time simultaneously. One can set the interpolation linear or quadratic as a Matlab lookup-tables property. In the simulations throughout the thesis work, inverse modelling to find necessary current inputs to generate desired damping forces is not used. The limits of the damping forces at a specified relative velocity across suspension are used as the feasible damping range. However, in the implementation of the control system or to be used in hardware in the loop simulations, inverse modelling will be required. The necessary current input may then be determined by an Embedded M-file block whose code is given in APPENDIX A. The Simulink block used for calculating the current to generate desired damping force uses interpolation. This interpolation is made between data points at the same relative velocity but at different current levels to find the right input current for the required control input. The MR characteristics used is given at APPENDIX E. The MR damper characteristics used is selected considering the vehicle parameters in APPENDIX B and existing dampers in section 1.3.1.2 in the light of the selection guide in section 1.3.1.2.

3.4 OPTIMAL CONTROL/ LINEAR QUADRATIC REGULATOR CONTROL STRATEGY

In the case of full car ride model there are seven degrees of freedom which is affected by four inputs from the road surface. In the case of controlling more than one parameter as in the case of the scope of this thesis, developing a control strategy

is a tedious task. The control inputs should be chosen according to physical constraints in the controlled plant and the semi-active damper force limitations.

Optimal control gives a systematic approach to solving this problem to minimize chosen performance criterion (performance index or cost function) while the equations of motion of the vehicle are satisfied. However when the control force inputs are semi-active damper forces present in the vehicle, additional control algorithms should be added to optimal control to satisfy semi-active damper physical constraints. These additional control algorithms are discussed at 3.4.3.

3.4.1 A THEORETICAL LOOK INTO LINEAR QUADRATIC REGULATOR CONTROL STRATEGY

The linear quadratic regulator is an optimal control problem where the plant state equations are linear, the cost function is quadratic, and the test conditions consist of random initial conditions and random disturbance inputs (B.Burl, 1999). The linear, time invariant plant state equation is written as

$$\dot{x}(t) = Ax(t) + Bw(t) + Cu(t) \quad (3.1)$$

where x is the vector of states in the full ride vehicle model, u is the semi-active damping forces, and w is the random road disturbances.

In the quadratic cost function of the type (Sinha, 2007):

$$J = \int_0^{\infty} (x^T(t)Qx(t) + u^T(t)Ru(t) + 2x^T Nu(t))dt \quad (3.2)$$

where Q is a symmetric, a positive semi definite matrix and R is a symmetric positive definite matrix. N is also positive a definite matrix.

The solution of the optimal control becomes (Naidu, 2003):

$$u(t) = -R^{-1}(B^T S + N^T)x(t) \quad (3.3)$$

where S is the solution of Algebraic Riccati Equation

$$A^T S + X S - X S S^T X + Q = 0 \quad (3.4)$$

In the thesis the cost function is:

$$J = \int_0^{\infty} [\rho_1(\ddot{z}_{cg})^2 + \rho_2(\theta)^2 + \rho_3(\phi)^2 + \rho_4(F_{\text{damperfl}}^2 + F_{\text{damperfr}}^2 + F_{\text{damperbl}}^2 + F_{\text{damperbr}}^2)]dt \quad (3.5)$$

where $\rho_1, \rho_2, \rho_3, \rho_4$ are weighting constants determined by trial and error process. The constant ρ_4 applies to the damping force inputs from four separate MR dampers.

3.4.2 THE LIMITATIONS OF TIME-INVARIANT LINEAR QUADRATIC REGULATOR

The limitations of the time invariant LQR control strategy to be stable and have a solution are given in (Matlab R2007b -The Language of Technical Computing, n.d.) as follows:

- 1-The pair (A, C) should be stabilizable.
- 2- $R > 0$ and $Q - NR^{-1}N^T \geq 0$
- 3- $(Q - NR^{-1}N^T, A - CR^{-1}N^T)$ has no unobservable mode on the imaginary axis.

The first condition holds for the system matrices A and C derived in section 2.2.4 for the vehicle data specified in APPENDIX B. All the modes are stable. The other criterions are to be checked for different cost functions. In this work Matlab (Matlab R2007b -The Language of Technical Computing, n.d.) is used to determine full state feedback gain matrix (K) . After specifying weighting factors; Q, R, and N matrices are computed and fed to Matlab. The computation of a full state feedback matrix (K) solution is only possible when all these criterions are met.

3.4.3 FEASIBILITY OF LQR CONTROL INPUTS FOR SEMI-ACTIVE DAMPERS

The required damping forces determined by the controller are not always feasible since the forces do not lie in the admissible force region of the damper shown at Figure 3.2. The forces applicable at a certain relative velocity should be between the maximum force and the minimum force that can be attained by changing the current supplied.

If it were an ideal active system that has the capability to give right damping forces, the linear quadratic controller would work perfectly.

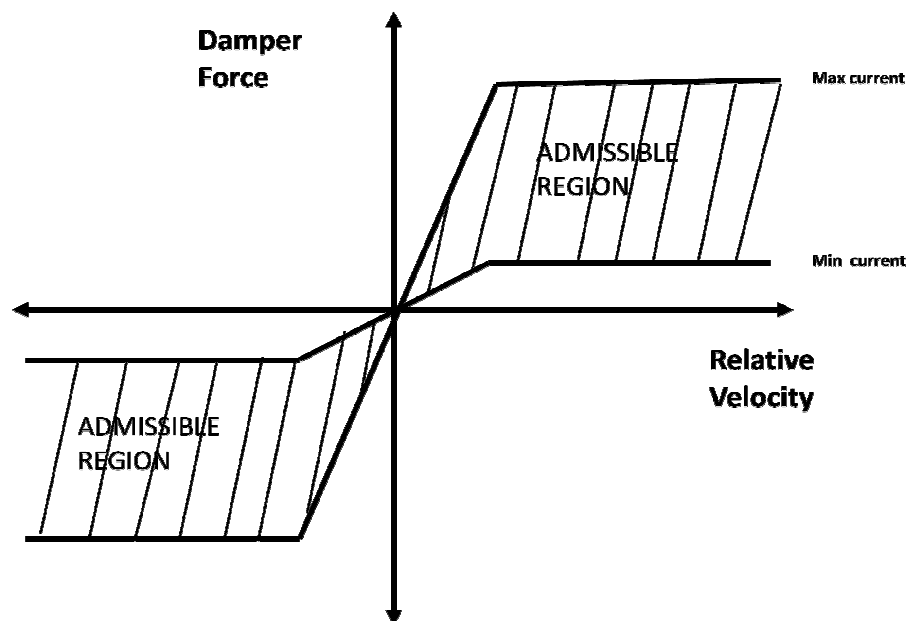


Figure 3.2 Admissible Damping Region of a Typical Semi-Active Damper

Possible approaches for this problem in feasibility of LQR inputs are discussed in the next section:

3.4.3.1 Constrained Optimal Control

The main constraint in LQR control for semi-active dampers is that the damping coefficient cannot be negative and cannot exceed some values. The work by (Butsuen, 1989) formulated a constrained optimal control problem for a full car ride model. He concluded that the difference in performance between clipped and constrained optimal control is negligible.

The constrained optimal control problem becomes very complicated to solve for full car ride models since it is a relatively complex model. The clipped optimal control will be discussed in the next section as a potential solution.

3.4.3.2 Clipped Optimal Control

Clipped optimal control makes sure that if the desired force from the controller is in the admissible region then it is applied by the MR dampers. If it is outside the region, the control input forces are clipped to give the closest damping force to the desired input as much as possible. The process is illustrated in Figure 3.3.

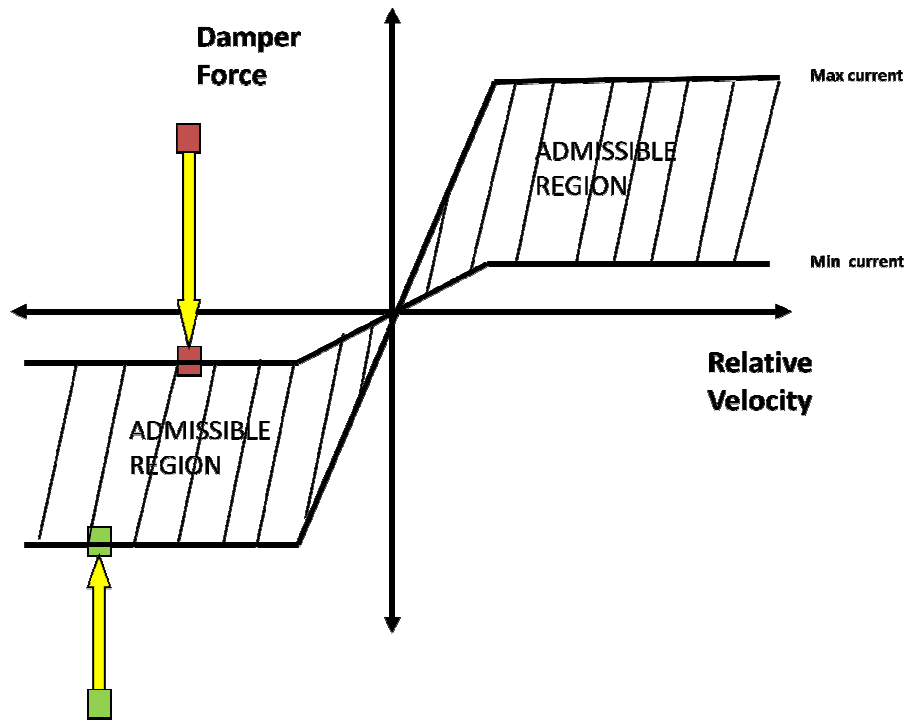


Figure 3.3 Process of Clipping Optimal Forces to Admissible Damping Region

First of all the set of weighting constants that will be used in the quadratic performance index given in equation 3.6 is chosen.

$$J = \int_0^{\infty} [\rho_1(\ddot{z}_{cg})^2 + \rho_2(\theta)^2 + \rho_3(\phi)^2 + \rho_4(F_{\text{damperfl}}^2 + F_{\text{damperfr}}^2 + F_{\text{damperbl}}^2 + F_{\text{damperbr}}^2)]dt \quad (3.6)$$

This cost function index with the weighting constants is equivalent to the expression

$$J = \int_0^{\infty} (x^T(t)Qx(t) + u^T(t)Ru(t) + 2x^T Nu(t))dt \quad (3.7)$$

Then the Q, R, and N matrices in the equivalent performance index are determined by considering the equations of motion of the seven degree of freedom vehicle model. The state space representation used in the cost function was determined at section 2.2.4. Afterwards the necessary states are collected and the full state feedback is computed by the LQR strategy while simulating the response of the vehicle to road inputs. The closest damping force lying in the admissible region to the required optimal force is determined and taken from the damper.

The weighting constants used in the cost function should be tuned. This tuning needs an iteration process on different road conditions. From the simulations based on specific road profiles, the weighting constants should be decided on user preference to give emphasis to which parameter to be minimized. The tuning process must begin with initial guesses. To make the initial guess properly, the response to an input of the vehicle model with passive suspension should be examined. The scalar values of the parameters in the performance index can be set proportionally by just examining the values. As an example, the vehicle whose data is given at APPENDIX B can be simulated over a road bump. From the results if one tries to minimize the bounce acceleration, pitch angle or roll angle at the same importance level, one can start with the weighting factor set of $\rho_1 = 10^8$; $\rho_2 = 10^4$; $\rho_3 = 10^4$; $\rho_4 = 1$

3.4.3.3 Optimal Gain Switching Control

The main methodology is proposed by (Giua, Seatzu, & Usai, 1999). As mentioned in the literature survey, Section 1.4, Optimal Gain Switching method gives a bounded target control force by switching between different feedback gains. There exists two phases for the design. The cost function used in this strategy is as follows:

$$\int_0^{\infty} (\rho x^T(t) Q_m x(t) + v^T(t) R v(t)) dt \quad (3.8)$$

In the first phase, the Q_m and R matrices are constants which are decided by intuition, $v(t)$ is the control input, and ρ is the controlled parameter to design a good active suspension control law that will later be mimicked by the semi-active suspension. When the system is far from the origin, low ρ should be used and when the system is close to the origin large ρ can be used in order to satisfy the constraint that the semi-active the magnitude of damping force cannot exceed a limit. This method also calculates the region of state space in which the control forces are bounded. The initial conditions that the system can have without violating the constraint are analyzed for every ρ and stored as data. In the simulation, the largest ρ that will cause the damping force satisfying the force magnitude constraint is chosen. Then the force is the target control force is approximated by controlling the damper coefficient.

The most complex part of this theory is calculating the initial conditions that will satisfy the force magnitude constraint. If the work were to be carried on quarter car model, the computing power would be adequate. However the computation difficulty for 7 degree of freedom full-car ride model is a very serious complication.

3.5 SKYHOOK, GROUNDHOOK CONTROL STRATEGY

These control strategies are simple but also effective in controlling the body bounce motion. They are based on quarter car models and are not specially designed to control pitch and roll motions. Skyhook control strategy is effective on reducing sprung mass bounce acceleration and groundhook control strategy is very effective at unsprung mass acceleration (Ahmadian M. P., 2000). Skyhook control strategy applies damping force proportional to sprung mass velocity whereas groundhook control strategy applies damping force proportional to unsprung mass velocity. Both of these try to give no damping force depending on the sign of the relative velocity of the damper ends, specified by the particular methodology described in equations 3.9-12. The notation used for the quarter car model can be seen in Figure 3.4. A combination of the skyhook and groundhook methods is also commonly used and called hybrid control. In hybrid control, damping forces computed by skyhook and groundhook controls are added in a proportion determined by the designer. Hybrid control is a compromise between two classical strategies in minimizing sprung and unsprung mass motions.

Skyhook control strategy is widely used in present applications. There are also constraints in the skyhook control strategy. As in the LQR optimal control the requested force is clipped towards the damper capability. For minimal damping force, no current is supplied to the damper. However it still provides some damping. If the requested damper force is larger than the maximum possible damping force, the maximum input current is supplied to the damper. If the force is between the limits, the requested force can be applied.

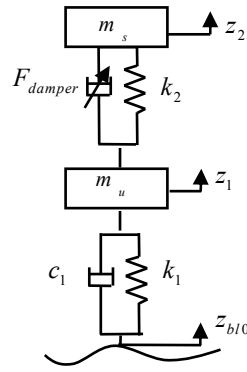


Figure 3.4 Quarter Car Model

Classical Skyhook Control Strategy:

$$\begin{aligned} F_{\text{damper}} &= G_s \dot{z}_2 \text{ if } \dot{z}_2 (\dot{z}_2 - \dot{z}_1) > 0 \\ F_{\text{damper}} &= 0 \text{ if } \dot{z}_2 (\dot{z}_2 - \dot{z}_1) \leq 0 \end{aligned} \quad (3.9)$$

Groundhook Control strategy:

$$\begin{aligned} F_{\text{damper}} &= G_g \dot{z}_1 \text{ if } \dot{z}_1 (\dot{z}_2 - \dot{z}_1) < 0 \\ F_{\text{damper}} &= 0 \text{ if } \dot{z}_1 (\dot{z}_2 - \dot{z}_1) \geq 0 \end{aligned} \quad (3.10)$$

Hybrid Control Strategy:

$$F_{\text{damper}} = \alpha \sigma_{\text{sky}} + (1 - \alpha) \sigma_{\text{groundhook}} \quad (3.11)$$

where

$$\begin{aligned} \sigma_{\text{skyhook}} &= G_s \dot{z}_2 \text{ if } \dot{z}_2 (\dot{z}_2 - \dot{z}_1) > 0 \\ \sigma_{\text{skyhook}} &= 0 \text{ if } \dot{z}_2 (\dot{z}_2 - \dot{z}_1) \leq 0 \\ \sigma_{\text{groundhook}} &= G_g \dot{z}_1 \text{ if } \dot{z}_1 (\dot{z}_2 - \dot{z}_1) < 0 \\ \sigma_{\text{groundhook}} &= 0 \text{ if } \dot{z}_1 (\dot{z}_2 - \dot{z}_1) \geq 0 \end{aligned} \quad (3.12)$$

CHAPTER 4

SIMULATION MODEL

4.1 SIMULINK MODEL

The simulation model and its graphical user interface are constructed using Matlab. In the Simulink model, nonlinear seven degree of freedom ride model is built. Its general structure is given in the Appendix A. The equations used to build the Simulink model have been given in chapter 2. The main difference of the model from a normal ride model is the additional embedded semi-active suspensions. The Simulink model should contain an MR damper model and the block sets to control the dampers independently. The MR damper models consist of lookup tables and the block sets to control the dampers. The control blocks are built for optimal control. In addition to optimal control blocks, the skyhook control blocks are also constructed for comparison purposes between skyhook and optimal control. These blocks are given at the next section.

4.2 OPTIMAL CONTROLLER BLOCKS

The optimal control blocks consist of products of the system states and the feedback gains computed before the simulations. The optimal control block of front left damper is illustrated in Figure 4.1

However the computed force for optimal control is not always feasible, so the block given in Figure 4.2 should also be embedded. If the requested damping force is outside the admissible damping region, the control input forces are redetermined to

give the closest damping force to the desired input as much as possible. If the desired force is between the bounds of the available damping forces, no modification is done.

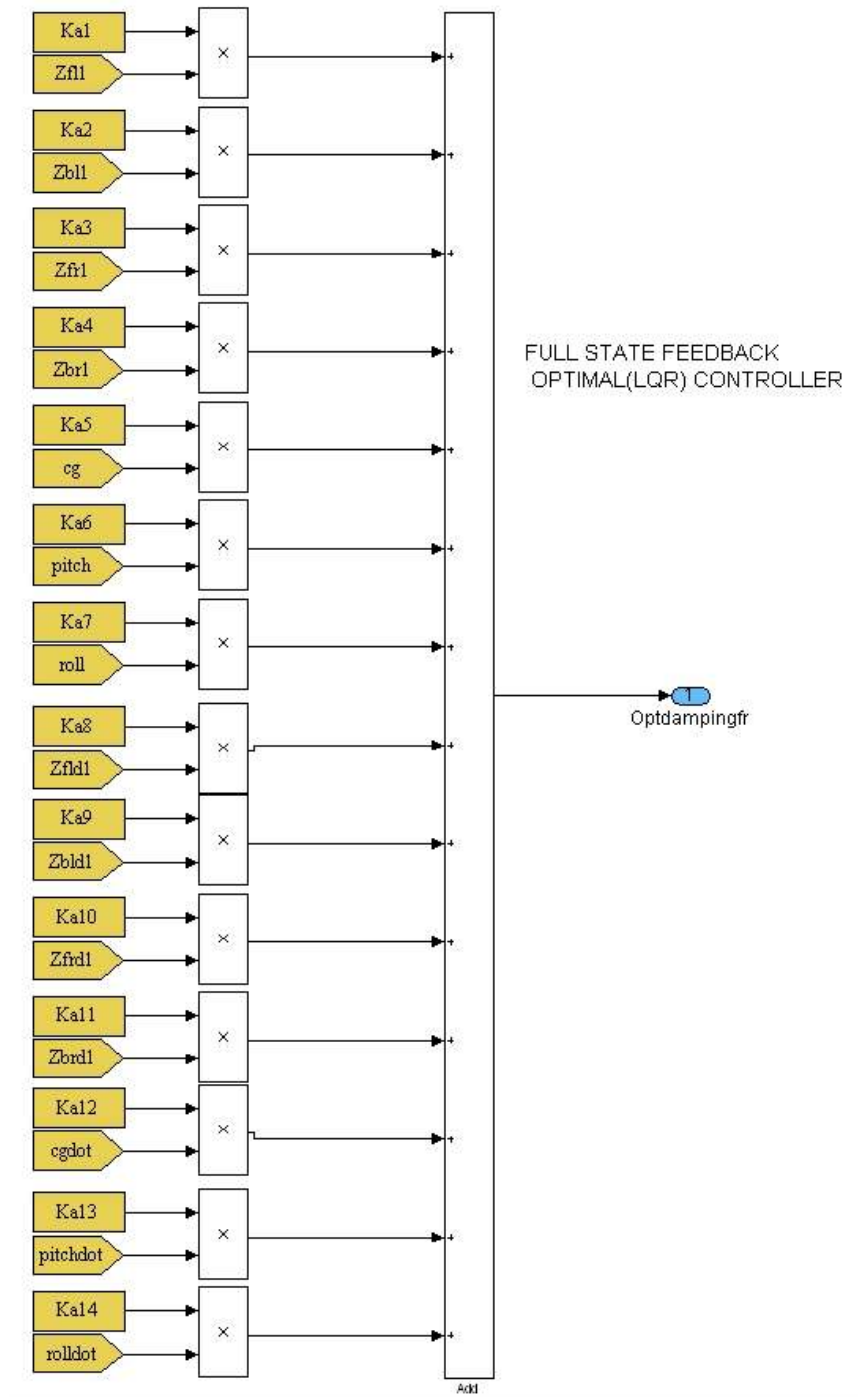


Figure 4.1 Full State Feedback Optimal Control Simulink Model

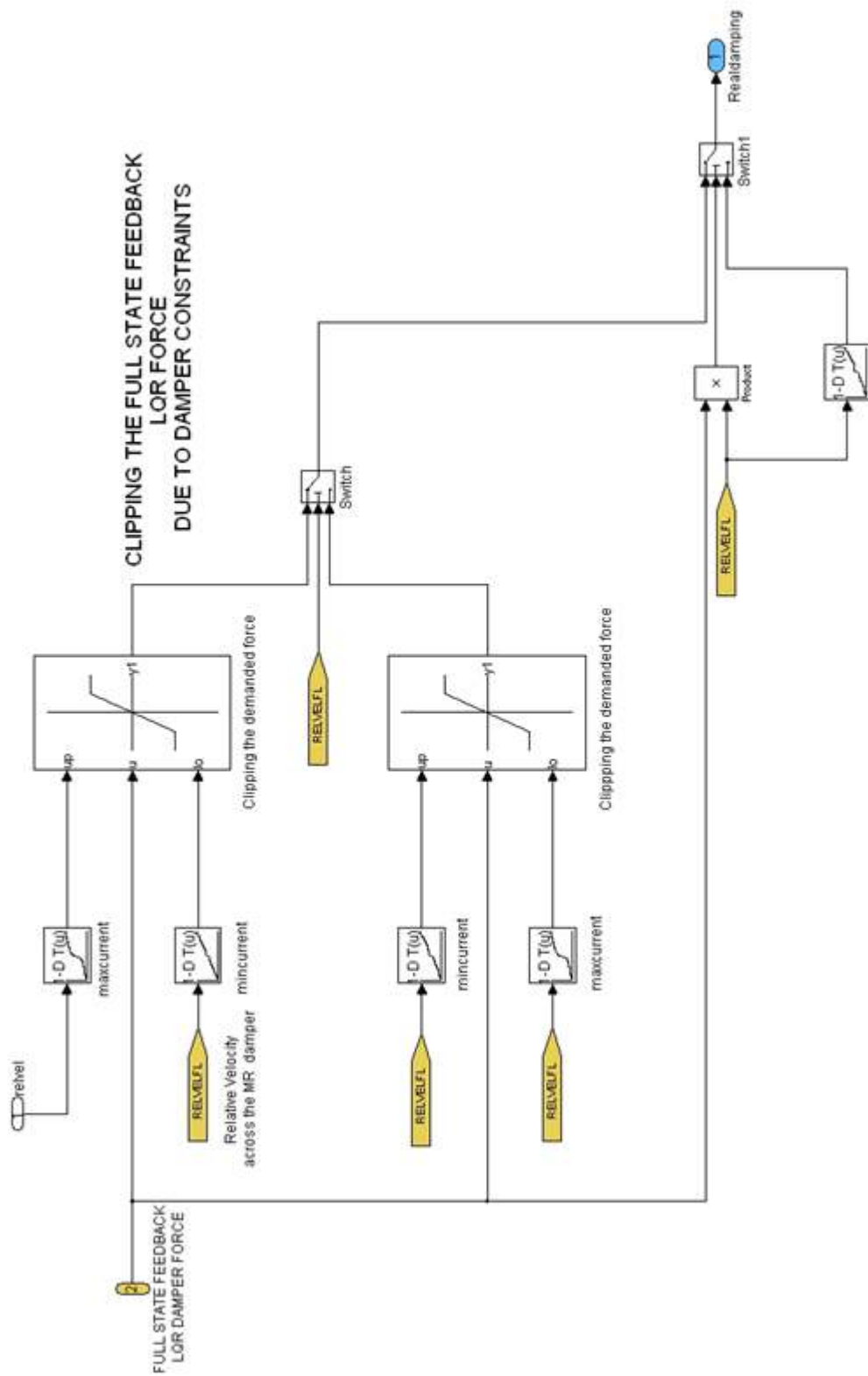


Figure 4.2 MR Modelling And Force Clipping Simulink Model

CHAPTER 5

OPTIMIZATION PROCESS

5.1 THEORETICAL BACKGROUND

5.1.1 TRANSMISSIBILITY ANALYSIS OF QUARTER CAR MODEL

Any control strategy of a semi-active damper is dependent on the characteristics of the vehicle. In this study, a quarter car model, given in Figure 5.1 is utilized in order to get in depth information about the controlled behaviours of suspensions, which will eventually be useful to understand the nature of bounce motion of the sprung mass, and the rattle space motion of the vehicle suspension. To control sprung and unsprung mass motions, semi-active suspensions are widely used. Semi-active dampers can provide both low and high damping ratios, of which the effects on responses of the vehicle vary due to road inputs frequency. The effects of the damping constants can be examined from the transmissibility plots of the quarter car model given Figure 5.2, Figure 5.3, Figure 5.4, Figure 5.5, and Figure 5.6. The transmissibility plots are also interpreted for different road input frequencies in this section.

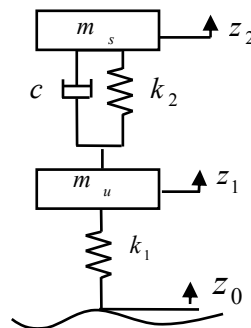


Figure 5.1 Quarter Car Model

Transmissibility of Sprung Mass Acceleration with respect to Road Input

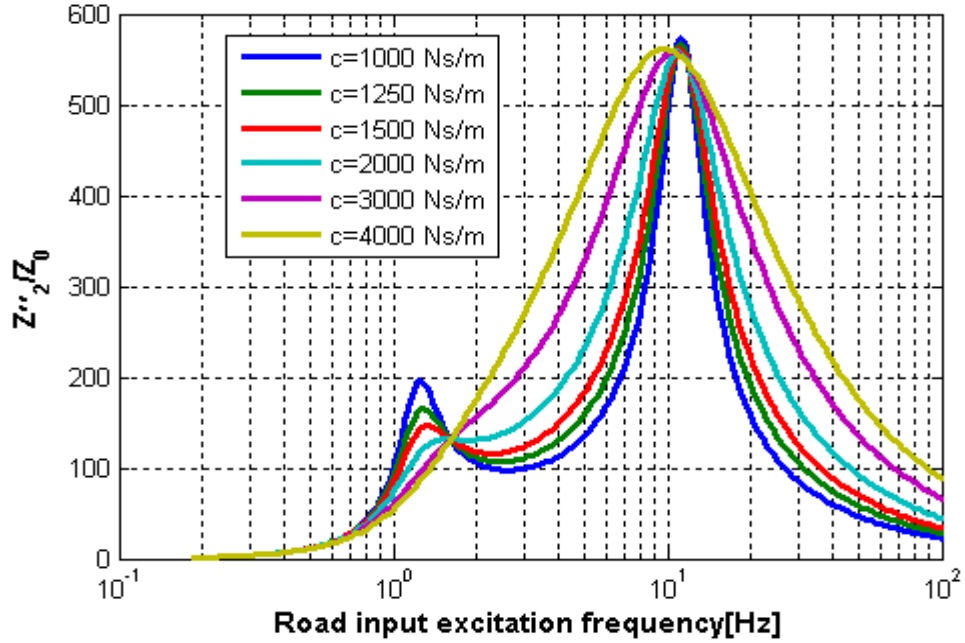


Figure 5.2 Transmissibility of Sprung Mass Acceleration with Respect to Road Input

Transmissibility of Sprung Mass Displacement with respect to Road Input

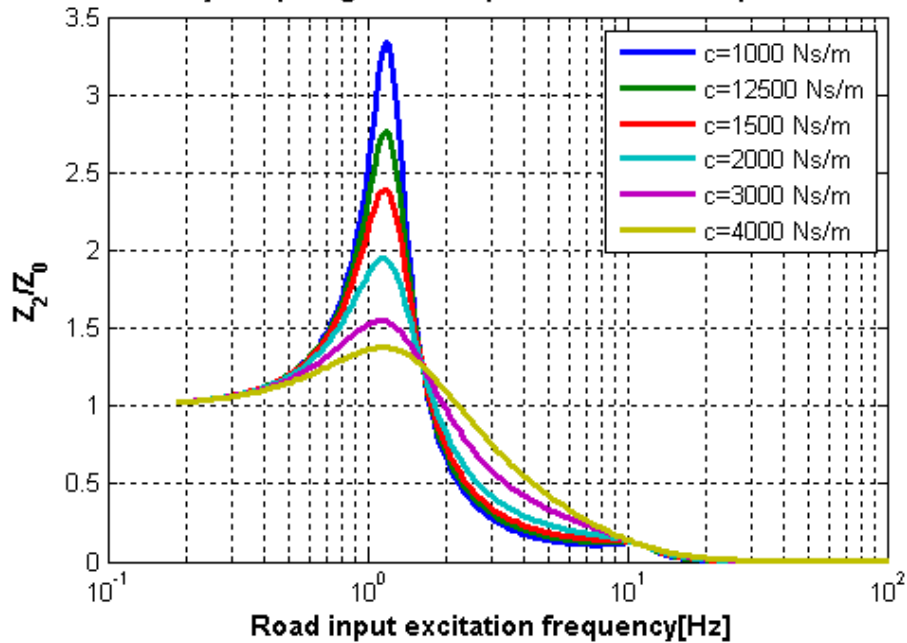


Figure 5.3 Transmissibility of Sprung Mass Displacement with Respect to Road

Input

The body bounce natural frequency of the quarter car model, which represents a typical passenger car with parameters given in APPENDIX B, is approximately 1.28 Hz whereas the wheel hop frequency is approximately 11.34 Hz. From the sprung mass acceleration transmissibility plot in Figure 5.2, it is seen that high damping coefficient selection is effective in the frequency range (0-1.6Hz), and at higher frequencies low damping coefficient selection is effective in minimizing bounce acceleration transmissibility. As expected, the same results are valid for bounce displacement transmissibility.

Rattle space motion (suspension displacement) is important since the suspension system has physical limits on the suspension stroke. In analyzing the transmissibility plot (Figure 5.4), it is seen that high damping coefficient selection is the best choice over all input frequencies.

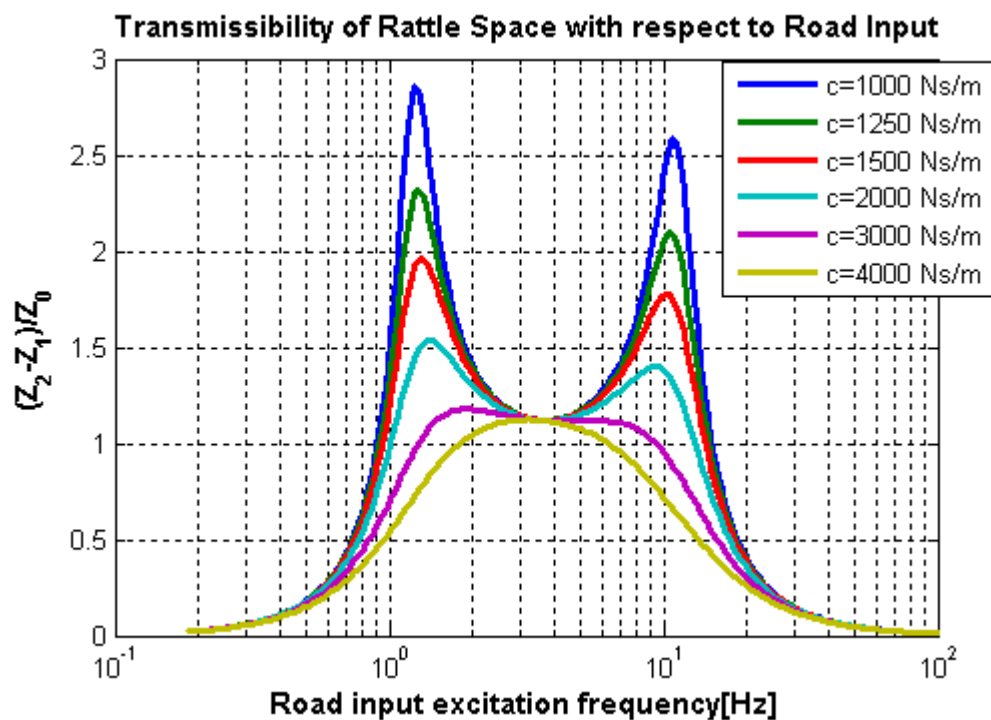
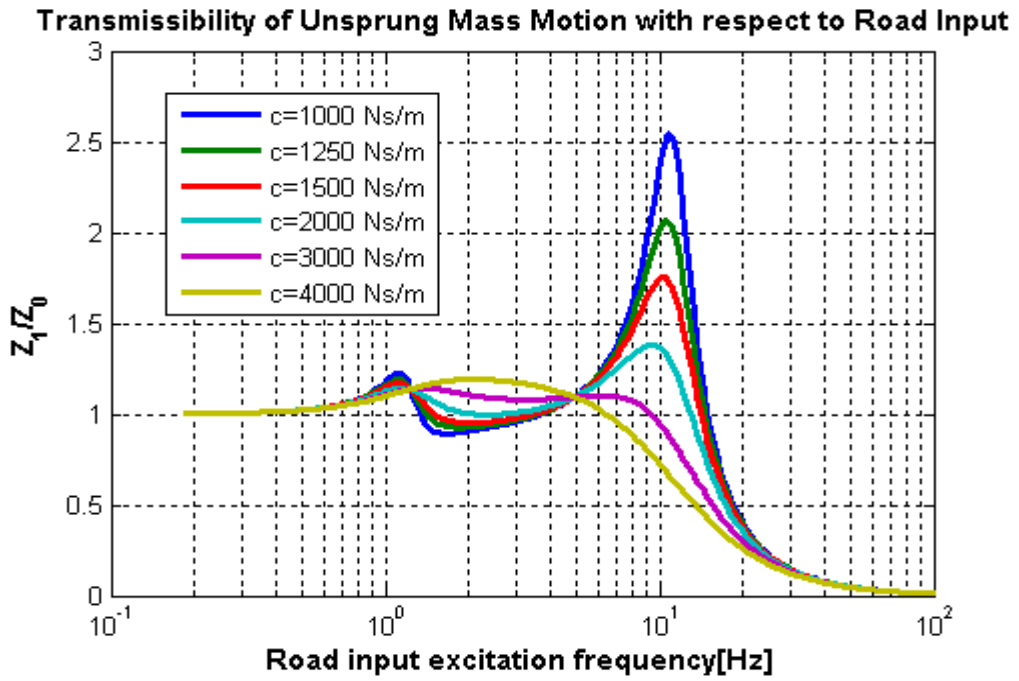
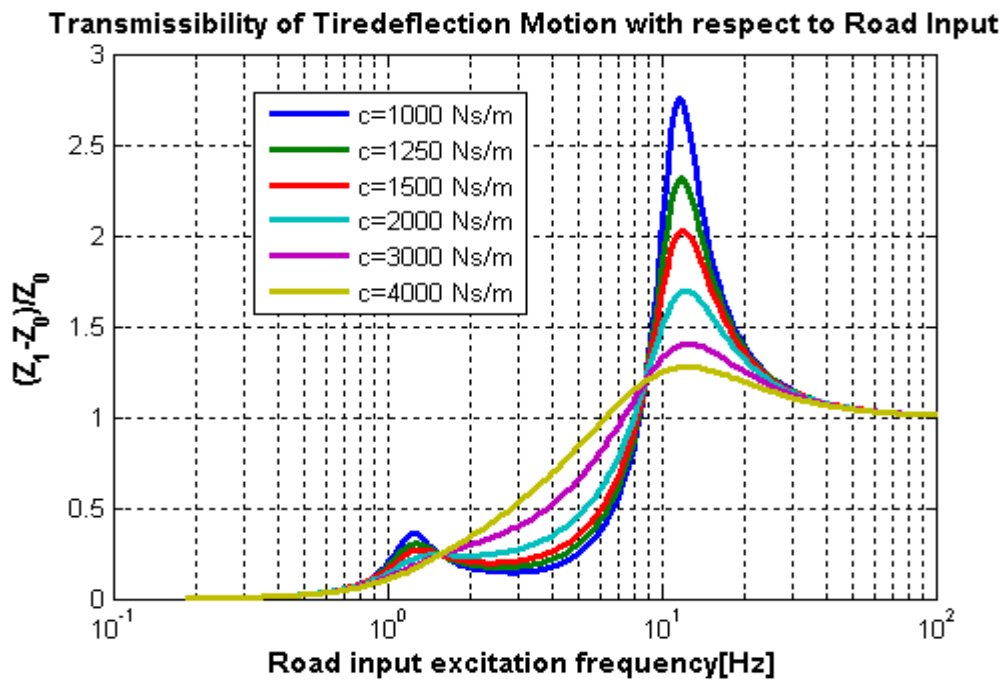


Figure 5.4 Transmissibility of Rattle Space with respect to Road Input



Input



Input

It is observed that the transmissibility plot of unsprung mass displacement in Figure 5.5 is mainly affected by the damping coefficient of the suspension damper at the wheel hop natural frequency. The unsprung mass motion together with tire deflection transmissibility (Figure 5.6) is of concern in relation to vehicle handling rather than ride comfort. On the other hand, excessive tire deflection may affect the vehicle performance drastically. As can be seen from both plots, higher damping coefficient selection is the best choice for isolation at frequencies greater than approximately 5 Hz and frequencies lower than 1.28 Hz. Selection of low damping coefficient proves to be useful for input frequencies between 1.28 Hz and 5 Hz.

To sum up the results, one can divide the frequency range in 3 sections roughly as:

Region 1 - up to nearby body bounce natural frequency (1.3 Hz)

Region 2 - between body bounce natural frequency and 4.5 Hz

Region 3 - beyond 4.5 Hz

In region 1, minimizing the body bounce motion, sprung mass motion and rattle space motion all together is only possible by choosing a damper with a high damping coefficient. In region 2, minimizing body bounce motion and sprung mass motion is best achieved by choosing a damper with a low damping coefficient. The rattle space motion in region 2 is not very sensitive to damping coefficient changes, so its optimization may be omitted to avoid unnecessary complexity.

In region 3, minimizing body bounce motion, sprung mass motion and rattle space motion simultaneously is not possible. Therefore, a trade-off between these optimization parameters should be made by the control algorithm designer. The importance level of these motion transmissibilities defined by the control algorithm designer, leads the choice between high and low damping coefficients. The main advantage of the semi-active dampers is their ability to provide low, medium, and high damping coefficients. It should be kept in mind that if in region 3 sprung mass acceleration is wanted to be minimized so low damping coefficient will be selected such that sprung mass and rattle space motion will be adversely affected. In case of

optimal control, if only bounce acceleration is chosen to be minimized, the damping constant is chosen as low as possible in region 3 such that the transmissibilities of rattle space and unsprung mass motion around wheel hop frequency increase. Naturally semi-active dampers can be controlled based on the feedback of velocity, and displacement measurements on vehicle states by supplying necessary current inputs to them. For minimizing bounce acceleration the semi-active control supplies maximum feasible current in the frequency regions 1 and 2. In region 3, the semi-active damper should supply zero current to provide the lowest damping possible like in the uncontrolled case where no current is supplied. Another drawback of lowering the damping in region 3 is the tendency of increasing oscillation magnitudes due to low damping. Although obtaining smaller bounce acceleration peak values, the RMS values have the affinity to increase.

The optimal dampers attempt to maintain the most convenient damping forces based on the states of the vehicle. Discussions about transmissibility plots are necessary to analyze the potentials of a control method. A suitable control law for a quarter car model can be defined as supplying maximum feasible current in the frequency region 1 and probably in region 2. In region 3, if only bounce acceleration is important, the semi-active damper should supply null current, in which case the results will be the same as those of uncontrolled case. Although low damping coefficients are desirable in the frequency region 3, low damping levels can cause the vehicle to have oscillations such that the settling time of the system is increased. If one has to compromise between different optimization parameters in region 3, the damper current should be regulated accordingly.

As a last statement, the study is carried on a quarter car model; however in the actual control model the pitch and roll angles are also controlled. The LQR control strategy will make the compromise between bounce acceleration, roll and pitch angle minimization. The damper current will take values between maximum and minimum current inputs possible to accomplish the compromise.

5.1.2 VIBRATION ANALYSIS OF FULL CAR RIDE MODEL

Quarter car model has the ease of transmissibility analysis since it is a single input single output (SISO) system. The natural frequencies of the full car model are obtained to justify the quarter car model and to gain insight information of the vehicle behaviour within the frequencies where roll and pitch motions are dominant. To carry out the frequency analysis, instead of the state space representation derived in chapter 2, equations of motion written in the form of equation 5.1 can be used. These matrices can be found at APPENDIX D. In equation 5.1, M is the mass matrix, C is the damping matrix, and K is the stiffness matrix.

$$[M]\{\ddot{x}\} + [C]\{\dot{x}\} + [K]\{x\} = 0 \quad (5.1)$$

$$\{x\}^T = [z_{fl} \quad z_{bl} \quad z_{fr} \quad z_{br} \quad z_{cg} \quad \theta \quad \phi]$$

Looking at the eigenvectors of the equation 5.2 where ω is the natural frequencies of each mode, the modes that the natural frequencies belong, can be identified. These natural frequencies found are given in Table 1.

$$[-M\omega^2 + K]\{x\} = 0 \quad (5.2)$$

Table 1 Natural Frequencies of Full Car Ride Model

Mode	Natural Frequency
Body bounce dominant mode	1.09 Hz
Pitch motion dominant mode	1.22 Hz
Roll motion dominant mode	1.39 Hz
Wheel hop dominant modes	11.29 Hz (front sprung masses)
	11.35 Hz(rear sprung masses)

5.2 OPTIMIZATION FOR OPTIMAL CONTROL USING BUMP INPUT

In this section, an optimization process is carried out in order to demonstrate the design procedure. A half sinusoidal bump with height of 3.5 cm and width of 1 m, which represent a typical high speed trap, will be used as the input for the optimization routine. The velocity of the vehicle will be varied from 5 kph to 90 kph to make the input frequencies dominantly cover the range of 0.7Hz-15Hz. This frequency range is selected since it covers the body bounce and wheel hop frequencies and the range of frequencies in which the human body is the most sensitive. The optimization for optimal control using bump input will be divided into five stages for deeper analysis of the nature of optimization. In each stage, optimization is carried out to investigate the best weighing factors at each vehicle speed, followed by the decision process of a constant weighing factor covering all velocities. RMS values and peak to peak motion amplitudes are plotted for each case at every velocity. The stages are namely:

Stage 1: Optimization with respect to only bounce weighting factor

Stage 2: Optimization with respect to only pitch weighting factor

Stage 3: Optimization with respect to bounce acceleration and pitch weighting factor

Stage 4: Optimization with respect to bounce acceleration, pitch, and roll motion weighting factor

The vehicle data is used in this section is taken from (Zuo & Nayfeh, 2003) . However to get comparable results between uncontrolled case and passive case in section 5.2.1, the damping constants used in simulations are modified. The front damping constant is taken as 964 N.s/m and the rear damping constant is taken as 876 N.s/m. MR damper characteristic used is given at APPENDIX E.

5.2.1 STAGE 1: OPTIMIZATION WITH RESPECT TO ONLY BOUNCE WEIGHTING FACTOR

At this stage, different bounce acceleration weighting factors are used for each vehicle velocity in the range of 5-90 km/h which corresponds approximately the frequency range of 0.7-15 Hz. In an iterative manner different bounce acceleration weighting factors (ρ_1) are substituted for different vehicle velocities whereas $\rho_2 = 0$, $\rho_3 = 0$, and $\rho_4 = 1$. Then the outputs of the system are sorted with respect to RMS values of the power of the bounce acceleration, the best factors that brings the bounce acceleration RMS values to a minimum for each velocity are obtained. A constant weighting factor is chosen in a way the system outputs do not differ highly from minimal outputs. In figures, the weighting factors are plotted. In Figure 5.7, the selected weighting factors are marked on the resulting plot. In Figure 5.8 and Figure 5.9, the RMS and peak to peak body bounce acceleration values for uncontrolled and controlled cases of semi-active suspensions and also for the passive suspensions are plotted. In the charts of Figure 5.8 and Figure 5.9, the time span used for calculating the RMS values is between the time the front wheels encounter the road input and the time the rear wheels encounter the road input. This time span is selected to focus on the bounce motion rather than on both pitch and bounce motions.

It is seen from Figure 5.7 and Figure 5.8 that the constant weighting factor selection does not affect the RMS values of bounce acceleration or peak-to-peak acceleration values. The improvement in outputs of the car model for semi-active suspensions to passive systems can be seen from the plots. Another important remark is that the control strategy is effective at low velocities which mean low road frequency inputs. The improvement is not clear at high frequencies. When investigated, it can also be seen in the quarter car transmissibility plot in Figure 5.2 that the suspension needs a higher damping ratio to reduce bounce acceleration transmissibility whereas it needs lowest damping ratio at high frequencies. For high frequency regions, the lowest damping coefficient means the uncontrolled case.

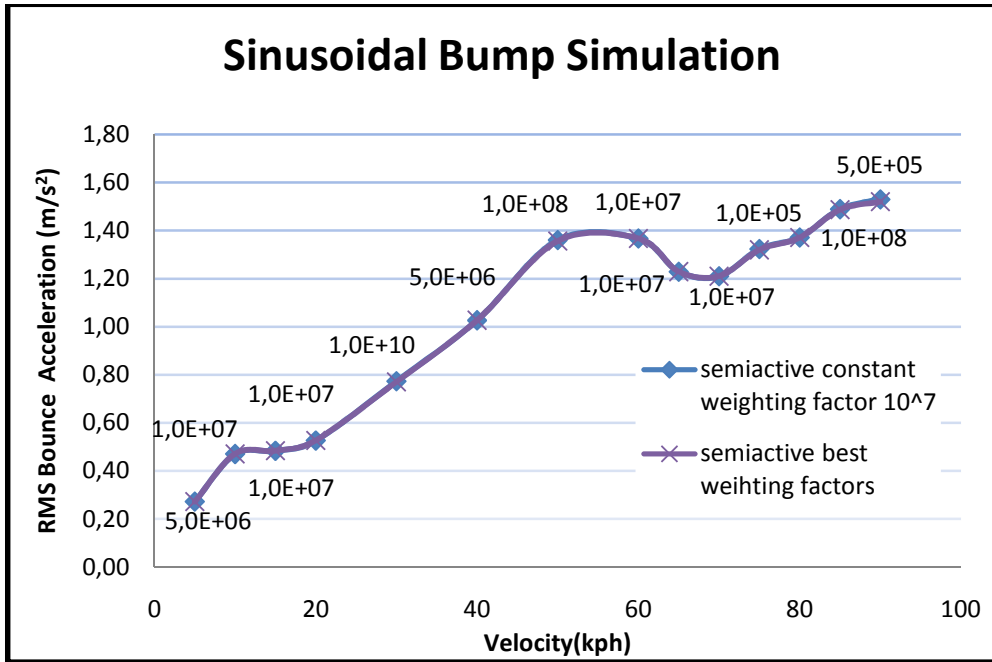


Figure 5.7 Weighting Constants for Sinusoidal Bump Body Bounce Acceleration Optimization

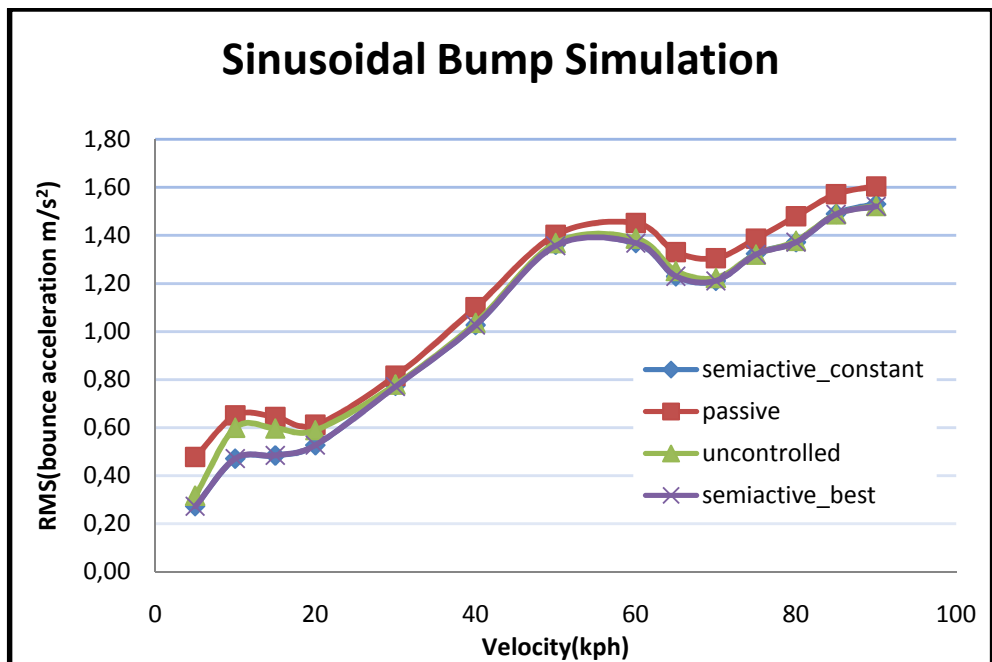


Figure 5.8 Bump Simulation Results (RMS Body Bounce Acceleration)

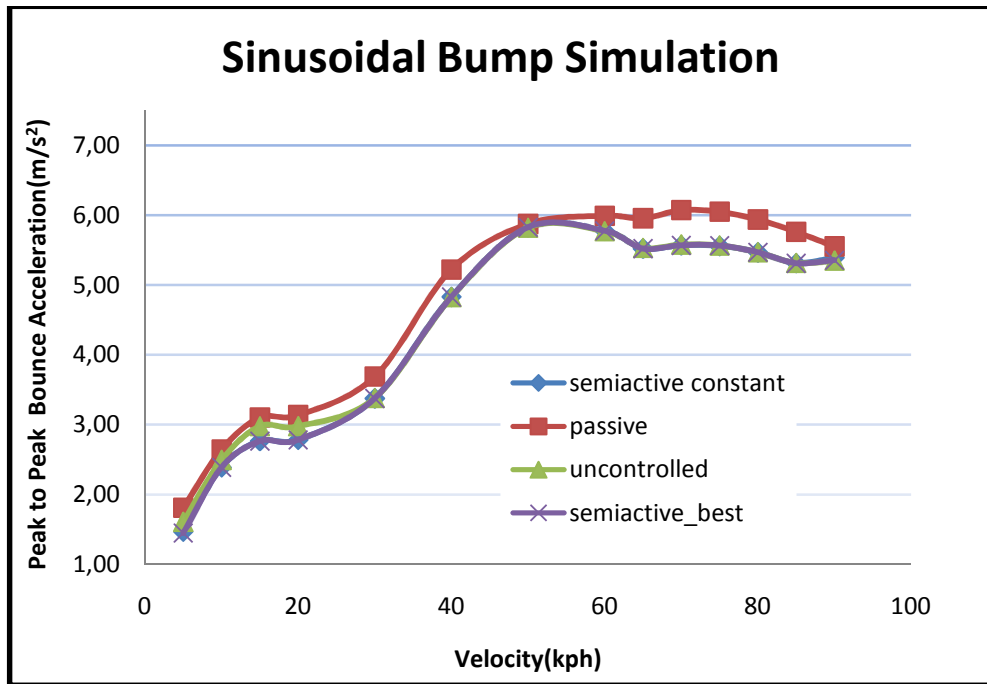


Figure 5.9 Sinusoidal Bump Simulation Results (Peak To Peak Body Bounce Acceleration)

5.2.2 STAGE 2: OPTIMIZATION WITH RESPECT TO ONLY PITCH WEIGHTING FACTOR

The optimization methodology is the same as in stage 1. Different pitch weighting factors are substituted for different vehicle velocities in an iterative manner. Then the outputs of the system are sorted with respect to RMS of the pitch motion, the best factors that result in the minimum RMS pitch angle values for each velocity are obtained. In Figure 5.10, these weighting factors found for different velocities are plotted. In Figure 5.11 and Figure 5.12, the peak-to-peak pitch angle values of semi-active suspensions and also for the passive suspensions are plotted for the uncontrolled and controlled cases.

The time span used in calculating RMS values is between the time the front wheels encounter the road input and two seconds after the rear wheels encounter the road input. This time span will also be used in section 5.2.3 and 5.2.4.

Figure 5.11 and Figure 5.12 illustrate the improvements in the outputs of the vehicle model with semi-active controlled suspensions as compared to the passive system and the case of uncontrolled.

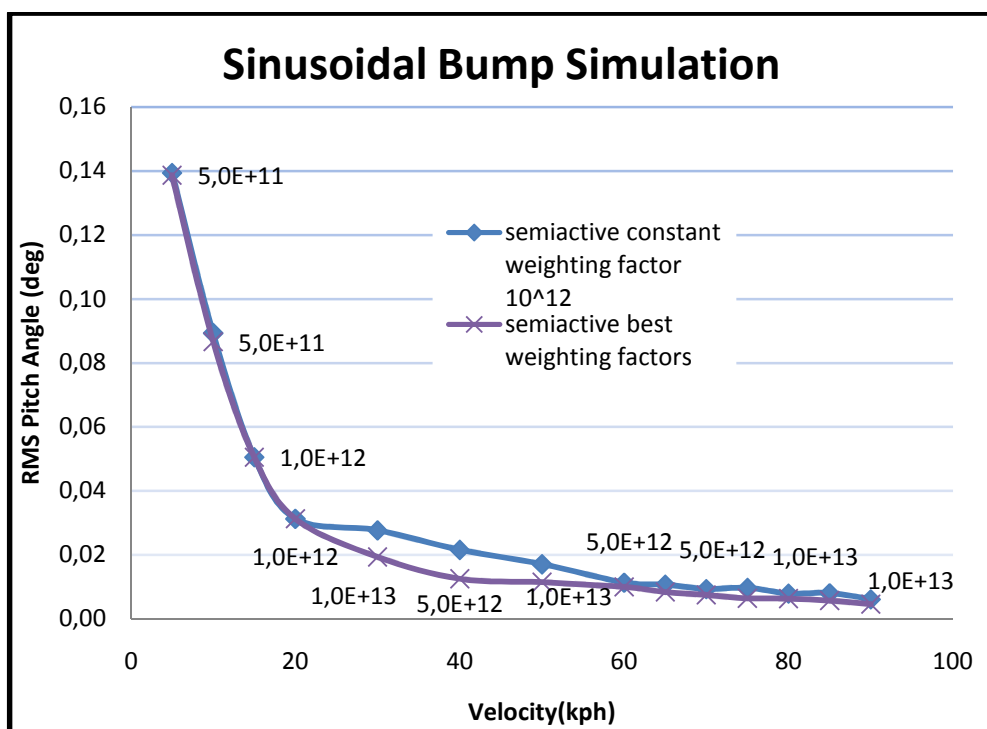


Figure 5.10 Weighting Constants for Sinusoidal Bump Pitch Angle Optimization

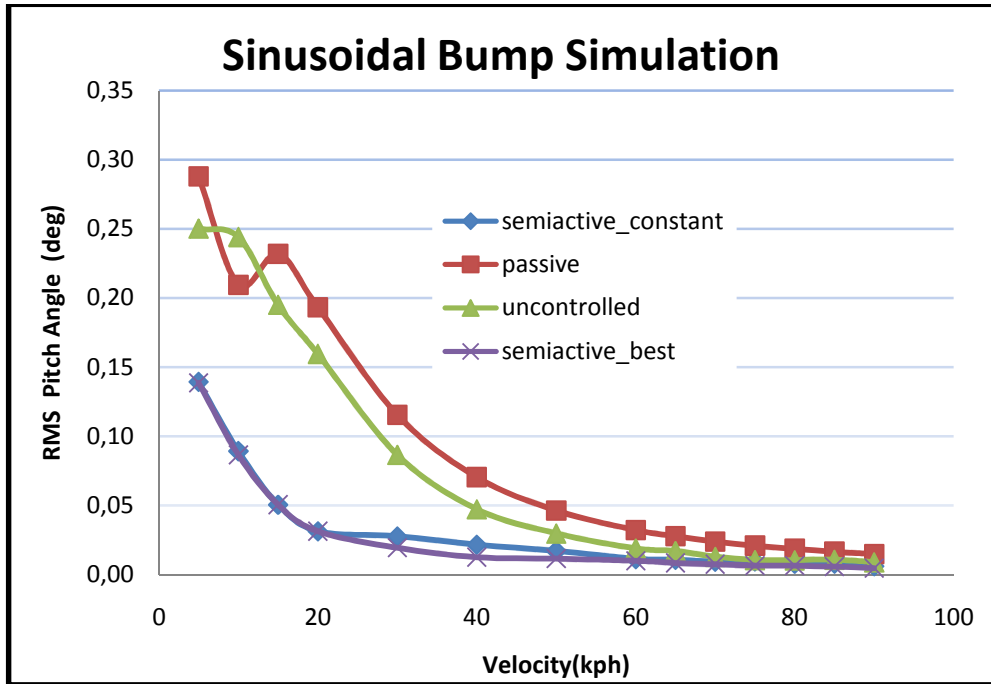


Figure 5.11 Sinusoidal Bump Simulation Results (RMS of Pitch Angle)

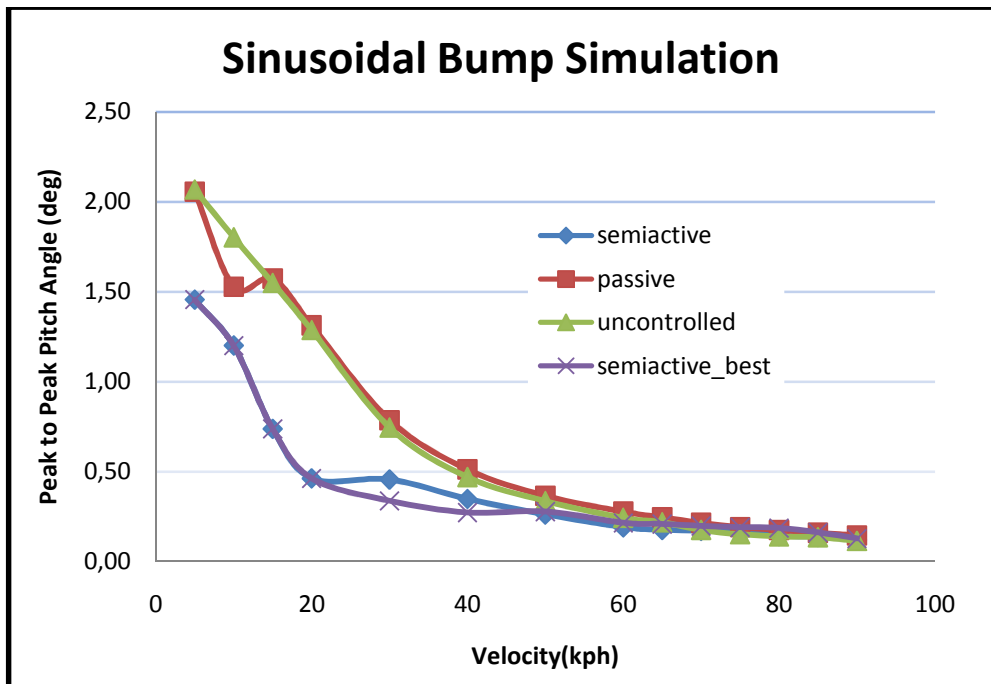


Figure 5.12 Sinusoidal Bump Simulation Results (Peak To Peak Pitch Angle)

5.2.3 STAGE 3: OPTIMIZATION WITH RESPECT TO BOUNCE ACCELERATION FACTOR AND PITCH WEIGHTING FACTOR

In this section, optimization to minimize both bounce acceleration and pitch angle are studied. In this section, optimization to minimize both bounce acceleration and pitch angle is 2D optimization which deals with two independent weighting factors. This procedure will be named as 2D bump optimization. Since the number of states to be minimized is increased, the complexity of optimization is also increased.

For the optimization process, the array of the bounce acceleration weighting factors is taken as:

$$\rho_1 = [10^6, 5 \cdot 10^6, 10^7, 5 \cdot 10^7, 10^8, 5 \cdot 10^8, 10^9, 5 \cdot 10^9, 10^{10}, 5 \cdot 10^{10}, 10^{11}, 5 \cdot 10^{11}]$$

The pitch angle weighting factor arrays is given as:

$$\rho_2 = [5 \cdot 10^8, 10^9, 5 \cdot 10^9, 10^{10}, 5 \cdot 10^{10}, 10^{11}, 5 \cdot 10^{11}, 10^{12}, 5 \cdot 10^{12}]$$

and the roll angle and the control input weighting factors are respectively:

$$\rho_3 = 0, \rho_4 = 1$$

The set of velocities considered during the optimization is:

$$\text{kph} = [5, 10, 15, 20, 30, 40, 50, 60, 65, 70, 75, 80, 85, 90]$$

In Table 2, the weighting constants to obtain minimum RMS values for bounce acceleration and pitch angle are listed for different vehicle speeds. Case A refers to the minimization of RMS values of bounce acceleration, whereas Case B refers to the minimization of RMS values of pitch angle. As seen from Table 2, when bounce acceleration is desired to be minimized, ρ_2 takes lower values; whereas ρ_1 takes lower values for the pitch angle minimization.

As a comparison, the minimal values that can be attained by one parameter optimization in 5.2.1 and 5.2.2 are examined in Figure 5.13 and Figure 5.14. The

time span used in calculating RMS values is between the time the front wheels encounter the road input and two seconds after the rear wheels encounter the road input. As can be seen from Figure 5.13, the two weighting factor optimization is better than only bounce acceleration minimization. However, as it can be observed in Figure 5.14 that there are no distinct performances differences in pitch angle minimization

Table 2 Weighting Constants for 2D Optimization

Case A: 2D Optimization of RMS Bounce Acceleration Values

Case B: 2D Optimization of RMS Pitch Angle Values

Vehicle Speed	CASE A		CASE B	
	ρ_1	ρ_2	ρ_1	ρ_2
5	5.E+08	1.E+11	5.E+06	5.E+11
10	5.E+06	1.E+10	5.E+06	5.E+11
15	1.E+07	1.E+10	5.E+06	1.E+12
20	1.E+07	5.E+09	1.E+06	5.E+12
30	5.E+06	1.E+09	1.E+07	5.E+12
40	5.E+10	5.E+10	1.E+08	5.E+12
50	5.E+09	5.E+08	1.E+08	5.E+12
60	1.E+11	5.E+11	1.E+11	5.E+12
65	1.E+07	5.E+10	5.E+08	5.E+12
70	5.E+09	1.E+11	1.E+07	5.E+12
75	1.E+07	5.E+08	1.E+06	5.E+12
80	5.E+06	5.E+09	5.E+07	1.E+12
85	5.E+10	5.E+10	5.E+06	5.E+11
90	1.E+06	5.E+08	5.E+07	1.E+12

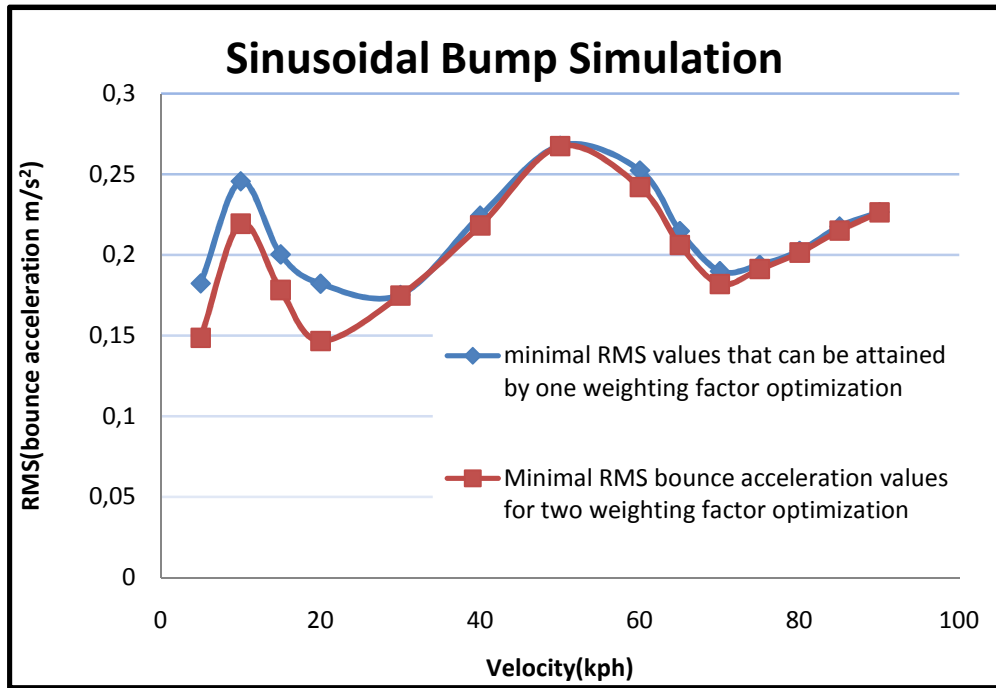


Figure 5.13 Sinusoidal Bump Simulation Results (RMS of Bounce Acceleration)

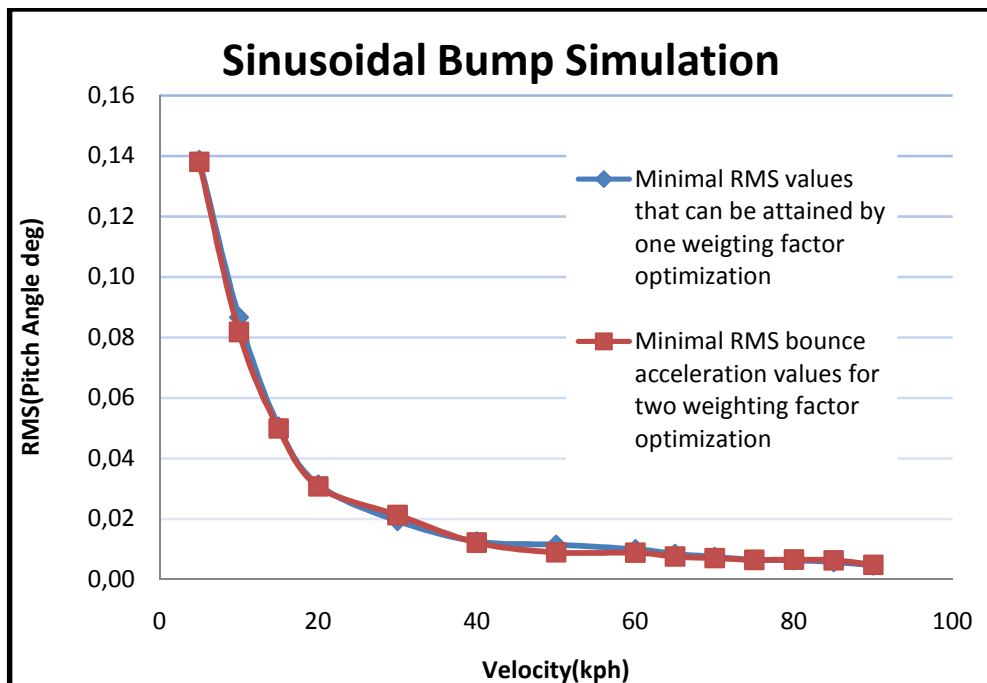


Figure 5.14 Sinusoidal Bump Simulation Results (RMS of Pitch Angle)

In this particular optimization procedure 1512 optimizations are carried, there should be some predefined criteria in sorting the results of the optimizations. In the previous study, with only one weighting factor optimization, it was seen that the bounce acceleration and pitch angle differences between controlled and uncontrolled results decrease as the vehicle velocity is increased. So the control effort is focused on low velocity optimization. This analysis was carried out for 0 to 70 kph. A performance criterion should be defined to measure the performance improvement in bounce acceleration and pitch angle at each vehicle velocity:

$$P_1 = \frac{\ddot{z}_{cg}(\text{uncontrolled}) - \ddot{z}_{cg}(\text{controlled})}{\ddot{z}_{cg}(\text{uncontrolled})} \quad (5.3)$$

$$P_2 = \frac{\phi(\text{uncontrolled}) - \phi(\text{controlled})}{\phi(\text{uncontrolled})} \quad (5.4)$$

In this index RMS values of bounce acceleration and pitch angle are used. The time to calculate RMS values is selected as two seconds after the bump enters the back wheels. This time is far adequate to damp the oscillations. The indices are unitless which make them easier to work with.

The following methodology is proposed for determining the optimum constant weighting factors. P_1 and P_2 defined in equations 5.3 and 5.4 are found for each weighting constant set and for different vehicle speeds. The weighting constants which make P_1 or P_2 negative are removed from the list, so any controlled response worse than uncontrolled responses is eliminated. Average P_1 for each velocity is calculated by calculating the average of the P_1 values of the reduced list which only contains superior performance than uncontrolled results. If bounce RMS minimization is set as the first priority, the weighting constant sets for each velocity that make P_1 better than average P_1 values should be emphasized. So by this manipulation the new list is further reduced to weighting factor sets that minimize the bounce acceleration more than average performance improvements at a specific velocity. Analyzing the reduced list further, suitable factors at different vehicle

speeds are examined and the set of most frequently appearing weighting factors. There can be several alternative solutions with which one can select good P_1 and P_2 indices. By this methodology, a suitable set for all vehicle speeds is chosen as $\rho_1 = 5 \cdot 10^6$ $\rho_2 = 10^{10}$ among several alternatives. The effect of this methodology to RMS values of bounce acceleration and pitch angle will be compared to minimal values that can be attained by two parameter optimization at each velocity

In Figure 5.15 and Figure 5.16 constant weighting factor optimization for 1D and 2D for all velocities, are also compared to passive and uncontrolled cases. As stated in the beginning of section 5.2.3, 2D optimization corresponds to bounce acceleration and pitch angle weighting factor optimization. 1D bump optimization corresponds to optimization of only bounce acceleration factor or only pitch angle weighting factor. 1D constant parameter optimization constants were evaluated in sections 5.2.1 and 5.2.2.

As can be seen from Figure 5.15 and Figure 5.16 constant weighting factor optimization for 2D cases is better in performance than other cases at low velocities. The performance improvement is not so clear at velocities higher than 40 kph. This result was expected because high frequency inputs as discussed in 5.1.1 needs minimum damping which corresponds to uncontrolled case.

As can be seen from Figure 5.16, constant weighting factor optimization for 2D cases is worse in performance than 1D case optimization. The reason is that the methodology sets priority on minimization of bounce acceleration values. Both 1D and 2D optimizations are better in performance than the uncontrolled cases.

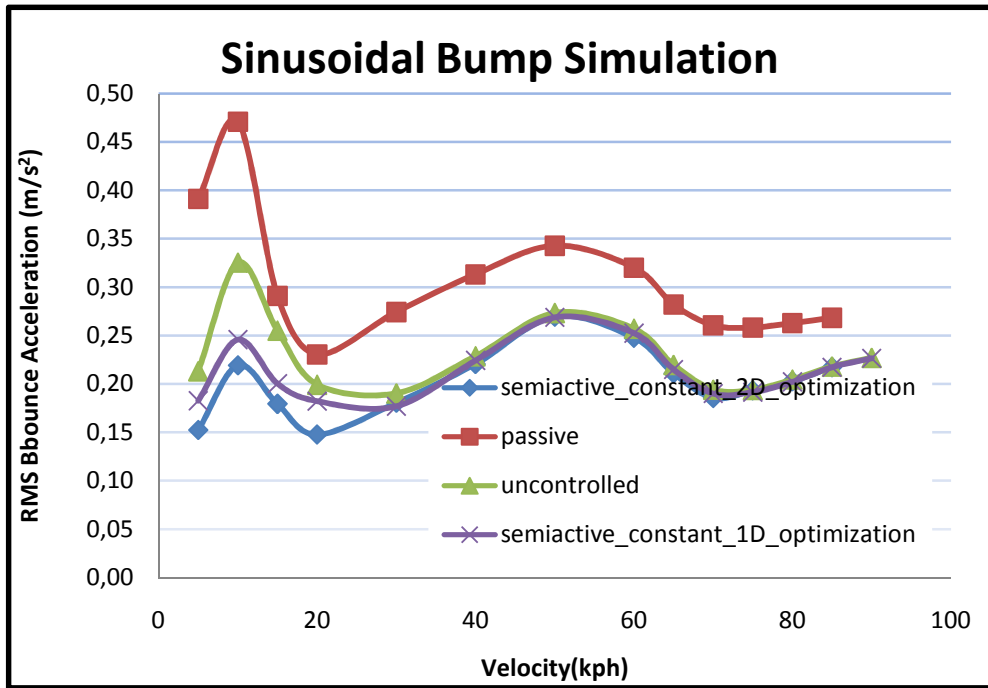


Figure 5.15 Sinusoidal Bump Simulation Results (RMS of Bounce Acceleration)

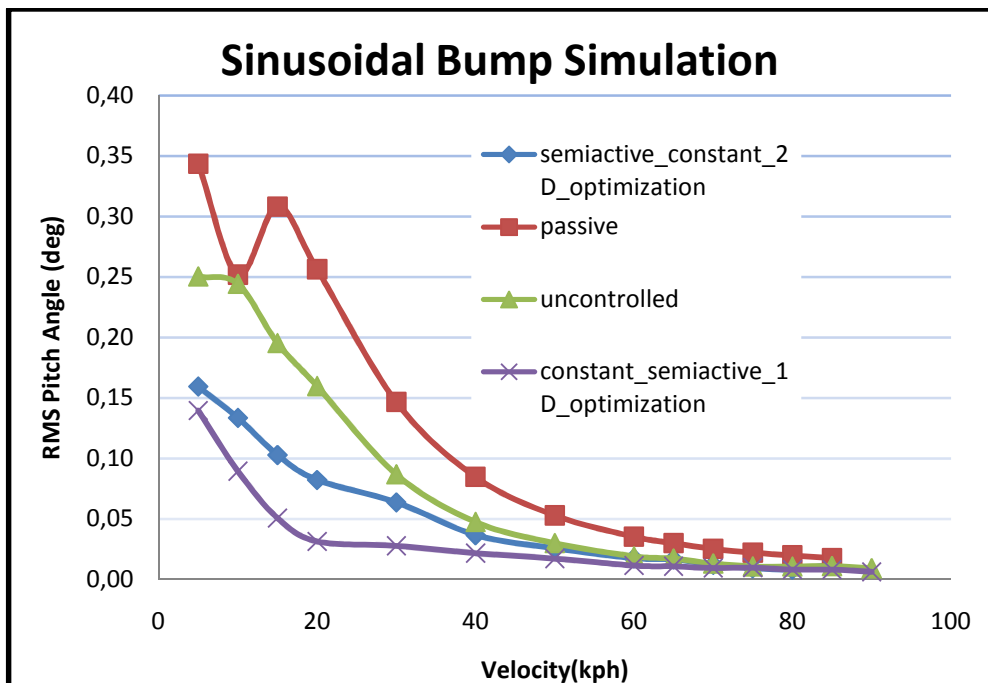


Figure 5.16 Sinusoidal Bump Simulation Results (RMS of Pitch Angle)

5.2.4 STAGE 4: OPTIMIZATION WITH RESPECT TO BOUNCE ACCELERATION, PITCH AND ROLL WEIGHTING FACTOR

In this stage bounce, pitch and roll motions are to be minimized, hence it is a 3D optimization which deals with three independent weighting factors. This procedure will be named 3D bump optimization. Since the computation complexity is increased for iterations with three weighting factors at different speeds, the iteration intervals of the variables should be selected for ease of computations. For the 3D iteration process, the bounce acceleration weighting factor is selected to vary as:

$$\rho_1 = [10^6, 10^7, 10^8, 10^9, 10^{10}, 10^{11}]$$

and the pitch angle weighting factor varies as:

$$\rho_2 = [5 \cdot 10^8, 10^9, 10^{10}, 10^{11}, 10^{12}, 10^{13}]$$

The roll angle and the input forces weighting factors are respectively:

$$\rho_3 = [5 \cdot 10^8, 10^9, 10^{10}, 10^{11}, 10^{12}, 10^{13}], \rho_4 = 1$$

The velocity range is selected up to 70 kph, since from previous studies it is seen that attainable control performance improvements in bounce acceleration and pitch angle minimization are not as good as the attainable improvements at velocities below 70 kph. The variation of the vehicle is selected is taken as:

$$\text{kph} = [5, 10, 15, 20, 30, 40, 50, 60, 70]$$

For the iterations, the input is the same half sine bump as in the previous stages except that there is a time delay between left and right wheels to induce roll movement of the vehicle. RMS values of each response is calculated up to the time interval which starts with the time the front wheel encounters the bump and ends 2 seconds after the time the rear wheel encounters the bump. The cases which minimize RMS values of roll, bounce and pitch motions separately is given in Table 3. In this table, case A consists of weighting constants that make the bounce acceleration minimal, case B consists of Constants for 3D optimization for minimal

pitch angles whereas case C consists of Constants for 3D optimization for minimal roll angles.

Table 3 Weighting Constants for 3D Bump Optimization

Case A: 3D Optimization for Minimal RMS Bounce Acceleration Values

Case B: 3D Optimization for Minimal RMS Pitch Angle Values

Case C: 3D Optimization or Minimal RMS Roll Angle Values

Vehicle	CASE A			CASE B			CASE C		
	ρ_1	ρ_2	ρ_3	ρ_1	ρ_2	ρ_3	ρ_1	ρ_2	ρ_3
5	1.E+06	1.E+11	1.E+11	1.E+06	1.E+12	1.E+11	1.E+06	5.E+08	1.E+12
10	1.E+08	1.E+10	1.E+09	1.E+06	1.E+12	1.E+11	1.E+06	1.E+09	1.E+12
15	1.E+10	1.E+10	1.E+09	1.E+08	1.E+12	5.E+08	1.E+08	1.E+09	1.E+12
20	1.E+10	1.E+10	1.E+11	1.E+07	1.E+12	5.E+08	1.E+08	1.E+10	1.E+12
30	1.E+08	1.E+10	1.E+11	1.E+08	1.E+12	1.E+09	1.E+11	1.E+09	1.E+12
40	1.E+10	1.E+11	1.E+10	1.E+07	1.E+12	1.E+12	1.E+06	1.E+11	5.E+08
50	1.E+06	1.E+11	5.E+08	1.E+07	1.E+12	1.E+11	1.E+11	1.E+11	1.E+11
60	1.E+06	1.E+11	1.E+11	1.E+06	1.E+12	1.E+12	1.E+09	1.E+12	1.E+11
70	1.E+06	1.E+12	1.E+09	1.E+09	1.E+12	1.E+09	1.E+11	1.E+12	1.E+11

The following methodology which was proposed in 5.2.3 is now extended for 3D optimization. P_1 , P_2 and P_3 which are defined in equation (5.5), (5.6) and (5.7) are found for each weighting constant set and for different vehicle speeds. The weighting constants which makes P_1 , P_2 , or P_3 negative is removed from the list, so any controlled response worse than uncontrolled responses is eliminated. Average P_1 for each velocity is calculated by calculating the average of the P_1 values of the reduced list which only contains superior performance achievements than uncontrolled results. If bounce RMS minimization is set as the first priority, the weighting constant sets that make P_1 better than average P_1 values should be emphasized. So by

this manipulation the new list is further reduced to weighting factor sets that minimize the bounce acceleration more than average at a specific velocity. The list can be further reduced by applying same procedure for P_2 and P_3 . However this type of overall reduction for P_1, P_2 , and P_3 . was not feasible in finding the most frequently appearing weighting factor sets for every vehicle speed, since a suitable weighting factor set could not be found after the overall reduction in the list. So the procedure is only carried for P_1 and P_3 . The emphasis is given to minimization of bounce acceleration and roll angle. Analyzing the reduced list, the suitable factors at different vehicle speeds are examined and are found. There can be several alternative solutions which one can select with good P_1 and P_3 indices. By this methodology, a suitable set for all vehicle speeds is chosen as $\rho_1 = 5 \cdot 10^6$ $\rho_2 = 10^{10}$ $\rho_3 = 10^{10}$ among several alternatives.

$$P_1 = \frac{\ddot{z}_{cg}(\text{uncontrolled}) - \ddot{z}_{cg}(\text{controlled})}{\ddot{z}_{cg}(\text{uncontrolled})} \quad (5.5)$$

$$P_2 = \frac{\phi(\text{uncontrolled}) - \phi(\text{controlled})}{\phi(\text{uncontrolled})} \quad (5.6)$$

$$P_3 = \frac{\theta(\text{uncontrolled}) - \theta(\text{controlled})}{\theta(\text{uncontrolled})} \quad (5.7)$$

The effect of this methodology for RMS values of bounce acceleration is given in Figure 5.17 . As can be seen there is a performance improvement of the control strategy between uncontrolled and controlled results. By using semi-active constant factors there is a slight performance decrease from optimal ones, the performance increase is better from uncontrolled and controlled results. The plots for roll angle and pitch angle RMS values are given in Figure 5.18 and Figure 5.19.

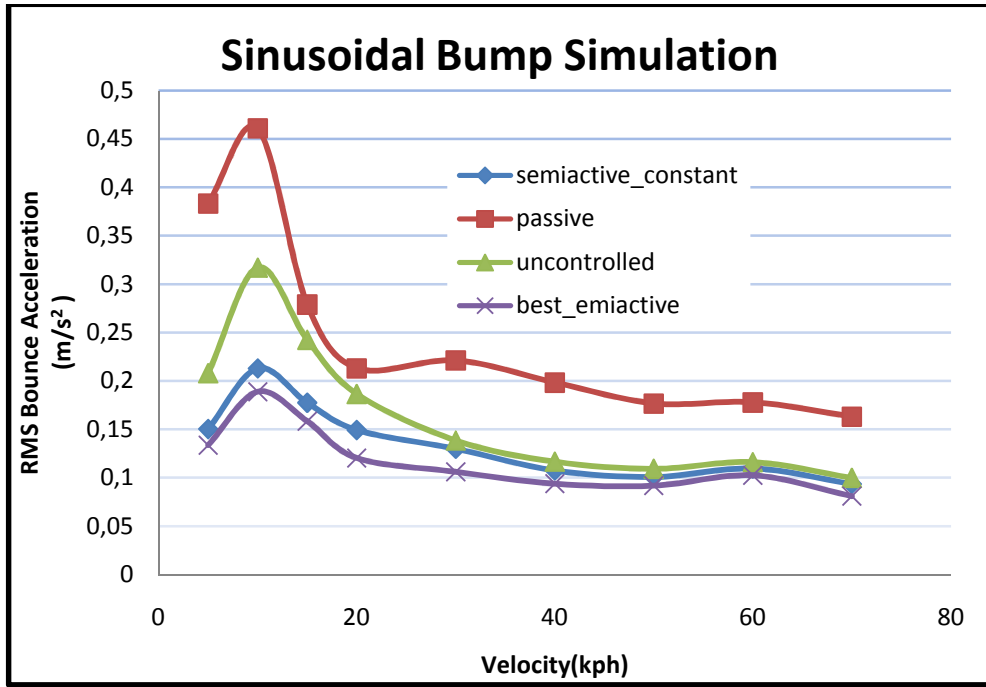


Figure 5.17 Sinusoidal Bump 3D Simulation Results (RMS of Bounce Acceleration)

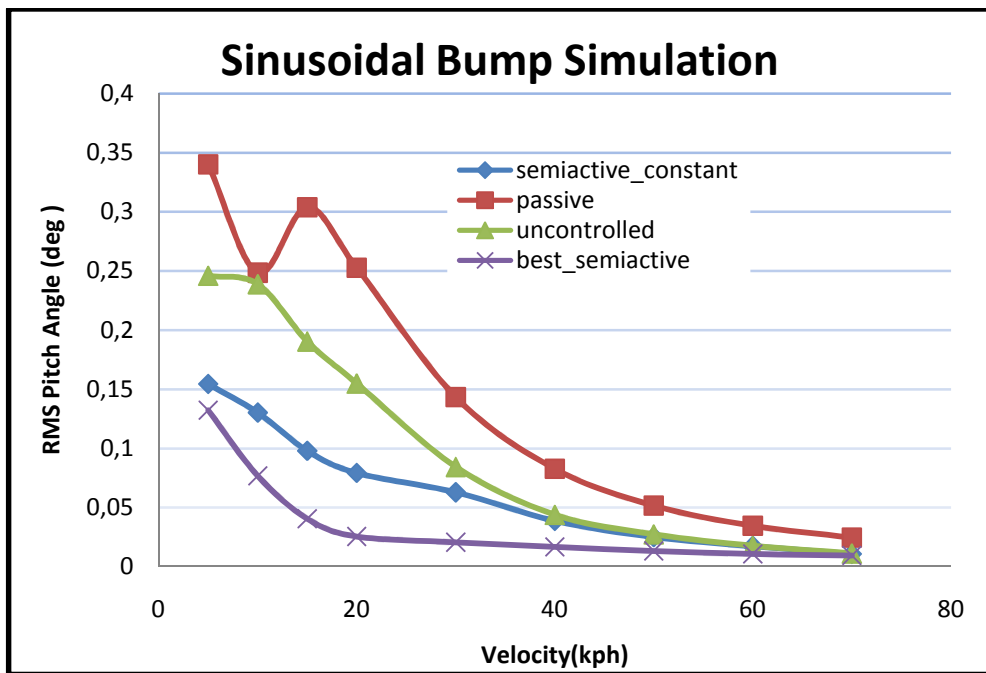


Figure 5.18 Sinusoidal Bump 3D Simulation Results (RMS of Pitch Angle)

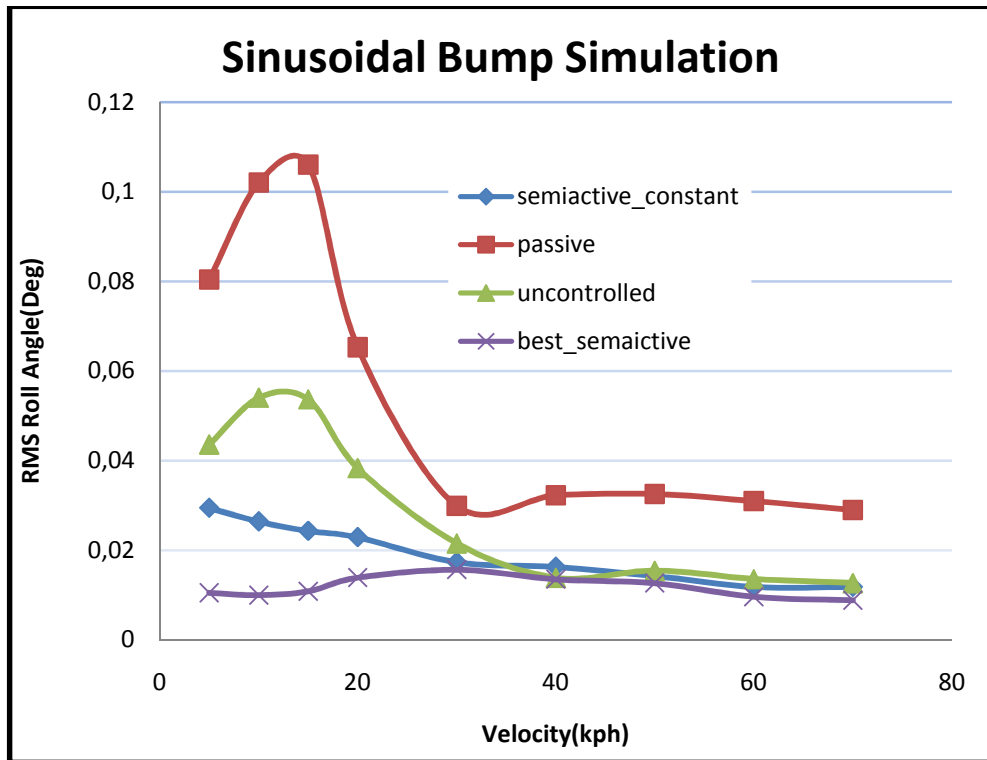


Figure 5.19 Sinusoidal Bump 3D Simulation Results (RMS of Roll Angle)

5.3 3D BUMP OPTIMIZATION FOR SKYHOOK CONTROL STRATEGIES

Skyhook control strategy for semi-active suspension control is widely used. So for comparison purposes with the optimal control approach used in this study, a reference skyhook controller will be developed and tested. The same optimization process described in section 5.2 should be done to find front and rear skyhook damping constants for skyhook control algorithm. Since the vehicle is symmetric about the roll axis, the optimization process is carried for front and rear skyhook constants. Also since the centre of gravity is close to the front side, the front damping constant is expected to be selected higher than or equal to the rear damping constants. The possible skyhook gains are selected as [1500 2500 3000 3500 4000 4500 5000 5500 6000 7000 8000 9000]. Some sample trials lead to a range of

skyhook damping values between 2500 and 6000. Hence the damping range between these constants is divided more finely than the entire range. The velocity variations are selected same as the section 5.2 and taken as [5 10 15 20 30 40 50 60 70] kph. The optimization procedure is done to minimize the bounce acceleration, pitch angle, and roll angle as was done in section 5.2. Suitable performance criterion for P1, P2, and P3 are evaluated for different vehicle speeds going on the same bump. The 3D optimization strategy for skyhook control procedure is easier to handle since only two damping constants are to be found whereas in 3D optimization three weighting factors were determined. The same methodology in section 5.2.4 is carried for this optimization. The front damping is selected as 5000Ns/m whereas the rear damping is selected as 4500 Ns/m. The results from skyhook control will now be compared with optimal control in section 5.4.

5.4 3D CHIRP INPUT ANALYSIS

When comparative results between different control strategies are needed to verify a design under general conditions, frequency response techniques are commonly used. Since the model is nonlinear, the classical approach for obtaining frequency response cannot be used. For nonlinear systems, hammer inputs and chirp inputs are generally used to find the frequency response.

The 7-dof vehicle ride model can be excited with a chirp signal to determine its frequency response. The chirp signal is generated in Matlab Simulink by a chirp signal block which generates a sine wave whose frequency increases at a linear rate with time. This simulation enables a frequency domain analysis. Although the chirp input test cannot be generalized, it gives an idea about the efficiency of the controller. The fast Fourier transform of the system outputs for a given chirp input gives an idea of the response of the system for different frequencies. The simulation input will contain all frequencies between 0.1 Hz to 17 Hz. This frequency range covers the basic frequency range interest of the ride comfort for passengers. Chirp input time is selected as 70 seconds. The sine input amplitude is selected as 0.035 m.

The inputs to left and right wheels should have a time delay difference to induce roll motion. The time difference between rear and front wheels is based on the vehicle speed. The time delay between wheels complicates the frequency response by dispersing the expected peaks at natural frequencies. This effect can be seen from Figure 5.20 which represents the bounce motion response when the chirp inputs applied at the front wheels. The same inputs are assumed to excite the back wheels with a time delay corresponding to a vehicle speed of 72 kph. Also a time delay of 0.05 seconds is applied to the right wheels with respect to left wheels to create roll motion.

To overcome the difficulty of four separate inputs, the inputs which have same characteristics at each wheel should be applied at the same time. There should also be no delay between the wheels for clarity in frequency response. Since the four inputs of same characteristics are meaningless, the vehicle is assumed to be affected from only one wheel to get a clear frequency response. This situation is evidently fictitious; however it gives a measure of the frequency response. Giving input to only one of the wheels can excite both roll, pitch, and bounce motions. The corresponding frequency responses are given for this special input in the following figures. In the legends, "SUBoptimal" is used to represent the clipped optimal law. To the rest of the chirp input analysis in this section and the simulations in section 6, the vehicle data (Zuo & Nayfeh, 2003) in APPENDIX B will be used.

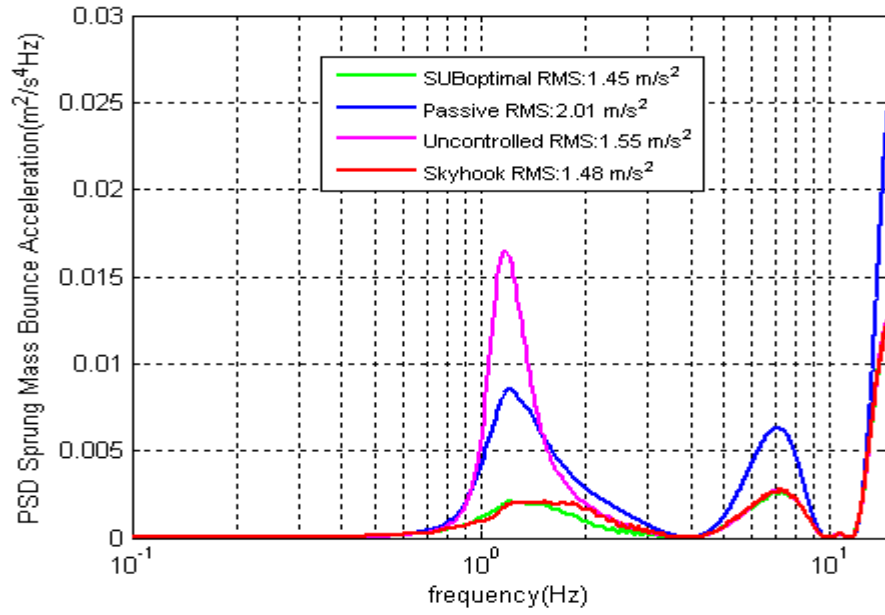


Figure 5.20 Power Spectral Density of Bounce Displacement and Acceleration - Chirp Input from 4 Wheels

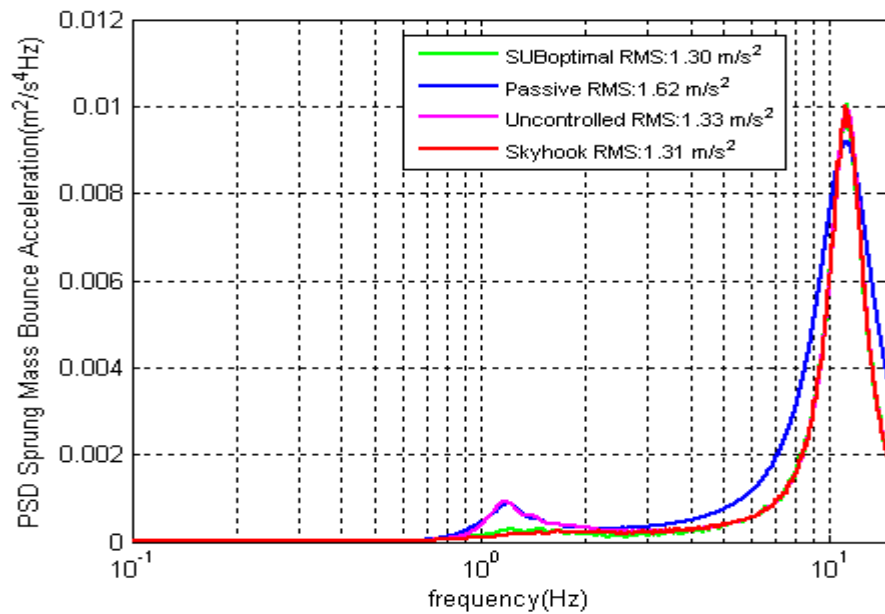


Figure 5.21 Power Spectral Density of Bounce Acceleration - Chirp Input from one Wheel

In Figure 5.21 it can be seen that there is some improvement in bounce acceleration minimization at low frequencies around 1 Hz for semi-active control among passive and uncontrolled cases. LQR strategy is slightly better than skyhook control.

In Figure 5.22 it can be seen that the peak at pitch natural frequency is minimized for semi-active control among passive and uncontrolled cases. The RMS value of pitch angle is better in LQR strategy although no clear improvement can be observed around 1 Hz. In bump optimization if the pitch motion was chosen as the most important criteria to minimize, the weighting coefficient of pitch motion would increase. However in that case the performance of bounce and roll motion minimization would deteriorate.

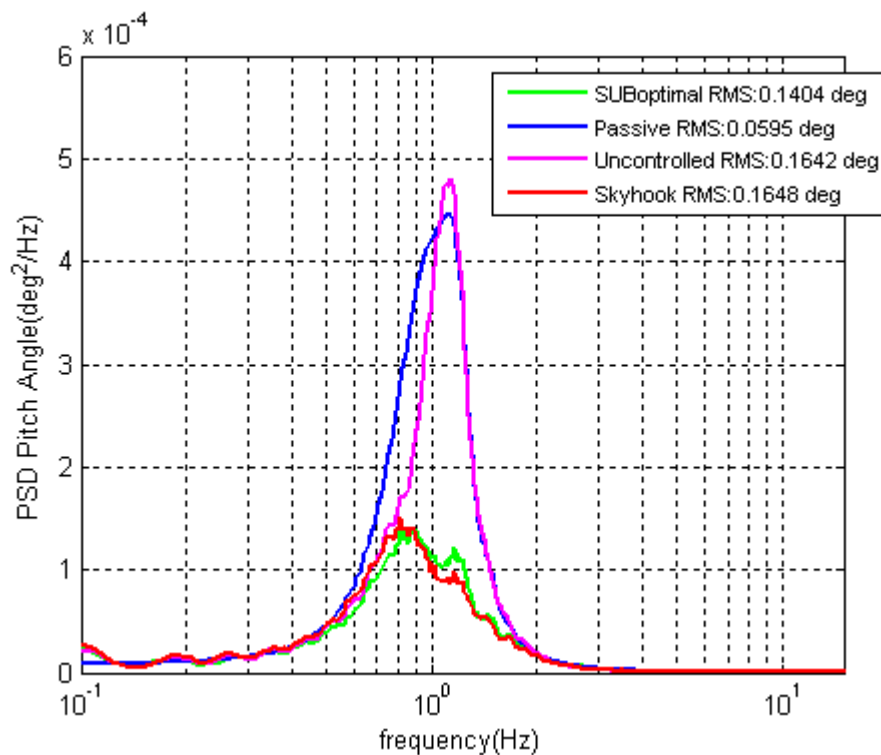


Figure 5.22 Power Spectral Density of Pitch Motion - Chirp Input from one Wheel

In Figure 5.23 it can be seen that there is also an improvement for semi-active suspensions in roll motion minimization at low frequencies around 1 Hz. The RMS values for both accelerations and motions are also minimal for semi-active control among passive and uncontrolled cases. In semi-active controls, the LQR controller performance is better than skyhook controllers.

As can be seen from Figure 5.24, rattle space movement is minimized at frequencies around 1 Hz.

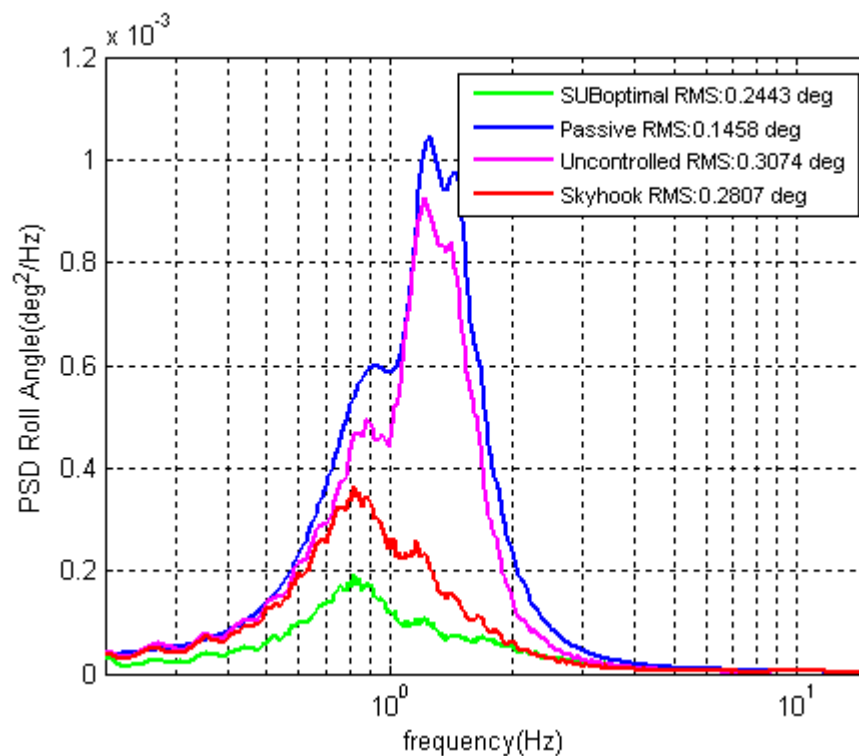


Figure 5.23 Power Spectral Density Of Roll Motion - Chirp Input From One Wheel

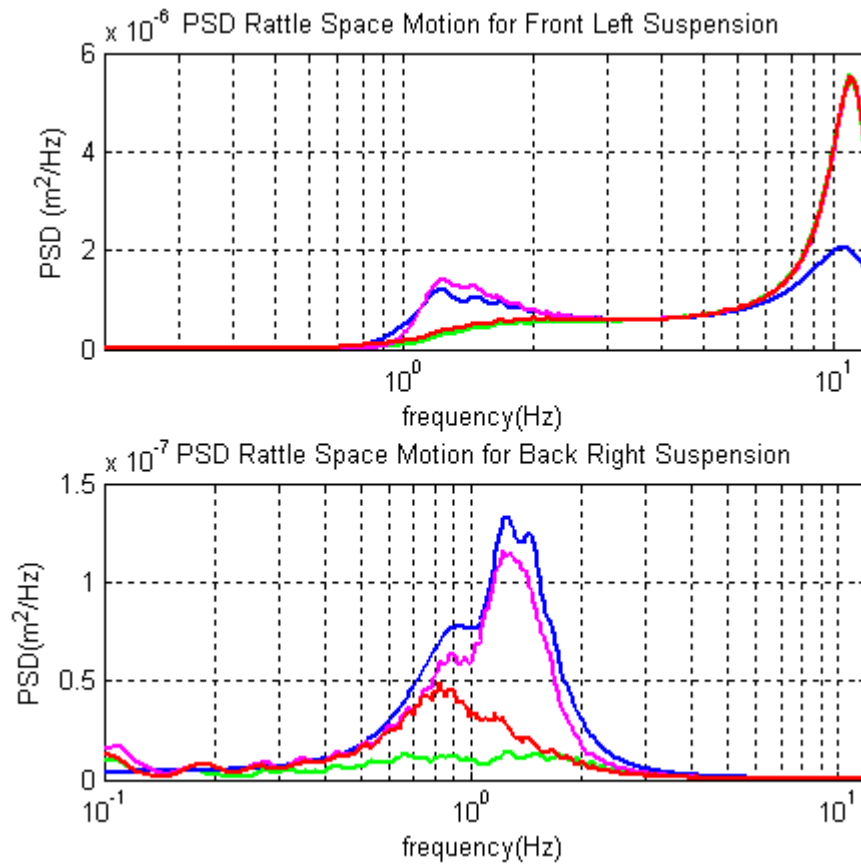


Figure 5.24 Power Spectral Density of Rattle Space Motion - Chirp Input from One Wheel

CHAPTER 6

SIMULATION TESTS

6.1 SINUSOIDAL INPUT TEST

This input is proposed to examine the response of the vehicle near the natural frequencies of bounce, pitch, and roll motions. The input is selected as a continuous 1 Hz sinusoidal input with an amplitude of 3.5 cm which corresponds to a width of 0.69 m and a velocity of 5 kph. There is a time delay between front and rear wheels dependent on the velocity of the car. To induce roll motion the sinusoidal input is only applied with a time shift of 0.2 radian between left and right sides of the car. The time responses are plotted in Figure 6.1, Figure 6.2, Figure 6.3, and Figure 6.4. The Root Mean Square values (RMS) for each control policy computed in the time span of 10 seconds can be seen in the legends of the plots.

In Figure 6.1, the bounce displacement is plotted. The transient behaviour is due to the time delay between front and rear wheels. There is high frequency oscillation added to 1 Hz oscillations in bounce acceleration due to the limits of semi-active control for the minimal and maximum damping forces. As can be seen there is a significant reduction of bounce motion for semi-active control.

In Figure 6.7 and Figure 6.8 the improvements of pitch and roll motions can be seen respectively.

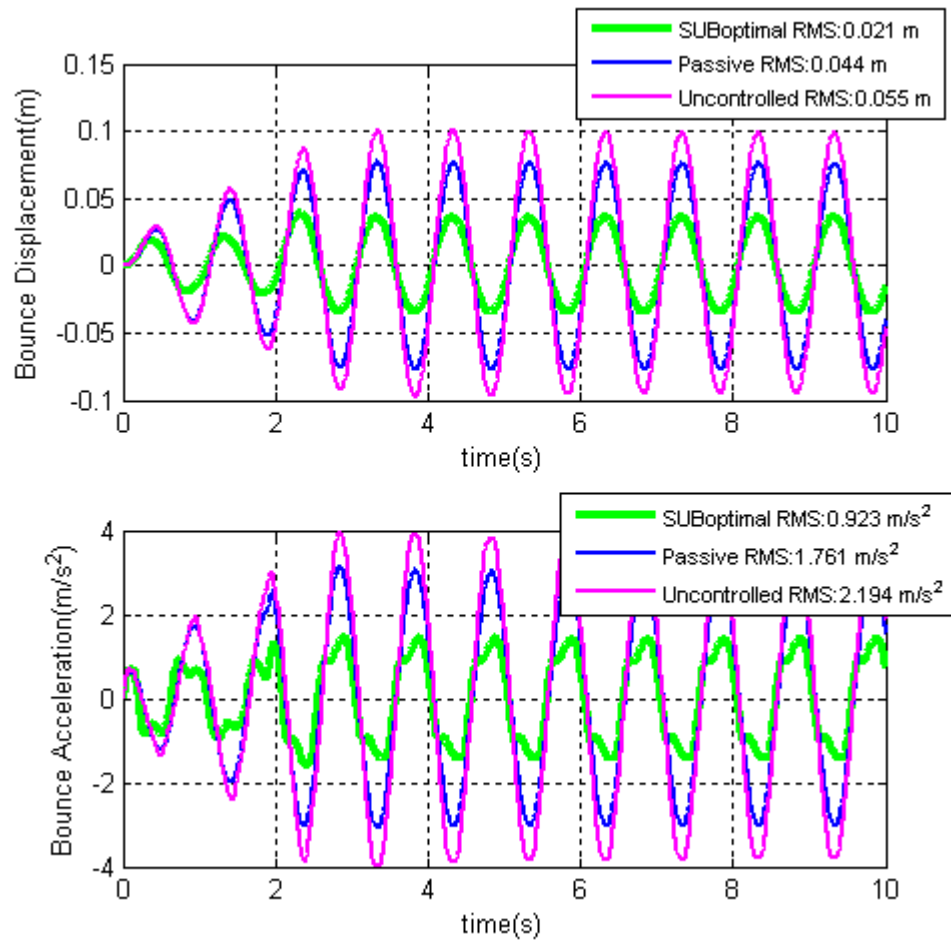


Figure 6.1 Bounce Displacement and Acceleration versus Time – Sinusoidal Input

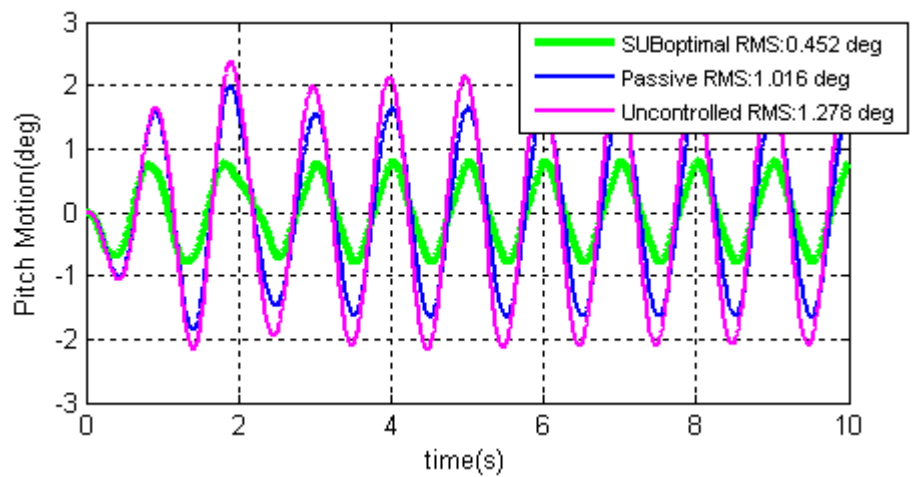


Figure 6.2 Pitch Angle versus Time - Sinusoidal Input

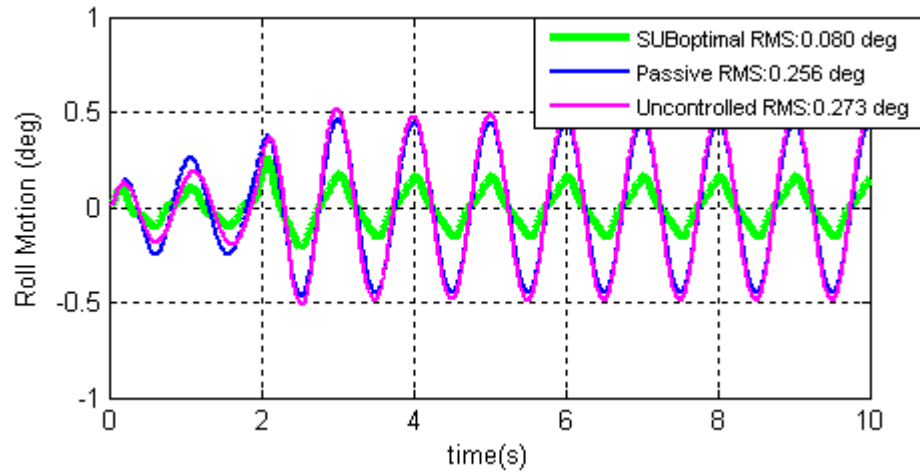


Figure 6.3 Roll Angle versus Time - Sinusoidal Input

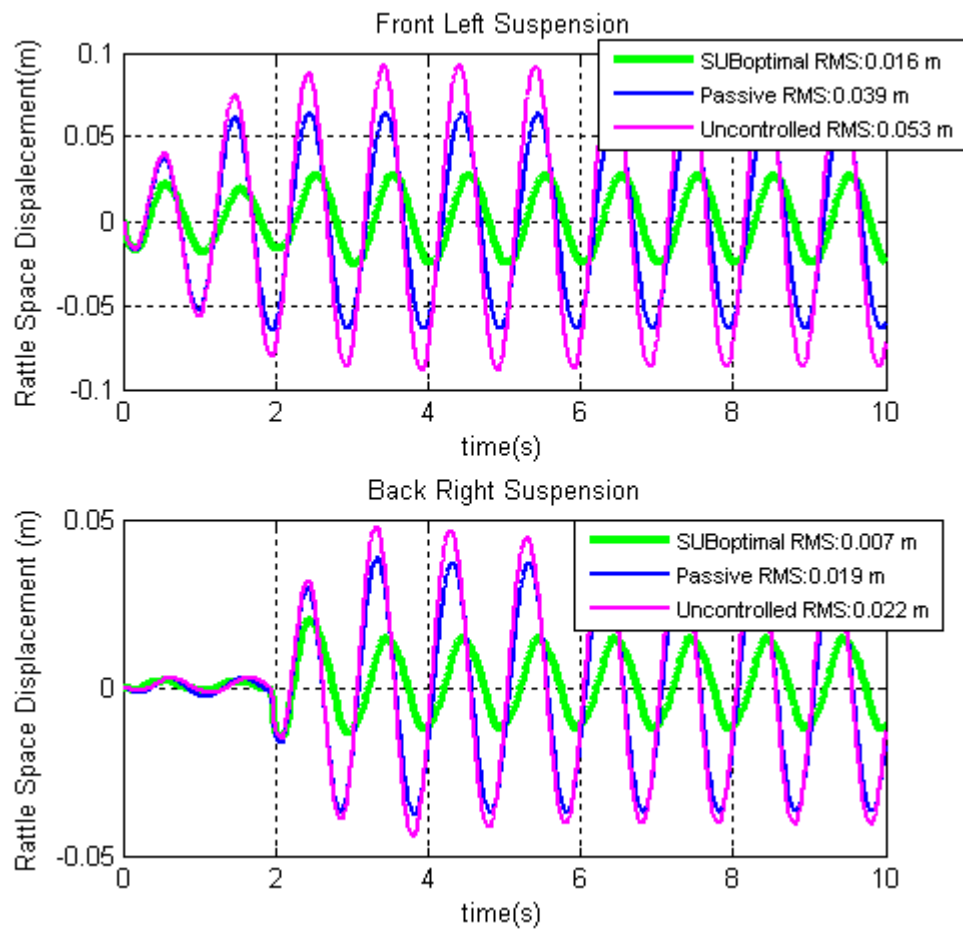


Figure 6.4 Rattle Space versus Time - Sinusoidal Input

6.2 BUMP&HUMP TEST

The inputs will correspond to single bumps or humps that will pass through two axles or only right or left wheels of the vehicle. The speed of the vehicle is taken as 30-50 kph since the speed limit in city centers where speed control humps is used. The geometrical information about more commonly used humps can be found from the document of TS 6283(Turkish Standard Institution, 1998). In this work it is stated that the length of the half sinusoidal flat humps is between 3.6 m to 3.8 m whereas the height of the bump is 7.5 to 10 cm.

In case of the half sinusoidal short bumps the width of the bump has the length 30 to 100 cm whereas the height of the bump is between 3 to 10 cm.

6.2.1 HALF SINUSOIDAL BUMP TEST SIMULATION 1

This input is proposed to examine the transient response of the vehicle due to bump inputs. The input is selected as a half sinusoidal bump with a height of 3.5 cm and with a width of 1 meter at a velocity of 9 kph. There is a time delay between front and rear wheels dependent on the velocity of the car. To induce roll motion the sinusoidal input is only applied to the left side of the car. The input can be also seen from Figure 6.5. The settling time of three control policies can be identified from the time response plots in Figure 6.6, Figure 6.7, Figure 6.8, and Figure 6.9. The RMS values for the time span of 5 seconds are given in the legends of the figures.

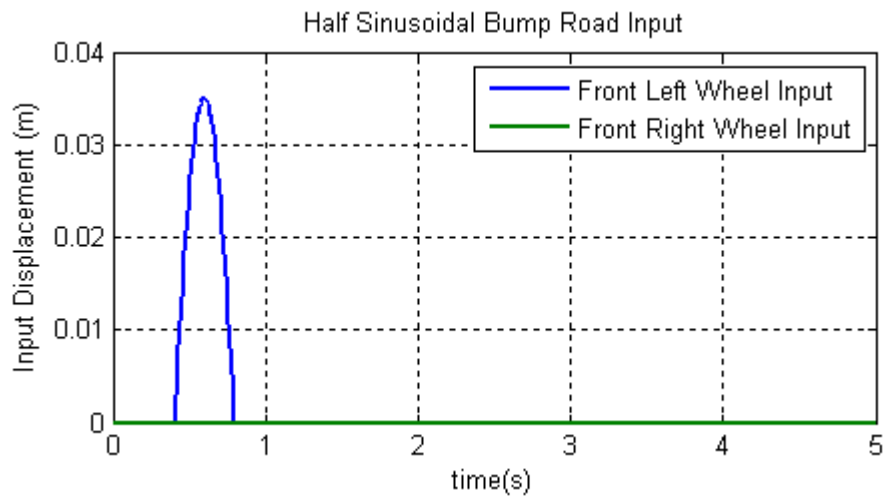


Figure 6.5 Road Input versus Time - Half Sinusoidal Bump Input Case 1

This type of input excitation is applied to give low frequency road inputs. The improvements are very clear for settling time, peak to peak value minimization, and RMS minimization of the system outputs. As was discussed in section 5.1.1 the improvement of ride comfort and handling is possible for low frequency range as can also be seen for the cases of this input.

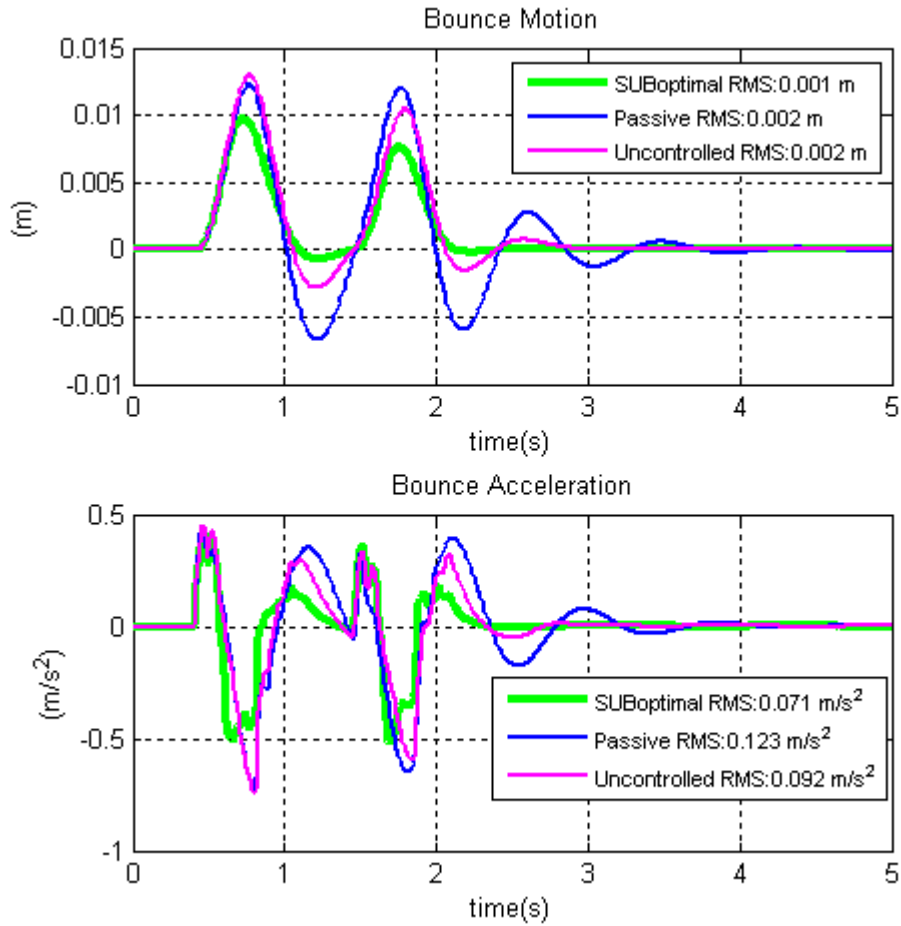


Figure 6.6 Bounce Displacement and Bounce Acceleration versus Time - Half Sinusoidal Bump Case 1

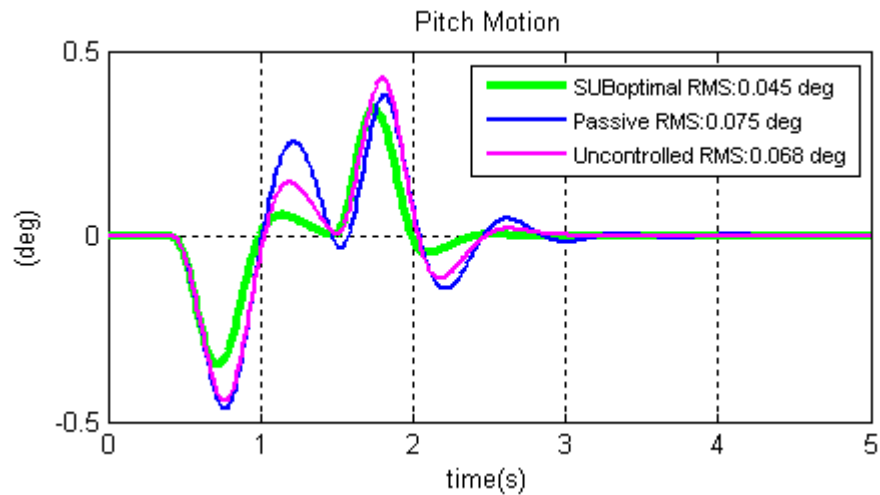


Figure 6.7 Pitch Angle versus Time - Half Sinusoidal Bump Case 1

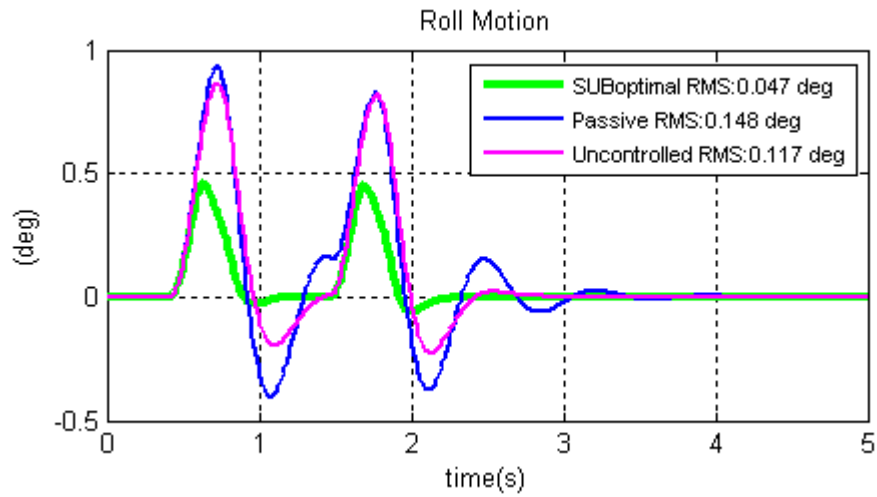


Figure 6.8 Roll Angle versus Time - Half Sinusoidal Bump Input Case 1

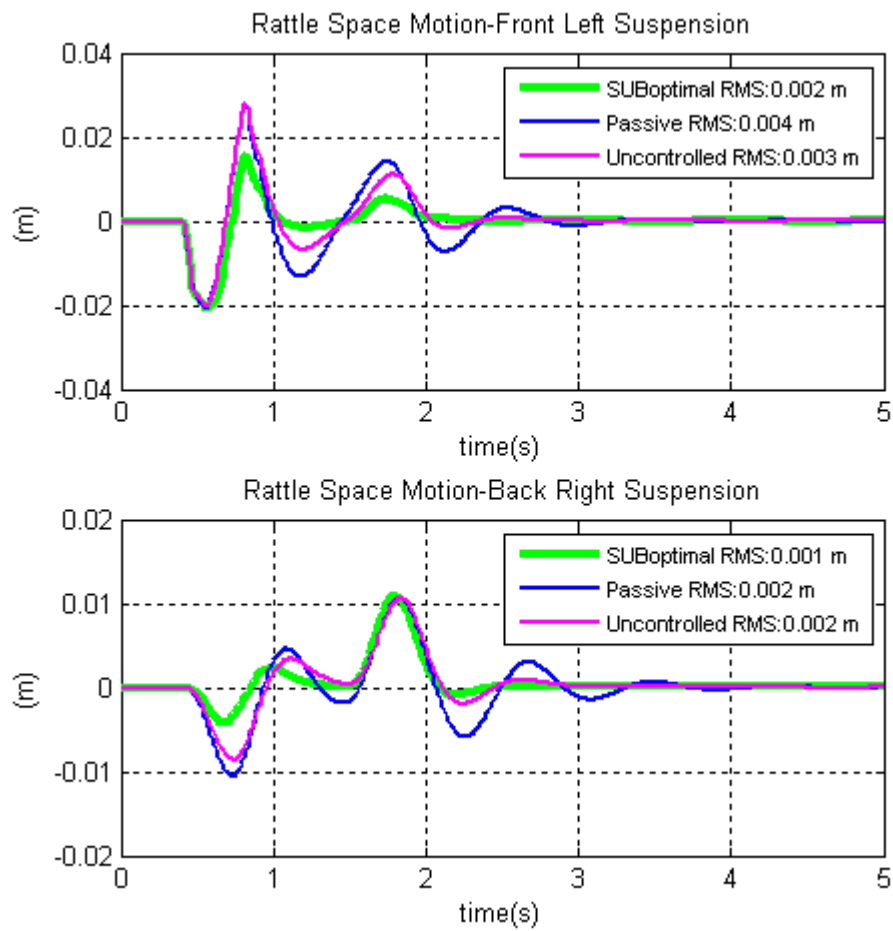


Figure 6.9 Rattle Space Motion of Front Left Suspension and Rear Right Suspension versus Time - Half Sinusoidal Bump Input Case 1

6.2.2 HALF SINUSOIDAL BUMP TEST SIMULATION 2

The input is selected as a half sinusoidal bump with a height of 7 cm and with a width of 0.8 m at a velocity of 30 kph. This bump is also used in the work (Choi, Han, Song, & Choi, 2007). The bump is modified to induce roll motion of the vehicle. The half sinusoidal input is only applied to the left side of the car. The input can be also seen from Figure 6.10

The settling time of three control policies can be identified from the time response plots in Figure 6.11, Figure 6.12, Figure 6.13 and Figure 6.14. The RMS values for the time span of 5 seconds are given in the legends of the figures.

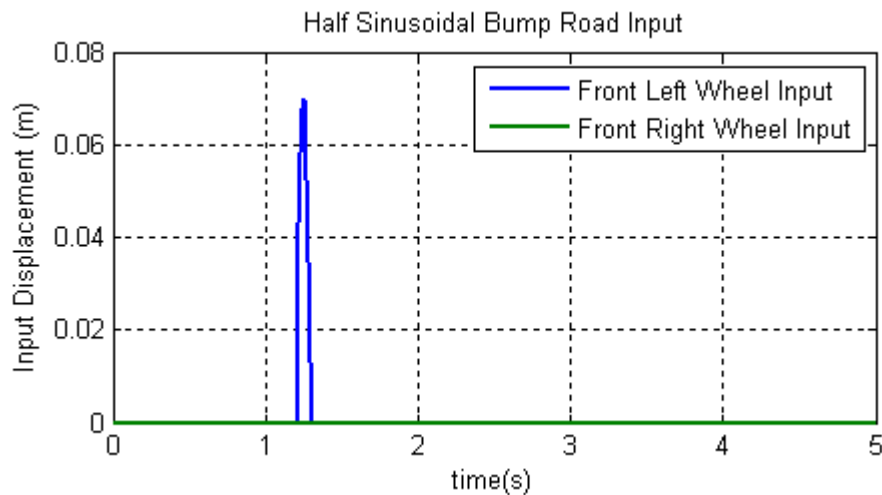


Figure 6.10 Road Input versus Time - Half Sinusoidal Bump Input Case 2

As can be seen from Figure 6.11 there is an improvement of bounce acceleration minimization with respect to passive suspensions, however this improvement is not clear between controlled and uncontrolled cases. The reason is for bounce acceleration minimization at high frequencies the damping force should be minimal. The settling time, RMS, and peak to peak values are minimal for semi-active suspension for bounce, pitch, and roll and rattle space motion.

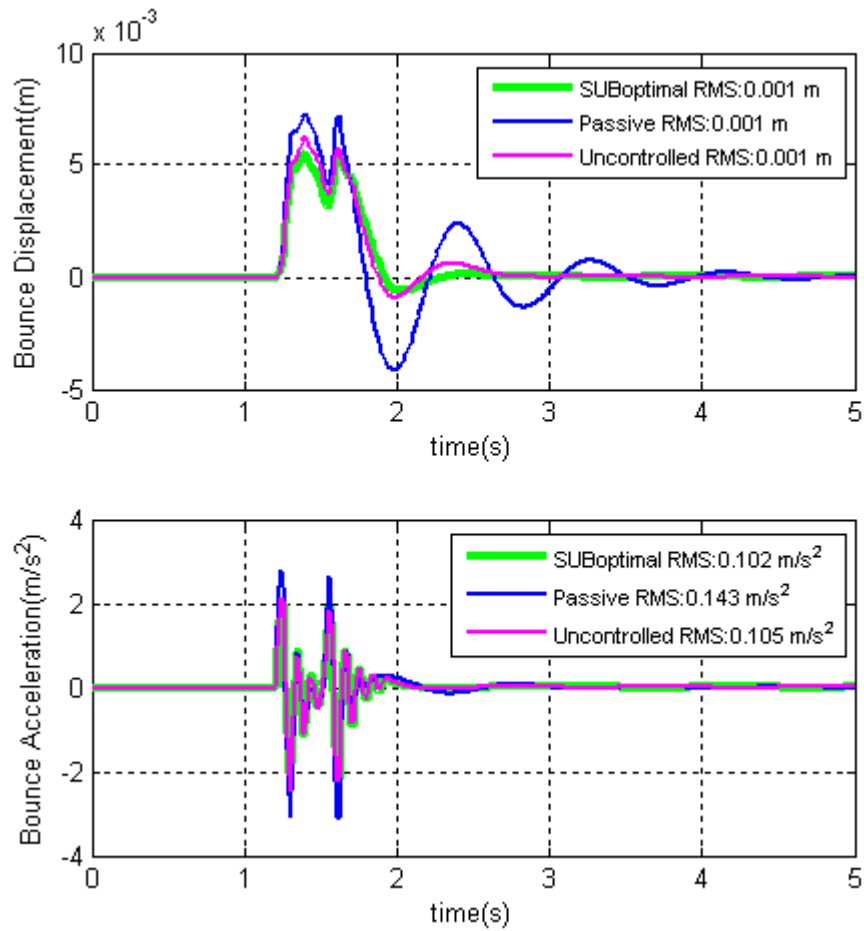


Figure 6.11 Bounce Motion And Bounce Acceleration versus - Half Sinusoidal Bump Input Case 2

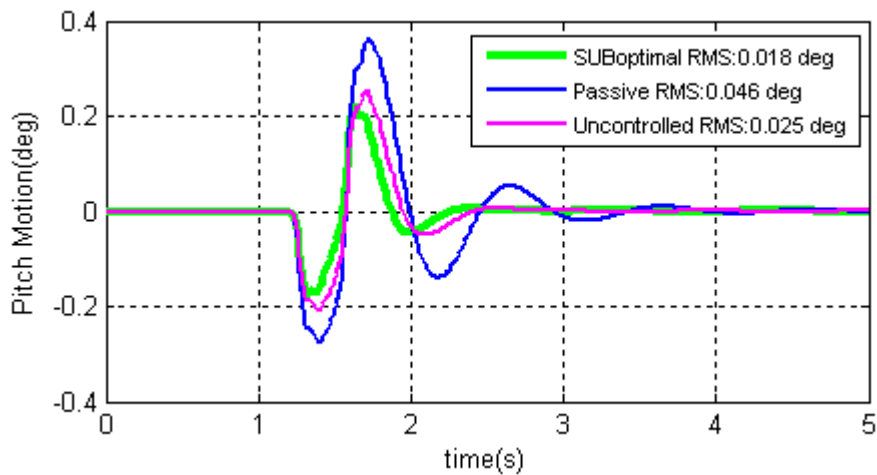


Figure 6.12 Pitch Motion versus Time - Half Sinusoidal Bump Input Case 2

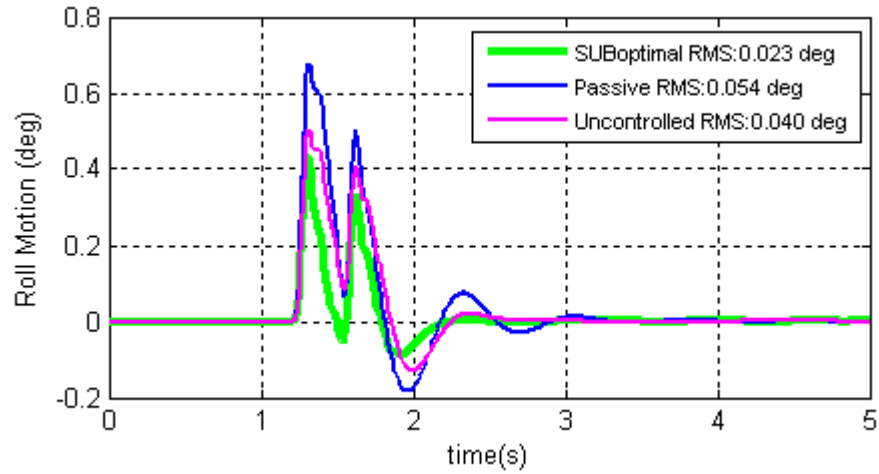


Figure 6.13 Roll Motion versus Time - Half Sinusoidal Bump Input Case 2

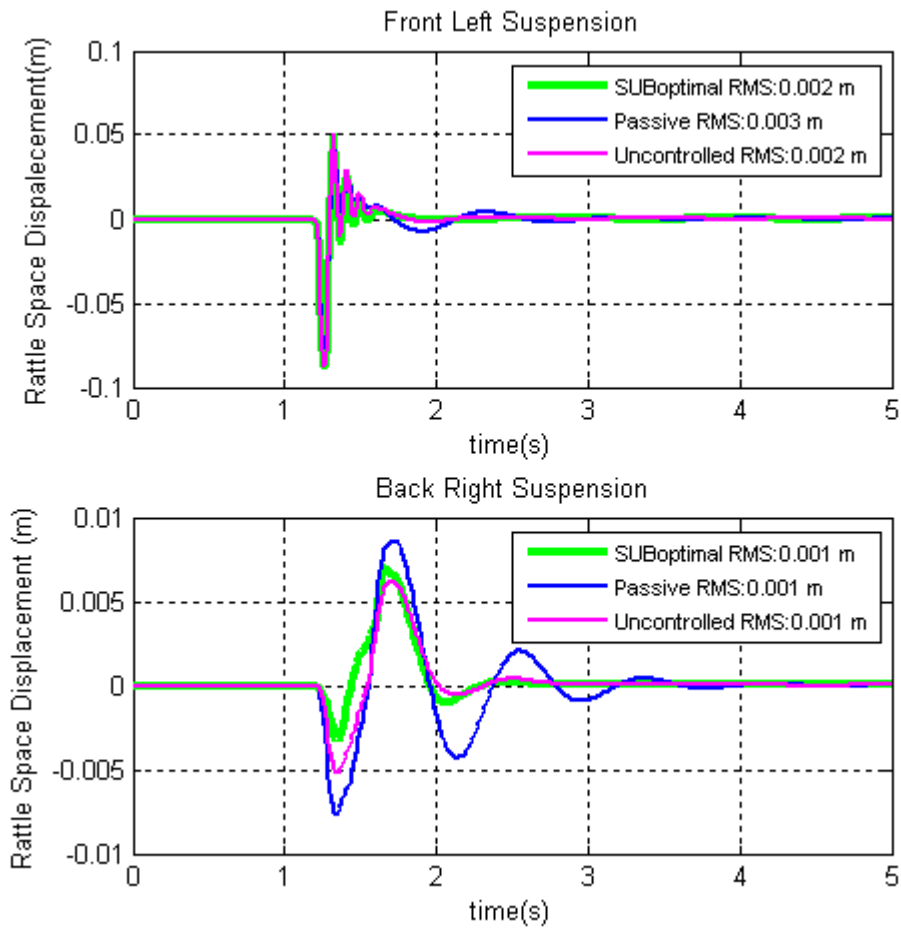


Figure 6.14 Rattle Space Motion of Front Left Suspension and Rear Right Suspension versus Time - Half Sinusoidal Bump Input Case 2

6.2.3 HALF SINUSOIDAL HUMP TEST

The input is selected as a half sinusoidal hump with a height of 9 cm and with a width of 3.6 m at a velocity of 40 kph. This half sinusoidal hump input is applied to both sides of the car for realistic driving conditions. The input can be also seen from Figure 6.15.

The settling time of three control policies can be identified from the time response plots in Figure 6.16, Figure 6.17, and Figure 6.18. The RMS values for the time span of 5 seconds are given in the legends of the figures.

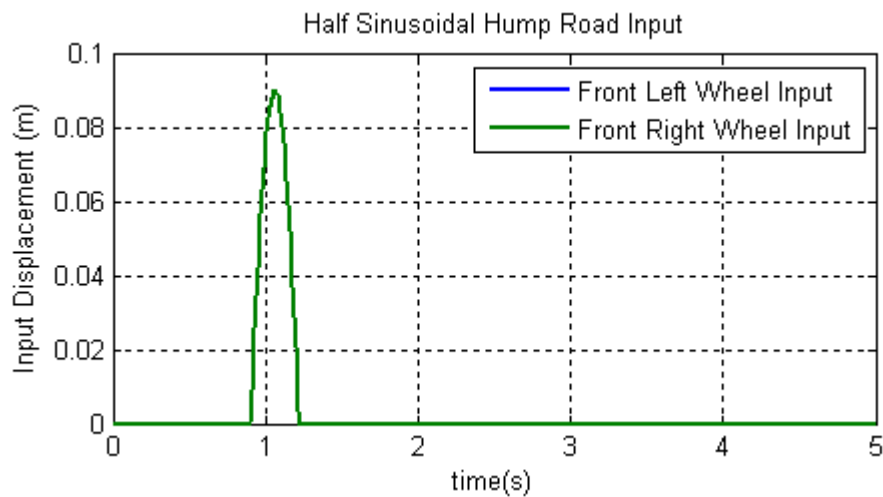


Figure 6.15 Road Input versus Time - Half Sinusoidal Hump Input

As can be seen from Figure 6.11 there is an improvement of bounce acceleration minimization with respect to passive suspensions, however this improvement is not clear between controlled and uncontrolled cases. The reason is for bounce acceleration minimization at high frequencies the damping force should be minimal. The settling time, RMS, and peak to peak values are minimal for semi-active suspension for bounce, pitch, and roll and rattle space motion.

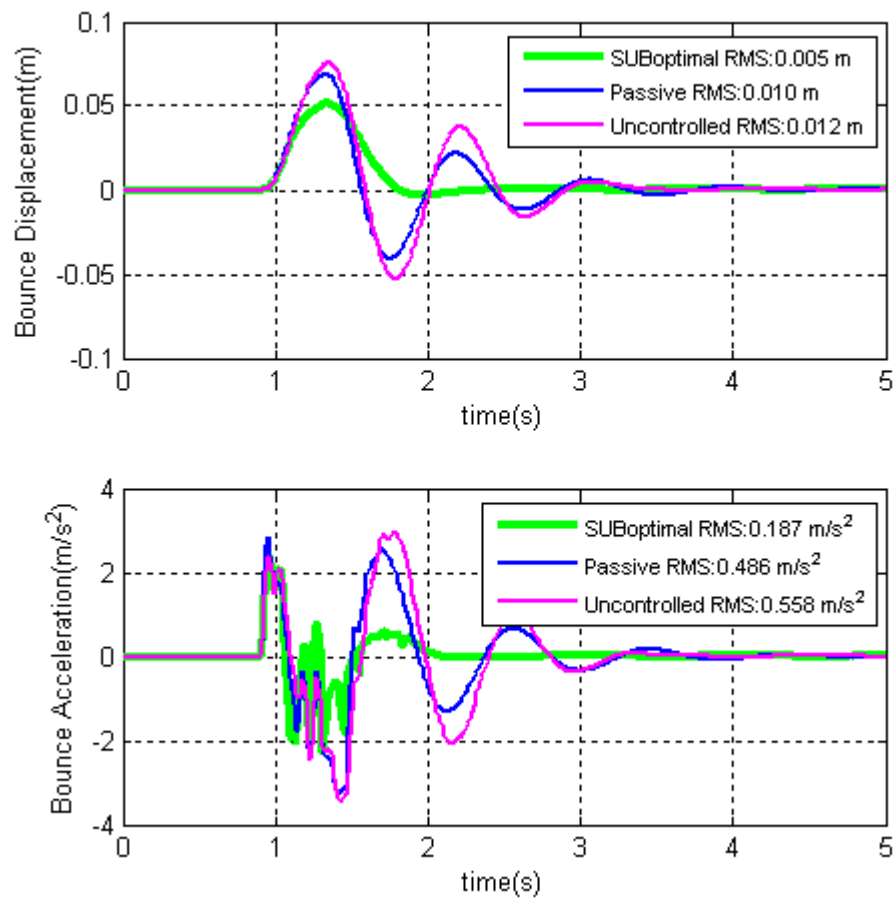


Figure 6.16 Bounce Motion And Bounce Acceleration versus - Half Sinusoidal Hump Input

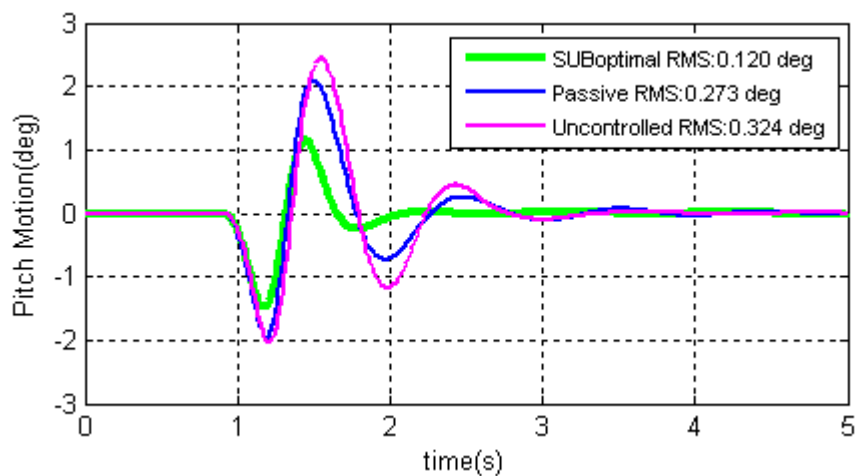


Figure 6.17 Pitch Motion versus Time - Half Sinusoidal Hump Input

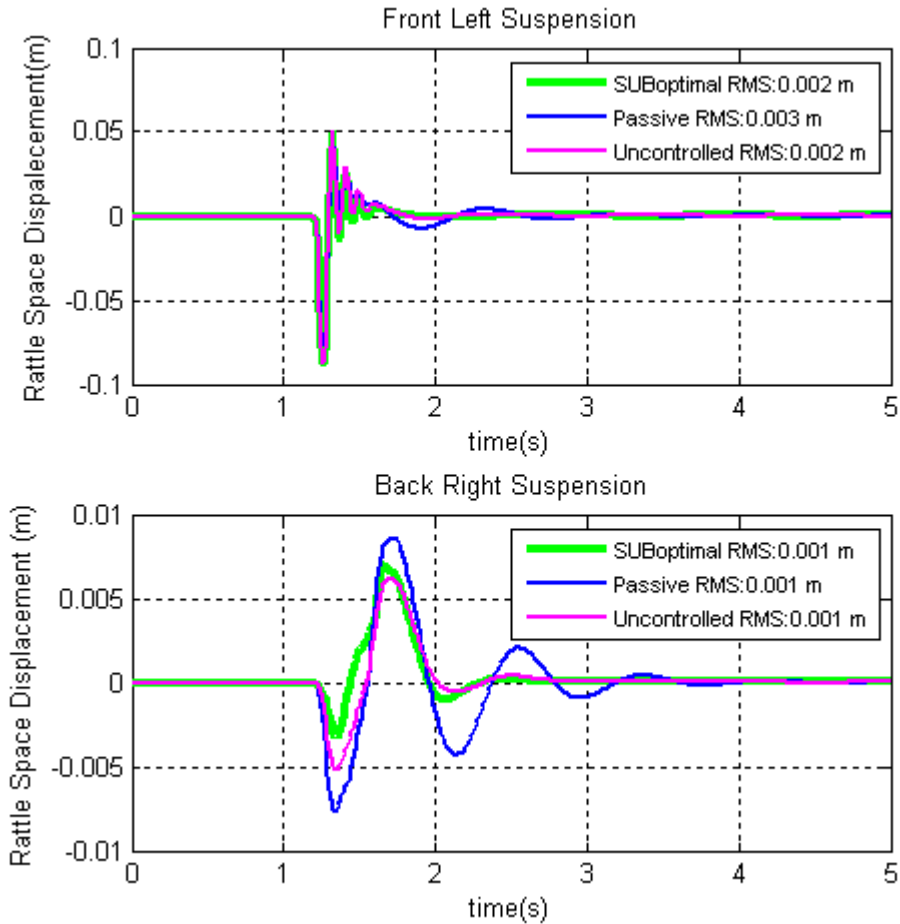


Figure 6.18 Rattle Space Motion of Front Left Suspension and Rear Right Suspension versus Time - Half Sinusoidal Hump Input

6.3 STEP INPUT TEST

This simulation is carried for determining transient response characteristics. The settling time can be seen from the plots. The step input height (Figure 6.19) is taken as 10 cm at a vehicle velocity of 60 kph. For this input the roll motion characteristics cannot be investigated, since the input does not differ for left and right side of the vehicle. In Figure 6.20 bounce motion characteristics are plotted whereas in Figure 6.21 and Figure 6.22 pitch angle and rattle space motion is plotted accordingly. As can be seen from the plots, the settling time for pitch, roll, and bounce motion

decreases considerable for Suboptimal control relative to passive and uncontrolled cases.

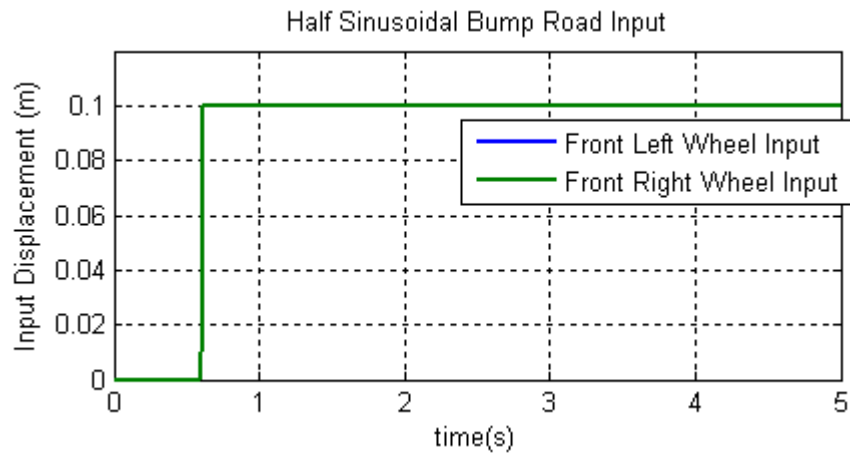


Figure 6.19 Step Road Input versus Time

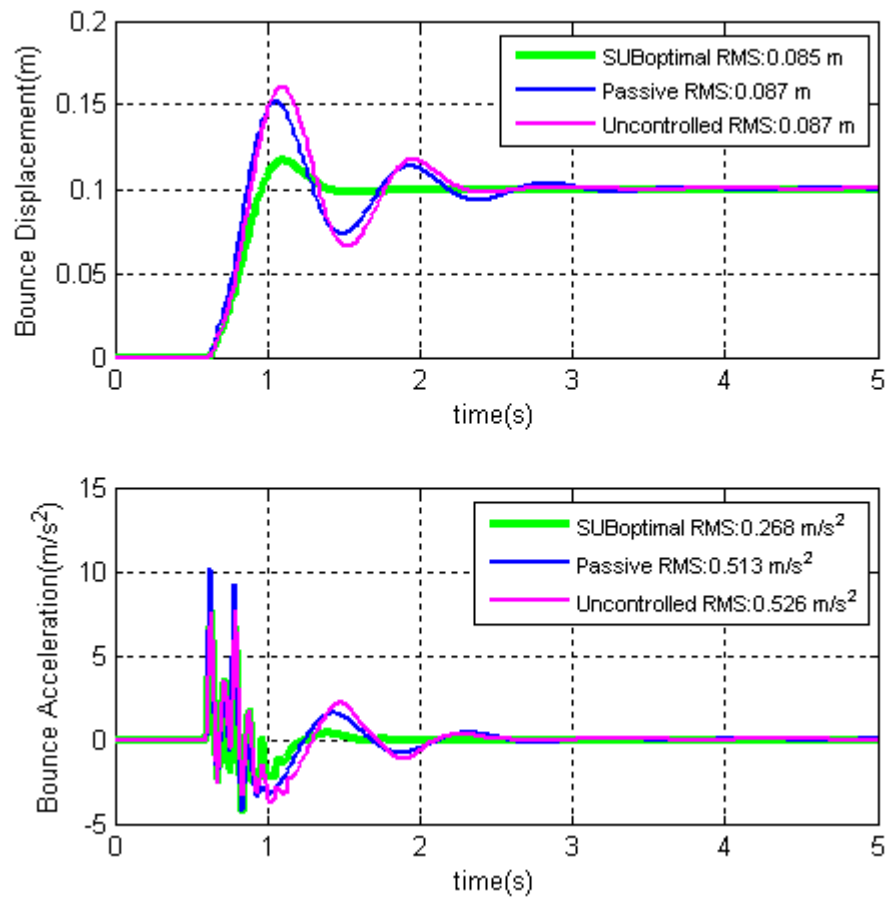


Figure 6.20 Bounce Motion versus Time Step Input

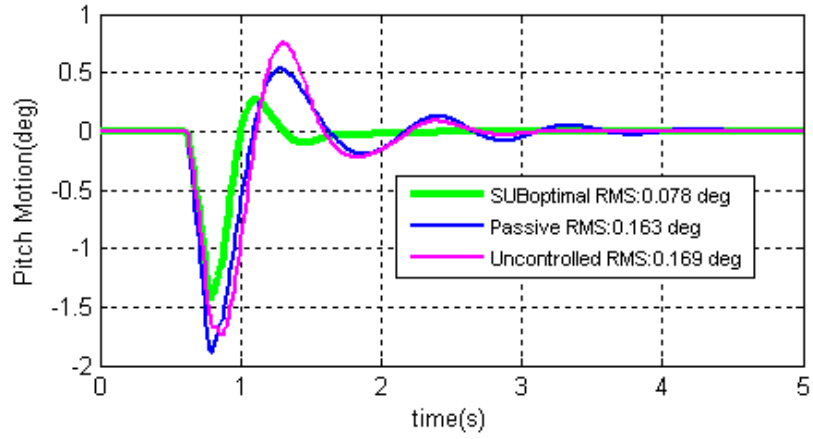


Figure 6.21 Pitch Motion versus Time Step Input

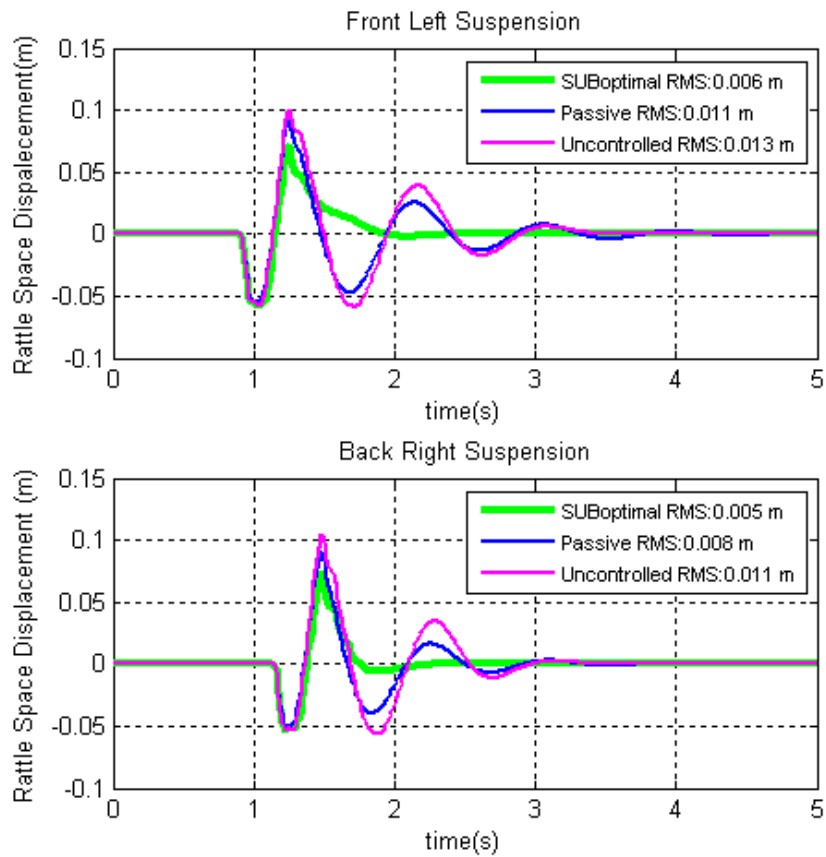


Figure 6.22 Rattle Space Motion of Front Left Suspension and Rear Right Suspension versus Time - Step Input

6.4 RANDOM ROAD INPUT TEST

Random road input test is carried with a white noise velocity input to have an idea of the frequency response of the vehicle. The random road input represents the general road conditions. The road excitation for a random process with a zero mean described by the equation:

$$\dot{z} + \rho V z = V W \quad 6.1$$

where V is the vehicle velocity, z is the road input, W is a white noise of power spectral intensity of $2\sigma^2\rho V$, σ^2 is the variance of road irregularity and ρ is the road roughness parameter. The road inputs are calculated separately for the left and right side wheels. The inputs generated for each side of the vehicle are transferred to the back axle with a time delay depending on the vehicle speed.

For this simulation, the velocity of the vehicle is assumed to be 72 kph, $\rho = 0,45\text{m}^{-1}$ and $\sigma^2 = 300\text{mm}^2$. In Figure 6.23, the time traces of left and right side road inputs are plotted.

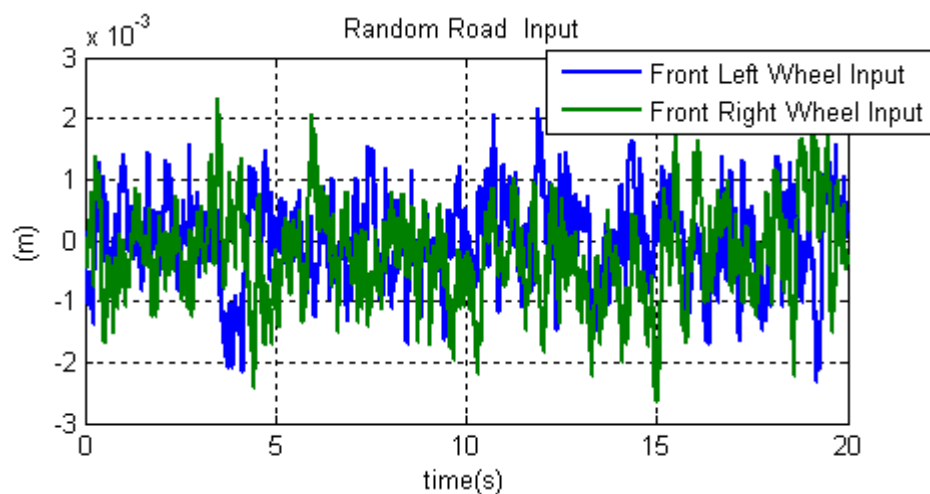


Figure 6.23 Random Road Input versus Time

The performance of the MR damper in minimizing bounce motion is seen in Figure 6.25. The vehicle parameters in APPENDIX B and the MR damper characteristics are adopted from the work of (Hong, Kim, & Kim, 2007). The relative velocity values across the damper for a random input is very low and at zero current level near these relative velocities, the MR damper is stiffer than passive dampers as can be seen from Figure 6.24. This deteriorates the performance of the controller. The PSD of the bounce motion shows that the passive damper behaviour becomes superior at high frequency inputs especially for bounce acceleration minimization.

If theoretically zero current damping forces of MR dampers (uncontrolled Mr damper characteristic) are reduced to 1/3 of the original damping force characteristic, the improvement between controlled, uncontrolled, and passive cases become clearer. The PSD of the fictitious MR damper under random road input is given in Figure 6.26.

To analyze the RMS values of bounce, pitch and roll motions for MR damper and fictitious MR damper, a performance criterion is proposed. The performance in minimizing RMS values is defined by the percentage of the difference between the obtained value and the passive suspension corresponding RMS value to the passive suspension RMS value. In the Table 4 the performance improvements are seen for MR damper. As expected the passive damper is better in bounce motion and pitch motion minimization, since the damper is stiffer in that region. For the fictitious damper whose minimum level damping is decreased to one third of the original there are tangible performance improvements in bounce, pitch and roll motions as shown in Table 5. As seen, semi-active dampers should be selected in a way that the feasible damping range should have a broadened damping range which also includes a suitable passive suspension damping characteristic inside.

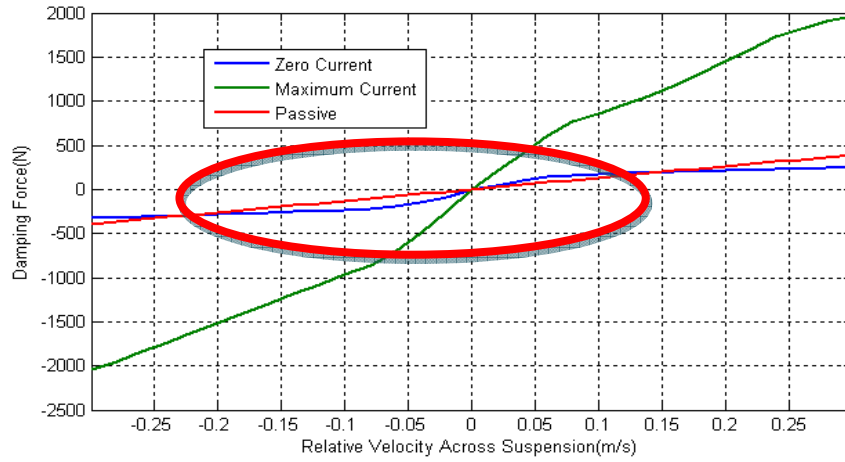


Figure 6.24 MR and Passive Damper Characteristics

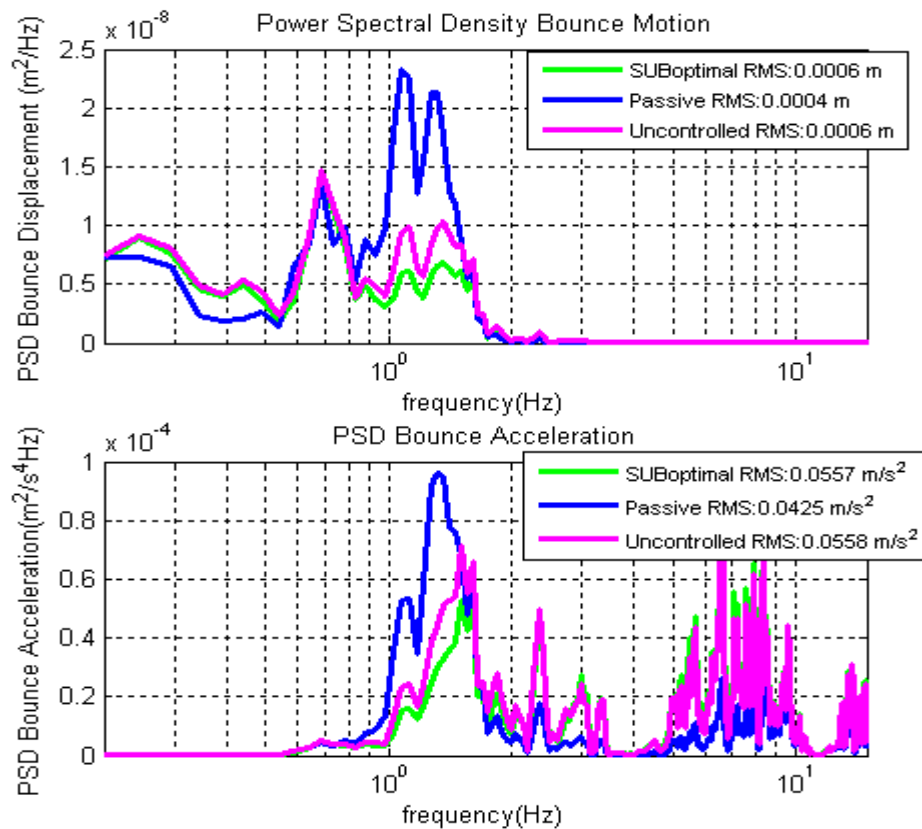


Figure 6.25 Power Spectral Density of Bounce Displacement and Bounce Acceleration of the existing MR damper

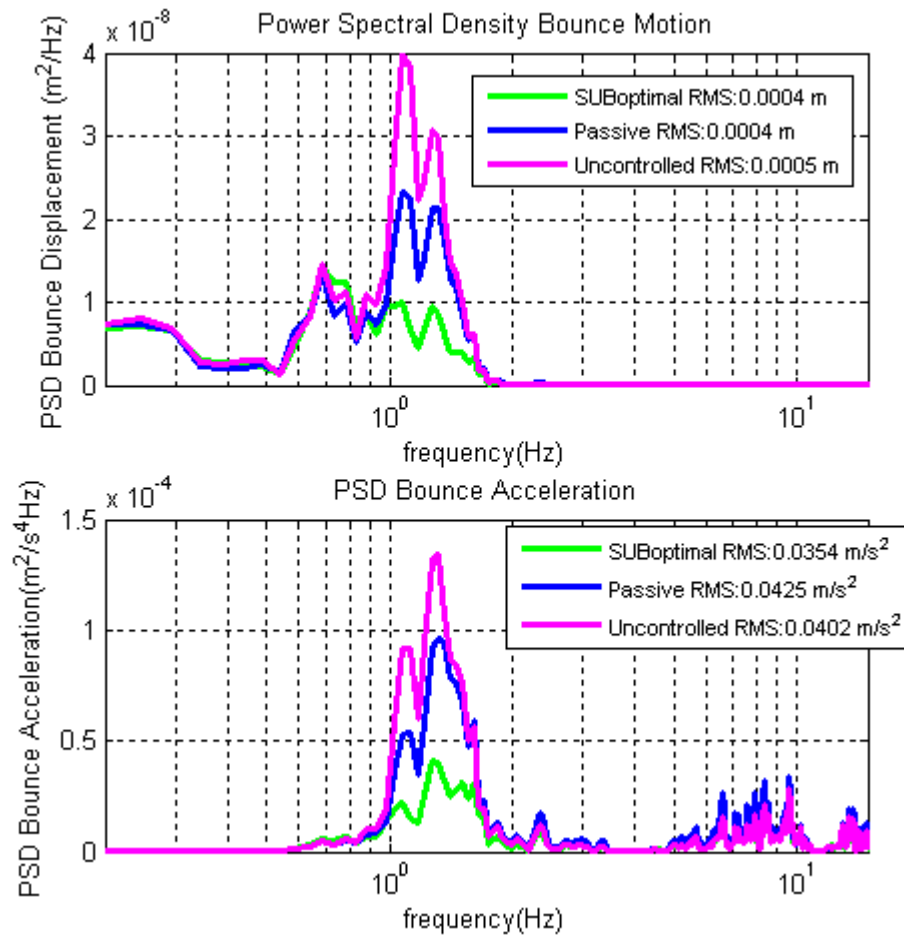


Figure 6.26 Power Spectral Density of Bounce Displacement and Bounce Acceleration of the fictitious MR damper

Table 4 Performance Results for the MR Damper under Random Road Input

	Performance Improvement of the Semi-active Control with respect to Passive Suspension	Performance Improvement of the Uncontrolled Dampers with respect to Passive Suspension
Bounce Motion	-50.0%	-50.0%
Bounce Acceleration	-31.1%	-31.3%
Pitch Motion	-12.5%	-18.8%
Roll Motion	30.6%	6.8%

Table 5 Performance Results for the Fictitious MR Damper under Random Road Input

	Performance Improvement of the Semi-active Control with respect to Passive Suspension	Performance Improvement of the Uncontrolled Dampers with respect to Passive Suspension
Bounce Motion	0.0%	-25.0%
Bounce Acceleration	16.7%	5.4%
Pitch Motion	17.2%	-12.5%
Roll Motion	42.8%	-7.3%

CHAPTER 7

CONCLUSION

Based on the simulation results, it was seen that semi-active MR dampers are capable of improving ride comfort by minimizing the bounce, pitch, and roll motion response with respect to passive dampers and uncontrolled case of semi-active MR dampers. The settling time and peak responses were reduced. The basic disadvantage of semi-active control is the worsening of rattle space responses. The increase in rattle space motion is not significant enough to create problems in suspension stroke limits. When implementing the semi-active controller, safety measures can be taken in case of extreme motions of rattle space motion by changing the control strategy.

For today the semi-active damping range for MR dampers is limited. Generally they are stiff in low relative velocities. This problem affects the random road input responses adversely. If the semi-active damping range could be broadened, the results would get better as was shown in section 6.4. The bigger the semi-active damping range, the more the performance of semi-active controllers improves.

LQR control algorithm is a systematic way to determine how to accomplish a given task. This strategy can be extended to take into account of the passenger seat motions and rattle space motion across dampers. The effectiveness of this strategy can be seen from the simulation results in section 6.1, 6.2, 6.3 and 6.4. The responses around 1 Hz which is near to body bounce frequency, show the improvement in ride comfort.

Skyhook control is an alternative control strategy which has nearly as significant improvements as LQR control does. Comparing the performances of skyhook and LQR control, LQR control is better in minimizing bounce acceleration and roll angle than skyhook control. The improvement of pitch angle minimization for LQR controllers is superior to classical passive suspensions; however the performance is not superior to skyhook controller. This was because more importance was given on reducing bounce and roll motion in LQR while tuning weighting constants.

The relative performance improvement is comparable to the easiness of implementation of the skyhook control strategy. LQR control for full car ride model needs full state feedback of 14 states whereas for skyhook control 8 state feedback is sufficient. The choice between two control strategies depends on the user expectations.

As a final remark, the main scope of optimal LQR control can be extended in various aspects. The LQR controller can be combined with fuzzy controller to compensate extreme conditions that deviates from normal road inputs. Different weighting factor sets can be used depending on the vehicle states. The genetic algorithm may be used in the optimization process of the weighting factors in the LQR controller. Also the seven degree of freedom model can be extended with additional degree of freedoms like the driver seat degree of freedom. In addition the cost function index can be extended to cover rattle space motion. Finally control techniques may be developed further with Hardware-in-the-Loop (HIL) simulations.

REFERENCES

- Ahmadian M., S. D. (2004). "Can Semiactive Dampers with Skyhook Control Improve Roll Stability of Passengers Vehicles?". *2004-01-2099*.
- Ahmadian, M. P. (2000). A Quarter-Car Experimental Analysis of Alternative Semi active Control Methods. *11*.
- Ahmadian, M. S. (2004). No-Jerk Skyhook Control Methods for semiactive Suspensions. *126*.
- B.Burl, J. (1999). *Linear Optimal Control H2 and Hinfinity Methods*. Addison Wesley.
- Butsuen, T. (1989). *The Design of Semiactive Suspensions for Automotive Vehicles*. Massachusetts Institute of Technology.
- Butz, T. v. (2002). Modeling and Simulation of Electro- and Magnetorheological Fluid Dampers. *82* (1).
- Choi, S. L. (2002). H_∞ Control Performance of a Full-Vehicle Suspension Featuring Magnetorheological Dampers. *38* (5), 341-360.
- Choi, S.-B., Han, Y.-M., & Sung, K.-G. (2008). Vibration control of vehicle suspension. s. 189-204.
- Choi, S.-B., Han, Y.-M., Song, H. J., & Choi, H. J. (2007). Field Test on Vibration Control of Vehicle Suspension System Featuring ER Shock Absorbers. *Journal of Intelligent Material Systems and Structures* , *18*.
- Choi, Y. P. (2000). A Sliding Mode Control of a Full-Car Electrorheological Suspension System Via Hardware in-the-Loop Simulation. *122*.
- Dominguez, A. S. (2004). Modeling the Hysteresis Phenomenon of Magnetorheological Dampers. *13*, 1351-1361.
- Du, H. S. (2005). Semi-active H_∞ Control of Vehicle Suspension with MR Dampers. *283*, 981-996.

- Giua, A. M. (2004). "Design of a Predictive Semiactive Suspension System. *41* (4), 277-300.
- Giua, A. S. (2000). A Mixed Suspension System for a Half-Car Vehicle Model. *10*, 375-397.
- Giua, A., Seatzu, C., & Usai, G. (1999). Semiactive Suspension Design with an Optimal Gain Switching Target. *Vehicle System Dynamics International Journal of Vehicle Mechanics and Mobility* .
- Grad, P. (2006, December). Against the flow - Smart fluids that can change their viscosity in real time. *Engineering & Technology* , *1* (9), s. 34-37.
- Guglielmino, E. S. (2008). *Semi-active Suspension Control - Improved Vehicle Ride and Road Friendliness* . Springer.
- Hong, K.-S., Kim, T.-S., & Kim, R.-K. (2007). Sensitivity Control of a Semi-Active Suspension System Equipped with MR-Dampers. *International Conference on Control, Automation and Systems*. Seoul, Korea: IEEE Xplore.
- Hong, K.-S., Kim, T.-S., & Kim, R.-K. (2007). Sensitivity Control of a Semi-Active Suspension System Equipped with MR-Dampers. *International Conference on Control, Automation and Systems 2007*. COEX, Seoul, Korea.
- Karkoub, M. Z. (2006). Active/semi-active suspension control using magnetorheological actuators. *37* (1), 35-44.
- Kim, R. H. (2007). Skyhook Control Using a Full-Vehicle Model and Four Relative Displacement Sensors.
- Klingenberg, D. J. (2001). Magnetorheology: Applications and Challenges. *Aiche Journal* , *17* No:2 249, 246-249.
- Li, R. C. (2004). Fuzzy Intelligent Control of Automotive Vibration via Magnetorheological Damper. *1-3*.
- Liu, Y. M. (2004). Controllable Vibration of the Car-Body Using Magnetorheological Fluid Damper. *41*, 627-636.
- Lu, J. (2004). A Frequency-Adaptive Multi-Objective Suspension Control Strategy,. *126*.

- Mark R. Jolly, M. R. (1999). Properties and Applications of Commercial Magnetorheological Fluids.
- Martynowicz, P. S. (2007). Experimental Study of Vibration Control in a two Degree of Freedom Pitch-Plane Model of a Magnetorheological Vehicle Suspension. *26* (2).
- Matlab R2007b -The Language of Technical Computing. (n.d.). LQR. *Control System Toolbox* .
- MR Fluid Techology*. (n.d.). Retrieved 01. 07, 2009, from LORD Corporation-Adhesives, Coatings, Vibration, Shock & Motion Control: <http://www.lord.com/Home/MagnetoRheologicalMRFluid/MRFluidTechnology/WhatisMR/tabid/3772/Default.aspx>
- (n.d.). Retrieved 01 07, 2009, from LORD Corporation – Adhesives, Coatings, Vibration, Shock & Motion Control.: www.lord.com
- Naidu, D. S. (2003). *Optimal Control Systems*. CRC PRESS.
- Ogata, K. *Modern Control Engineering-Fourth Edition*. Upper Saddle River,New Jersey: Prentice Hall.
- Primary Suspension*. (2008). Retrieved 05 08, 2008, from LORD Corporation – Adhesives, Coatings, Vibration, Shock & Motion Control: <http://www.lord.com/Home/MagnetoRheologicalMRFluid/Applications/PrimarySuspension/tabid/3329/Default.aspx>
- Rajamani, R. (2006). *Vehicle Dynamics and Control*. Springer.
- Sinha, A. (2007). *Linear Systems Optimal and Robust Control*. CRC Press.
- Song, X. A. (2005). Modeling Magnetorheological Dampers with Application of Nonparametric Approach. *16*.
- Sung, K. C. (2005). Performance Comparison of Mr Dampers with Three Different Working Modes: Shear, Flow and Mixed Mode. *19* (7,8,9), 1556-1562.
- Sung, K.-G., Han, Y.-M., Cho, J.-W., & Choi, S.-B. (2008). Vibration control of vehicle ER suspension system using fuzzy moving sliding mode controller. *Journal of Sound and Vibration* , 1004-1019.
- Technology Compared*. (n.d.). Retrieved 01 07, 2009, from Lord Corporation-Adhesives,Coatings,Vibration,and Shock& Motion Control:

<http://www.lord.com/Home/MagnetoRheologicalMRFluid/MRFluidTechnology/TechnologyCompared/tabid/3773/Default.aspx>

Tsang, H. S. (2006). "Simplified inverse dynamics models for MR fluid dampers. 28, 327-341.

Turkish Standard Institution. (1998). Speed Control Humps. *Turkish Standard, TS 6283/T3* .

Wang, H. H. (2005). Optimal Fuzzy Control of a Semi-active Suspension of a Full-Vehicle Model using MR Dampers. *19* (7,8,9), 1513-1519.

Yu, M. L. (2006). Study on MR Semi-active Suspension System and its Road Testing.

Zhang, C. O. (2006). Parameter optimization and analysis of a vehicle suspension system controlled by magnetorheological fluid dampers.

Zheng, L. L. (2007). The Design of a Fuzzy-sliding Mode Controller of Semi-active Suspension Systems with MR Dampers.

Zuo, L., & Nayfeh, S. A. (2003). Structured H2 Optimization of Vehicle Suspensions Based on Multi-Wheel Models. *Vol. 40*, 351–371.

APPENDIX A

A.1 GENERAL VIEW OF THE SIMULATION MODEL SIMULATION MODEL

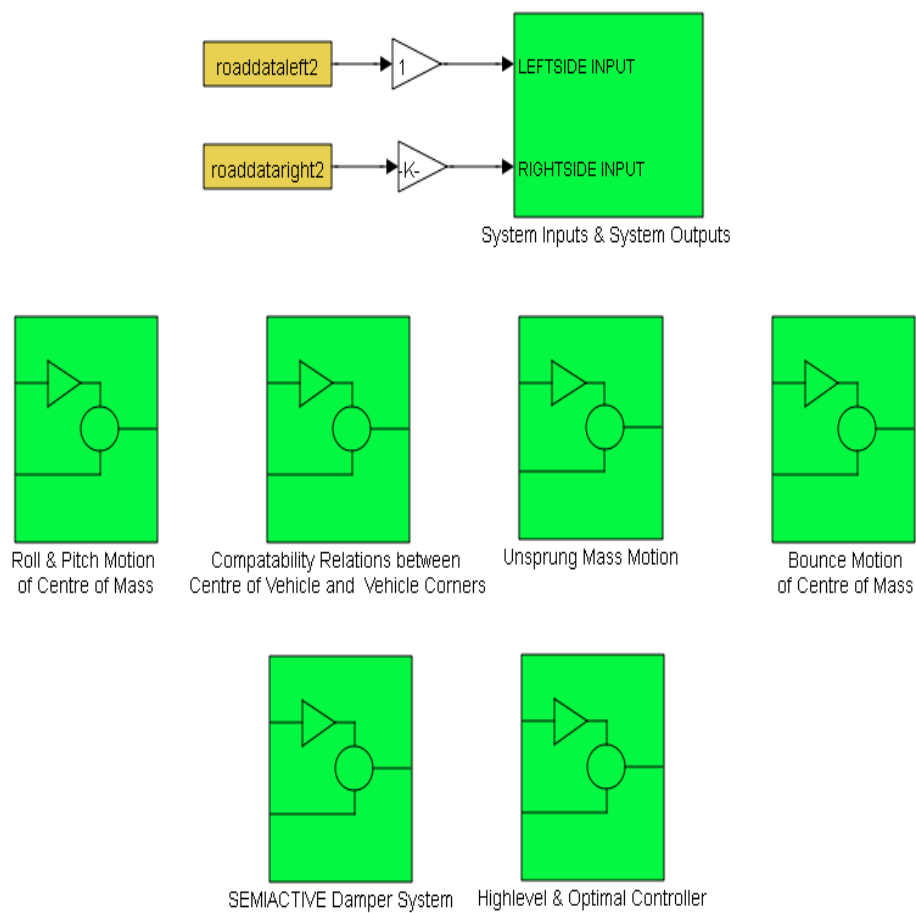


Figure A.1 General view of the Simulink Model

A.2 ROLL AND PITCH MOTION OF THE VEHICLE

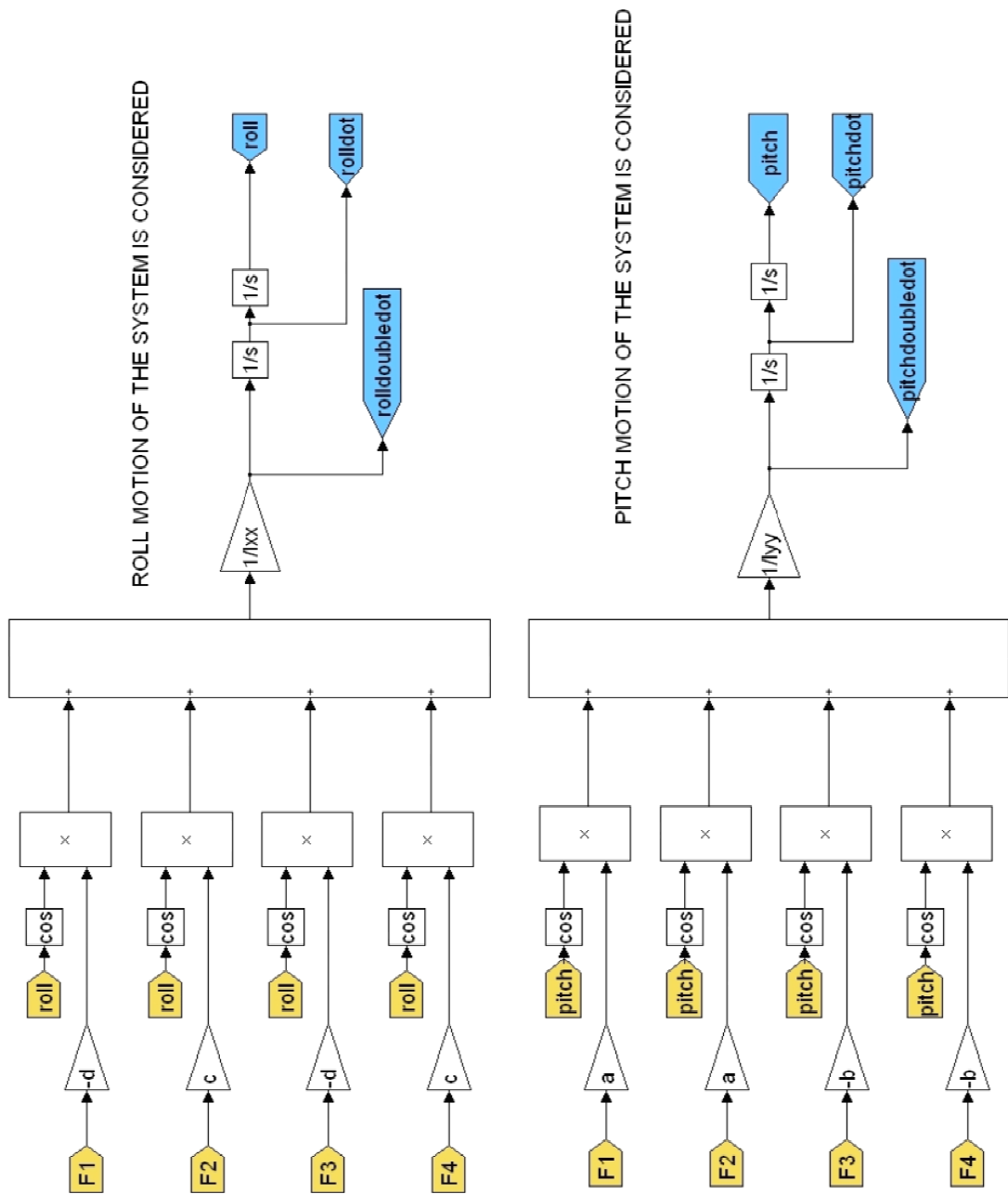


Figure A.2 Simulink Model for Roll and Pitch Motion

A.3 COMPABILITY EQUATIONS BETWEEN CENTRE OF MASS AND CORNERS OF THE VEHICLE

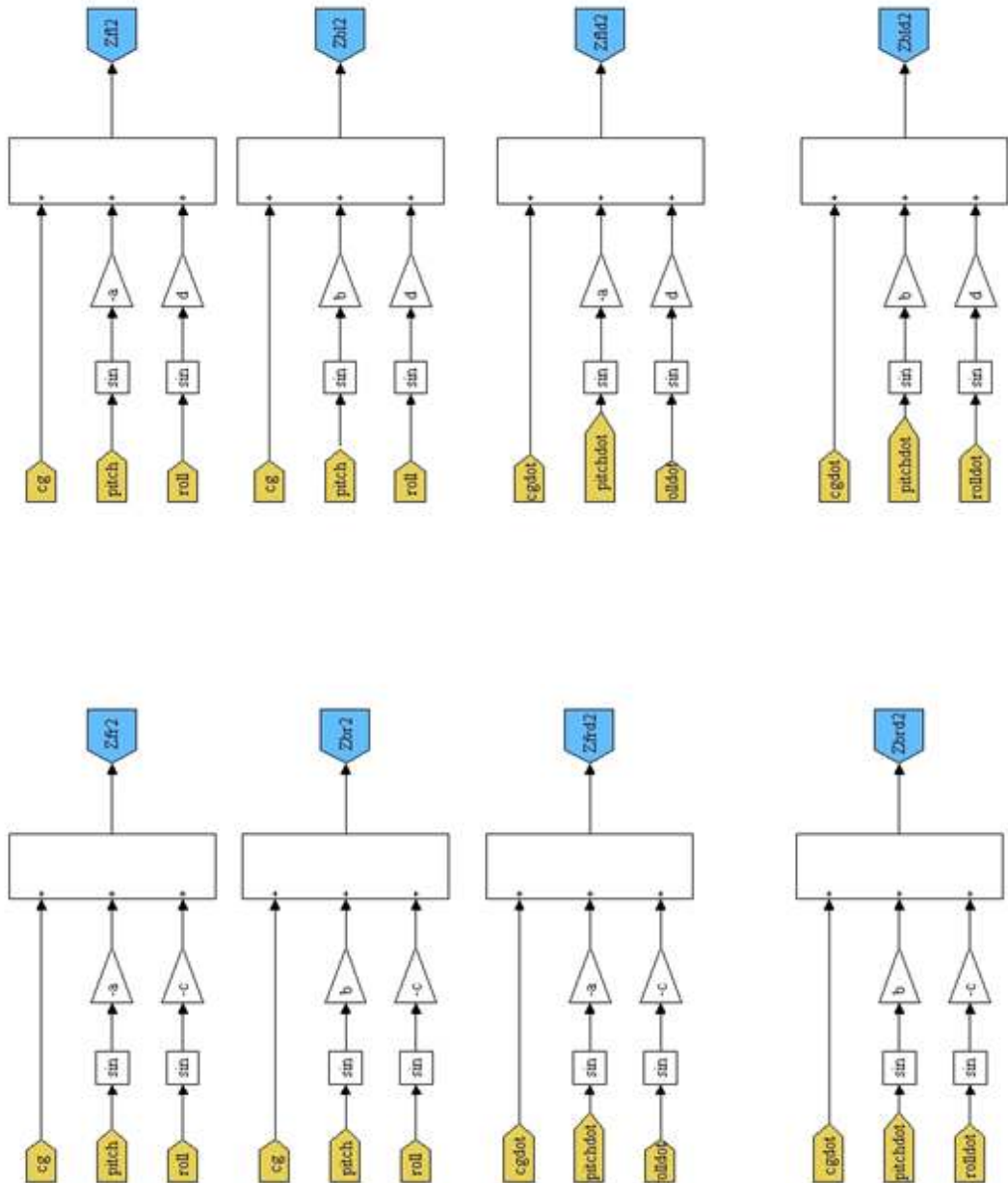


Figure A.3 Simulink Model for Compatibility Equations

A.4 UNSPRUNG MASS MOTION

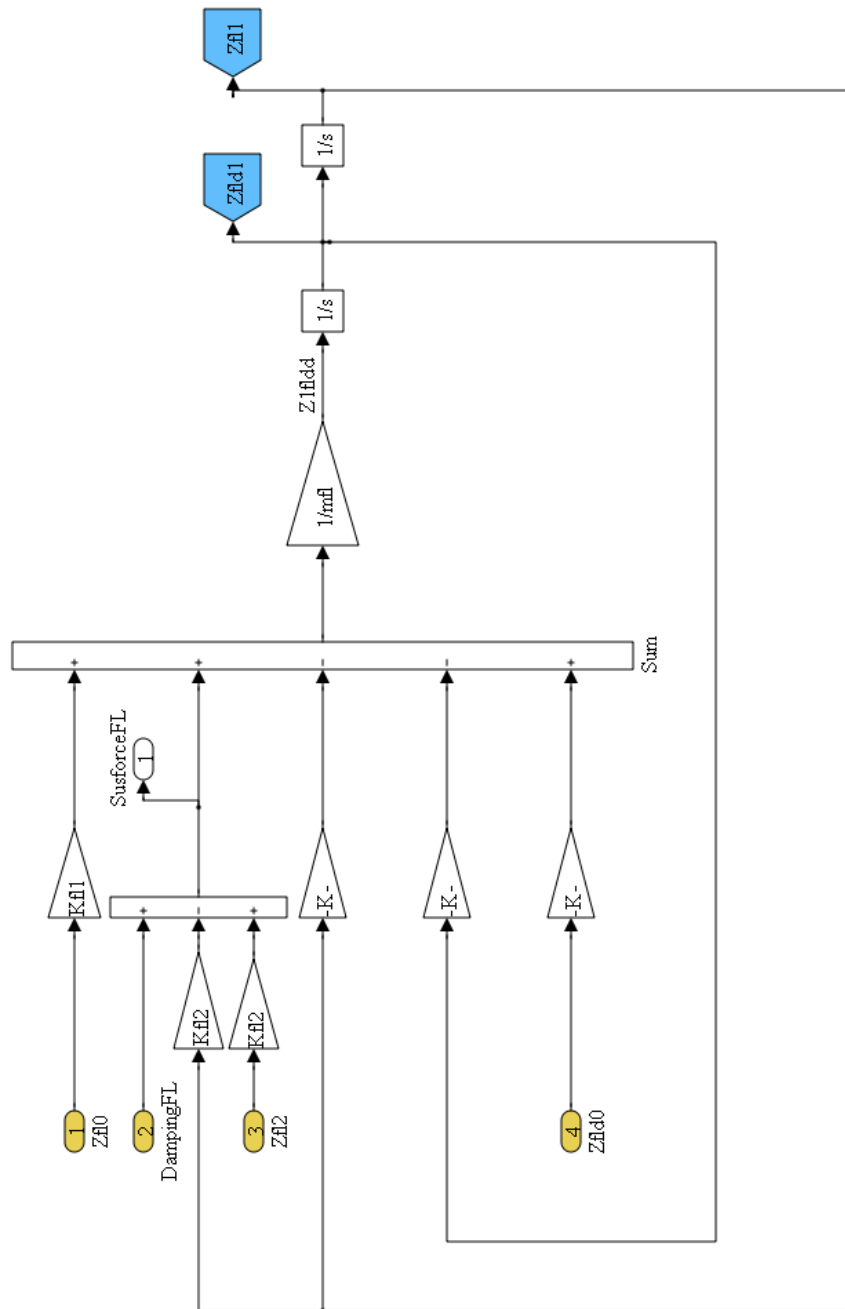


Figure A.4 Simulink Model of Unsprung Mass Motion

A.5 BOUNCE MOTION OF THE VEHICLE

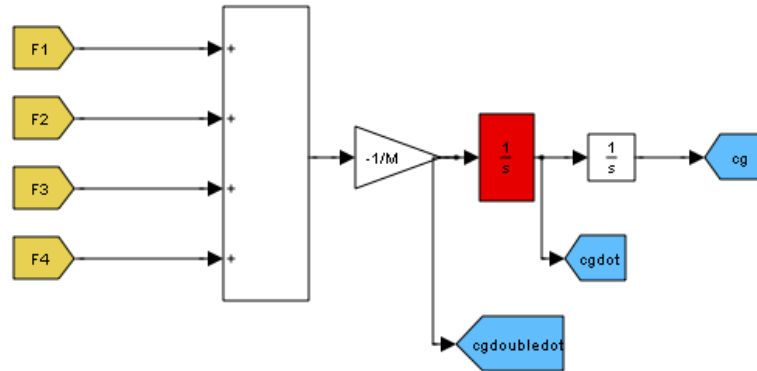


Figure A.5 Simulink Model for Bounce Motion

APPENDIX B

Table 6 Vehicle Data Used in Vehicle Simulations

(Zuo & Nayfeh, 2003)

Sprung Mass	1376 kg
Front Unsprung Mass per suspension	40 kg
Rear Unsprung Mass per suspension	40 kg
Spring Constant per tire	182087 N/m
Suspension Spring rate for tire(front)	20985 N/m
Suspension Spring rate for tire(rear)	19122 N/m
Front Damper Coefficient per tire	1306 N.s/m
Rear Damper Coefficient per tire	1470 N.s/m
Roll Moment of Inertia	484 kg.m ²
Pitch Moment of Inertia	2344 kg.m ²
Distance between front tires and centre of gravity	1.125 m
Distance between rear tires and centre of gravity	1.511 m
Distance between front tires and centre of gravity	0.72 m

APPENDIX C

The m-file code used in embedded Matlab/Simulink block to find necessary input currents for requested damping forces is given here. The logic of this code is briefly:

- 1-The lookup tables are separately prepared for each current.
- 2-At a given relative velocity, the damping forces that can be generated at each current is fed to the embedded function block.
- 3-By the function of “min”, the two current values which give closest forces to desired force is found.
- 4-Linear interpolation is carried between the two currents to find the necessary currents.
- 5-As will be discussed if the current is not feasible, the current will be modified.

The code:

```
function [optcurrent,index,index2,opteski] =  
fcn(wanted,relvel,f1,f2,f3,f4,f5,f6,f7,f8,f9,current1,current2,current3,current4,current  
5,current6,current7,current8,current9,count,minlimited,maxlimited,forceminlimit)  
% This block supports an embeddable subset of the MATLAB language.  
% See the help menu for details.  
  
%the array of forces that can be generated at different current levels at a specific  
relative velocity:  
f=[f1 f2 f3 f4 f5 f6 f7 f8 f9];  
%the array of available current levels:  
current=[current1 current2 current3 current4 current5 current6 current7 current8  
current9];  
delta=[0 0 0 0 0 0 0 0 0];  
%each delta represents the difference between demanded force and available force  
%at a specific current level at a specific relative velocity  
delta(1)=wanted-f1;  
delta(2)=wanted-f2;  
delta(3)=wanted-f3;  
delta(4)=wanted-f4;  
delta(5)=wanted-f5;  
delta(6)=wanted-f6;
```

```

delta(7)=wanted-f7;
delta(8)=wanted-f8;
delta(9)=wanted-f9;

%finding smallest delta to find the smallest error between demanded force and
available force
[sortt,place]=sort(abs(delta));
%finding the limits of available damping force at a specific relative velocity
[sortt2,place2]=sort(f);
maks=sortt2(9);
minimum=sortt2(1);
index=place(1);
index2=place(2);

optcurrent=0;
check=1;

%finding the current input:

if wanted>=maks;%in this case demanded force is more than available damping
force
    index=place2(9);
    index2=place2(8);
    optcurrent=current(index)+abs(delta(index))/abs(f(index2)-
f(index))*abs(current(index2)-current(index))*-sign(current(index2)-current(index));

elseif wanted<=minimum;%in this case demanded force is less than available
damping force
    index=place2(9);
    index=place2(1);
    index2=place2(2);
    optcurrent=current(index)+abs(delta(index))/abs(f(index2)-
f(index))*abs(current(index2)-current(index))*-sign(current(index2)-current(index));
else%in this case demanded force is at the available damping range
    for i=2:9
        index2=place(i);
        if (f(index)<=wanted && wanted<=f(index2))|| ( f(index2)<=wanted &&
wanted<=f(index))&&check==1
            check=0;
            break
        end

    end
    optcurrent=current(index)+abs(delta(index))/abs(f(index2)-
f(index))*abs(current(index2)-current(index))*-sign(current(index2)-current(index));

end
end

```

```
opteski=optcurrent;  
  
%Clipping the input current levels:  
if optcurrent>maxlimited  
    optcurrent=maxlimited;  
elseif optcurrent<minlimited  
    optcurrent=minlimited;  
  
end  
  
y = optcurrent;
```

APPENDIX D

The mass matrix is given as:

$$M = \begin{bmatrix} m_{fl} & 0 & 0 & 0 & 0 & 0 & 0 \\ 0 & m_{bl} & 0 & 0 & 0 & 0 & 0 \\ 0 & 0 & m_{fr} & 0 & 0 & 0 & 0 \\ 0 & 0 & 0 & m_{fl} & 0 & 0 & 0 \\ 0 & 0 & 0 & 0 & M & 0 & 0 \\ 0 & 0 & 0 & 0 & 0 & I_{xx} & 0 \\ 0 & 0 & 0 & 0 & 0 & 0 & I_{yy} \end{bmatrix} \quad (D.1)$$

The stiffness matrix K is written as:

$$K = [K_1 \quad K_2 \quad K_3] \quad (D.2)$$

$$K_1 = \begin{bmatrix} (k_{fl1} + k_{fl2}) & 0 & 0 & 0 \\ 0 & (k_{bl1} + k_{bl2}) & 0 & 0 \\ 0 & 0 & (k_{fr1} + k_{fr2}) & 0 \\ 0 & 0 & 0 & (k_{br1} + k_{br2}) \\ -k_{fl2} & -k_{bl2} & -k_{fr2} & -k_{br2} \\ k_{fl2}a & -k_{bl2}b & k_{fr2}a & -k_{br2}b \\ -k_{fl2}d & -k_{bl2}d & k_{fr2}c & k_{br2}c \end{bmatrix} \quad (D.3)$$

$$\mathbf{K}_2 = \begin{bmatrix}
-k_{fl2} & -k_{fl2}d \\
-k_{bl2} & -k_{bl2}d \\
-k_{fr2} & +k_{fr2}c \\
-k_{br2} & +k_{br2}c \\
k_{fl2} + k_{bl2} + k_{fr2} + k_{br2} & +k_{fl2}d + k_{bl2}d - k_{fr2}c - k_{br2}c \\
-k_{fl2}a + k_{bl2}b - k_{fr2}a + k_{br2}b & -k_{fl2}ad + k_{bl2}bd + k_{fr2}ac - k_{br2}bc \\
k_{fl2}d + k_{bl2}d - k_{fr2}c - k_{br2}c & k_{fl2}d^2 + k_{bl2}d^2 + k_{fr2}c^2 + k_{br2}c^2
\end{bmatrix} \quad (\text{D.4})$$

$$\mathbf{K}_3 = \begin{bmatrix}
k_{fl2}a \\
-k_{bl2}b \\
k_{fr2}a \\
-k_{br2}b \\
-k_{fl2}a + k_{bl2}b - k_{fr2}a + k_{br2}b \\
+k_{fl2}a^2 + k_{bl2}b^2 + k_{fr2}a^2 + k_{br2}b^2 \\
-k_{fl2}da + k_{bl2}db + k_{fr2}ca - k_{br2}cb
\end{bmatrix} \quad (\text{D.5})$$

APPENDIX E

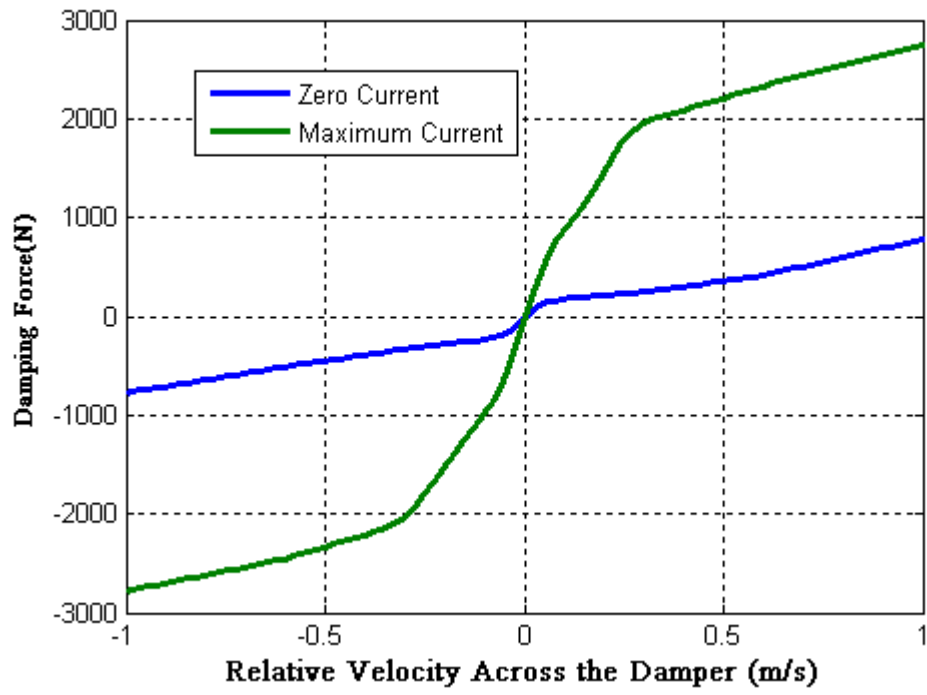


Figure E.1 MR Data used in Simulations